SKB

TECHNICAL REPORT 93-02

Hydrothermal field test with french candidate clay embedding steel heater in the Stripa mine

R Pusch[1], O Karnland[1], A Lajudie[2], J Lechelle[2], A Bouchet[3]

[1] Clay Technology AB, Sweden
[2] CEA, France
[3] Etude Recherche Materiaux (ERM), France

December 1992

SVENSK KÄRNBRÄNSLEHANTERING AB
SWEDISH NUCLEAR FUEL AND WASTE MANAGEMENT CO

BOX 5864 S-102 48 STOCKHOLM

TEL. 08-665 28 00 TELEX 13108 SKB S
TELEFAX 08-661 57 19

HYDROTHERMAL FIELD TEST WITH FRENCH CANDIDATE CLAY EMBEDDING STEEL HEATER IN THE STRIPA MINE

R Pusch[1], O Karnland[1], A Lajudie[2], J Lechelle[2], A Bouchet[3]

1 Clay Technology AB, Sweden
2 CEA, France
3 Etude Recherche Materiaux (ERM), France

December 1992

FINAL REPORT ON SKB/CEA

HYDROTHERMAL FIELD TEST WITH FRENCH CANDIDATE CLAY EMBEDDING STEEL HEATER IN THE STRIPA MINE

December 1992

CLAY TECHNOLOGY AB

R. PUSCH
O. KARNLAND

CEA

A. LAJUDIE
J. LECHELLE

ERM*

A. BOUCHET

* Etude Recherche Materiaux (Poitiers)

ABSTRACT (English)

Field experiments with French kaolinite/smectite clay heated up to 170°C in boreholes in granite were conducted for 8 months and 4 years. The clay heated for 8 months had a considerably higher water content and it had undergone much less changes in mineralogy and physical properties than the clay exposed to heating for 4 years. The drying of the latter clay was probably caused by hydrogen gas from corrosion of the heater. The clay next to the heater turned into claystone despite conversion of the kaolinite component to smectite.

ABSTRACT (Swedish)

Fältexperiment med värmning av fransk kaolinit/-smektitlera upp till 170°C i borrhål i granit utfördes under 8 månader respektive 4 år. Leran som värmdes under kortare tid hade högre vatteninnehåll och visade mindre förändring av mineralinnehåll och fysikaliska egenskaper än den som värmdes i 4 år. Uttorkningen av den sistnämnda leran orsakades troligen av vätgas bildad vid korrosion av värmaren. Leran närmast värmaren hade fått karaktären av lersten trots att kaolinitkomponenten omvandlats till smektit

TABLE OF CONTENTS

SUMMARY

Field hydrothermal experiments with kaolinite/smectite clay surrounding 70 mm heaters in 200 mm diameter boreholes were conducted for about 8 months and somewhat less than 4 years, respectively. The rock was granite with low-electrolyte groundwater giving a piezometric pressure at the base of the 3 m long holes of 0.5-0.9 MPa. The heater power was about 1 kW and the surface temperature of the centrally placed steel casing with the heater was in the range of 170-180°C at maximum at mid-height heater, at which level the temperature at the clay/rock interface was around 95°C.

Excavation and testing of the clay core from the 8 months long experiment showed that the degree of water saturation was high except for close to the casing, and both chemical and physical properties were practically unchanged. The clay excavated from the longer test had become much drier in the hot zone, indicating that it had first become rather well saturated and then dehydrated, a possible reason for this being expulsion of water by hydrogen gas produced by steel corrosion.

The innermost centimeter-thick annulus had turned very dark and stiff due to dissolution of quartz and coloring by neoformation of trioctahedral smectite, and it had turned into claystone by cementation of precipitated anhydrite and silicious compounds. The very significant neoformation of smectites in this zone, for which the almost completely dissolved kaolinite component supplied aluminum, did not yield ductility and swelling ability because of the cementation. The hydraulic conductivity of the claystone was about 1000 times higher than that of the virgin clay due to the increased amount of interconnected voids and fissures.

The rest of the clay core had undergone insignificant mineralogical and chemical changes but rather strong cementation by migrated and precipitated silica had taken place.

The clay/steel contact and the shallow steel were inspected by electron microscopy and pitting-type corrosion with a maximum cavern depth of about 30 μm was observed. The loss of iron by corrosion corresponds fairly well to the amount of hydrogen gas that would be required to yield the observed water expulsion.

1 INTRODUCTION

1.1 GENERAL

SKB and CEA agreed in late 1985 on conducting a joint venture project that aimed at finding out the sort and rate of physico/chemical changes that will take place in dense smectitic clay surrounding steel canisters with high surface temperature. The test site in the granitic rock mass was selected so as to yield nearfield conditions similar to those in the first decade after repository closure with respect to piezometric pressure and rock quality. The steel was of ordinary commercial type available in any country, while the clay was selected from a number of French candidate buffer materials by CEA.

The field test comprised two experiments of which one served as a pilot test of short duration (8 months) for checking equipment and for getting information on processes taking place in the first phase after emplacement, while the other, which ran for about 4 years, was intended to yield information on longterm alteration processes.

The entire field experiment could be pursued very successfully and turned out to give results of significant value. Most certainly the outcome of the project will be a guidance in designing future repositories.

1.2 SCOPE

The primary aim was to let the field experiments go on for a sufficiently long time to check the water uptake rate in the initially unsaturated clay and to find out possible chemically induced changes in physical properties in the saturation phase and well beyond that.

The testing philosophy was to emplace prefabricated units of clay blocks surrounding steel tubes with electrical heaters in vertical boreholes and to maintain the steel surface temperature at around 170°C whilst measuring the piezometric head at the bottom of the holes and the temperature and swelling pressure in the system. At the termination of the tests, the plans were to extract the clay from the rock so quickly, i.e. in a few hours, that no redistribution of water would take place before samples could be extracted for water content determination and for subsequent chemical, mineralogical and physical testing.

2 DESCRIPTION OF TESTS

2.1 GENERAL

Prefabricated clay/heater units were emplaced in two vertical boreholes with 200 mm diameter and 2.8 m length at 350 m depth in the "Time Scale" drift in the Stripa Mine in August and October 1986, respectively (Fig.2-1). This drift was excavated about 7 years earlier and used for various rock heating experiments in a preceding study conducted by Lawrence Berkeley Laboratory in a Swedish/American joint research project. One of the 200 mm boreholes (Hole I) coincided with an earlier drilled 147 mm diameter LBL hole which extended for several tens of meters from the tunnel floor. The other 200 mm hole was drilled for the present purpose, the drilling being preceded by making a 56 mm pilot hole.

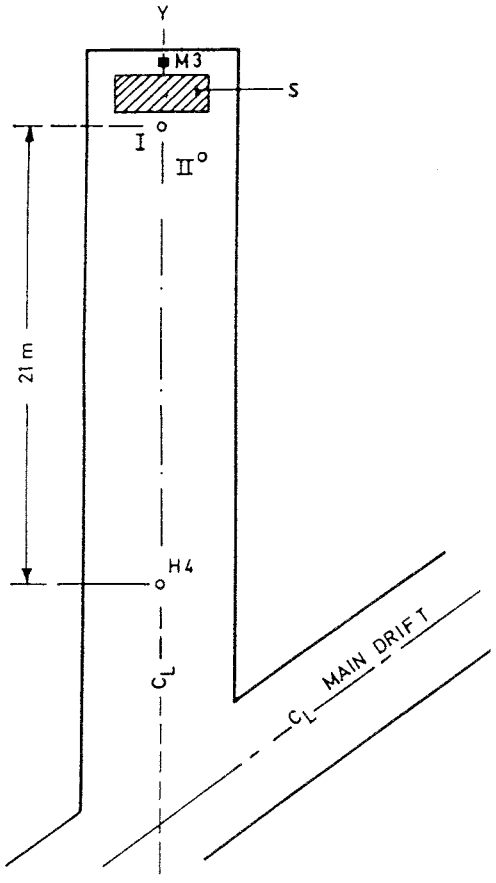

Figure 2-1 Schematic view of the drift at 350 m depth in the Stripa mine with the two test holes. Hole I coincides with the 147 mm hole H2 used by LBL in a preceding study

The test arrangement is illustrated by Fig.2-2, showing the instrumentation of Hole II with a somewhat larger number of thermocouples than in Hole I, in which a short-term pilot test was conducted. The fi-

gure also shows the emplacement of the clay/heater unit in Hole I, and the epoxy sealing of the lead-through of casing and cables.

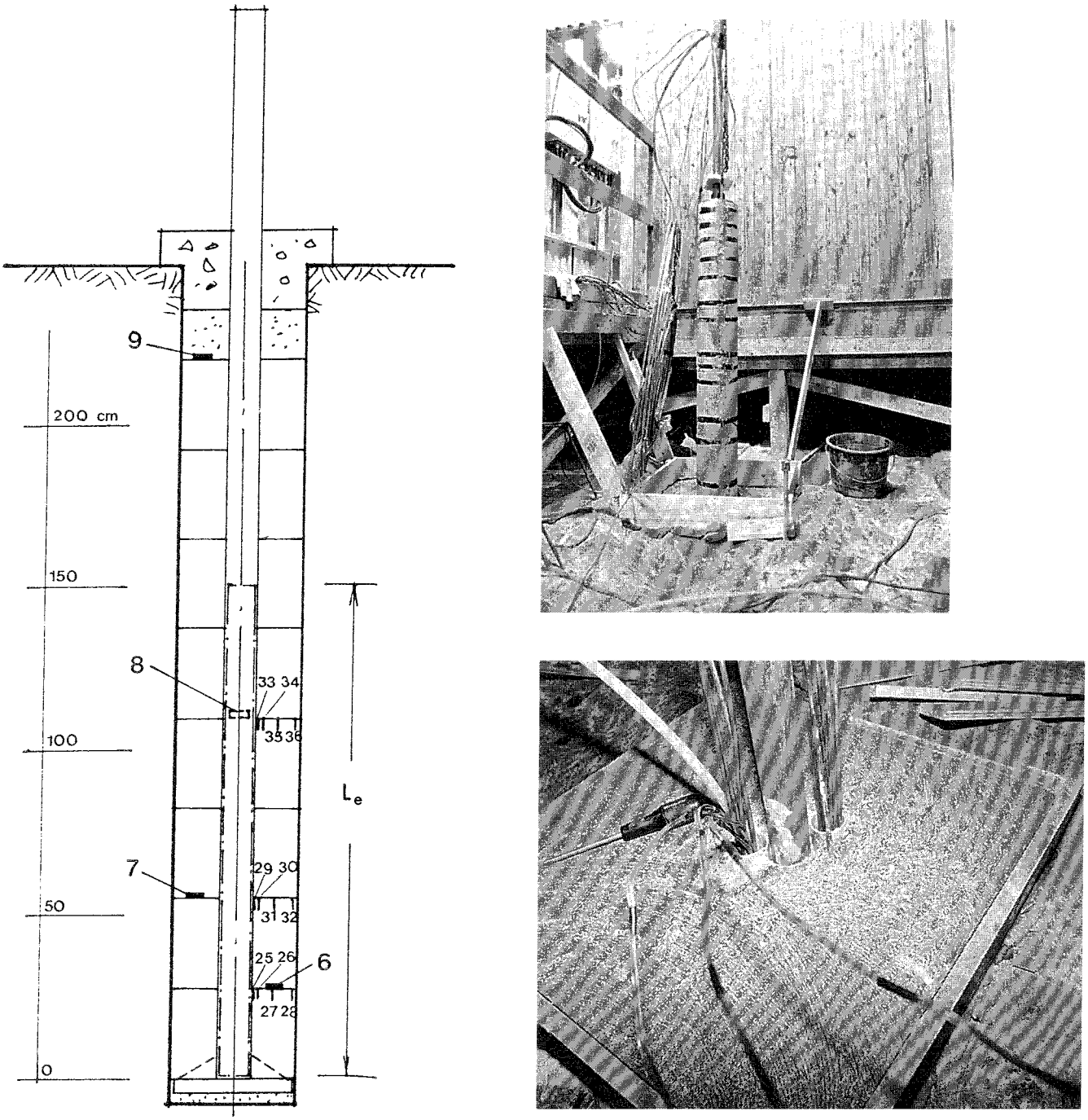

Figure 2-2 Test arrangement. Figures 25 to 36 denote thermocouples and 6-9 Gloetzl pressure cells. L_e is the effective part of the heater in the casing. The upper photo shows clay/heater unit ready for lowering after coating with clay paste. Lower photo shows epoxy grouting of lead-throughs of casing and cables in concrete lid

The ring-shaped clay blocks were produced in France by compressing air-dry clay powder to a dry density of 1.82 g/cm^3, a technique that was successfully introduced by the senior author in the preceding Buffer Mass Test (1). The degree of water saturation of the compacted clay, which was around 50 %, was expected first to drop close to the heaters and to increase at the rock contact, and then to increase throughout the clay as observed in this earlier project. Experience from earlier tests that the wetting rate depends on the piezometric pressure in the nearfield rock required information on this pressure.

The 275 mm high clay blocks, which had an outer diameter of 186 mm and an inner diameter of 52 mm, were fitted around a 51 mm steel casing, which contained a replaceable electric heater and served as "canister" material. The blocks were equipped with thermocouples and Gloetzl pressure cells for recording the swelling pressure at certain levels. The predicted dry density at complete expansion and homogenization in the lower and central parts of the hole was 1.53 g/cm^3, while it was expected to be somewhat lower in the uppermost part due to upward expansion in conjunction with compression of the upper 150 mm sandfill over which concrete had been cast.

2.2 TEST EQUIPMENT

2.2.1 Instrumentation

ISA T thermocouples (Pentronic) were used for temperatures recording, and F 5 QM 200 F VA pressure cells manufactured by the German company Gloetzl were used for recording total pressures. While the thermocouples operated very well throughout the entire experiment, the pressure cells, which were expected to sustain temperatures of at least 170°C for several years, failed with a few exceptions.

2.2.2 Data acquisition

Recording of temperatures was made automatically by use of the data acquisition system and measuring principles shown in Fig.2-3 and 2-4. Readings were made with a few hours intervals shortly after test start and with several days intervals late in the experiments. Swelling pressures and piezometric pressures were recorded manually with 1 week intervals.

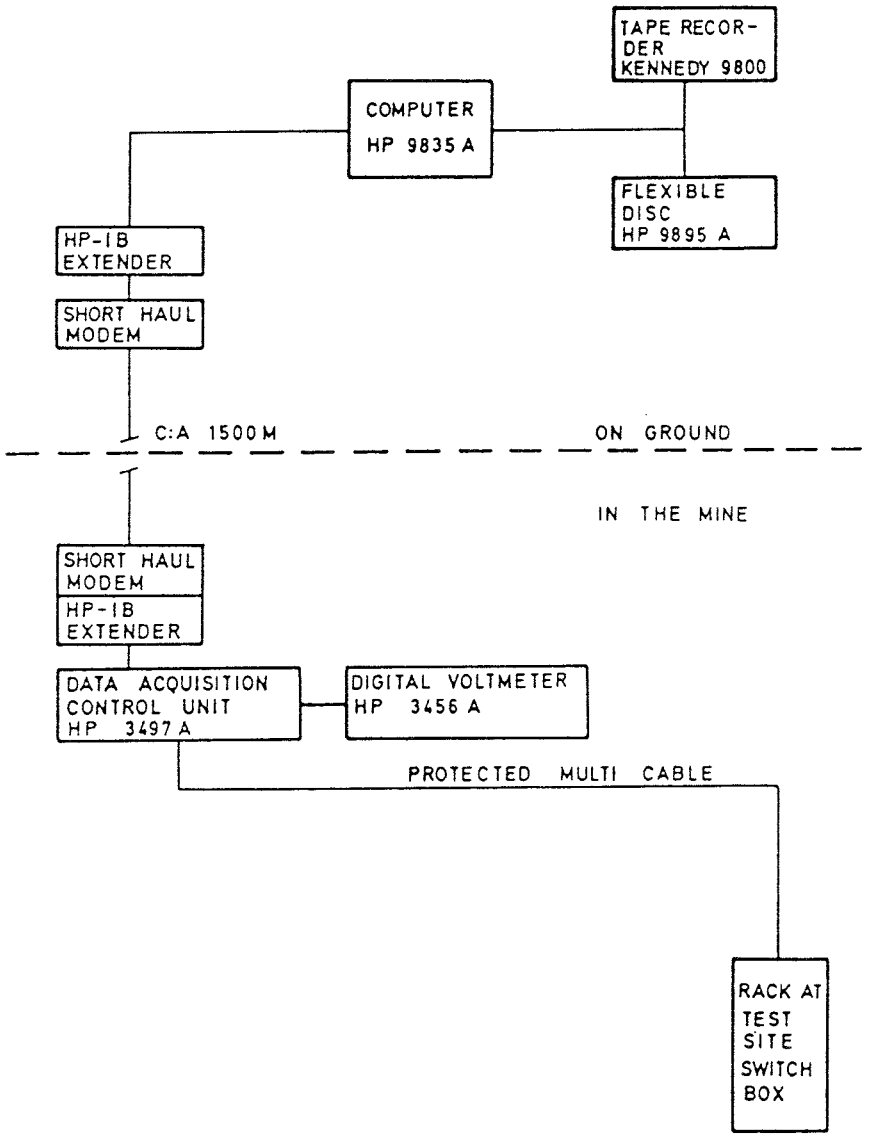

Figure 2-3 Layout of data acquisition system

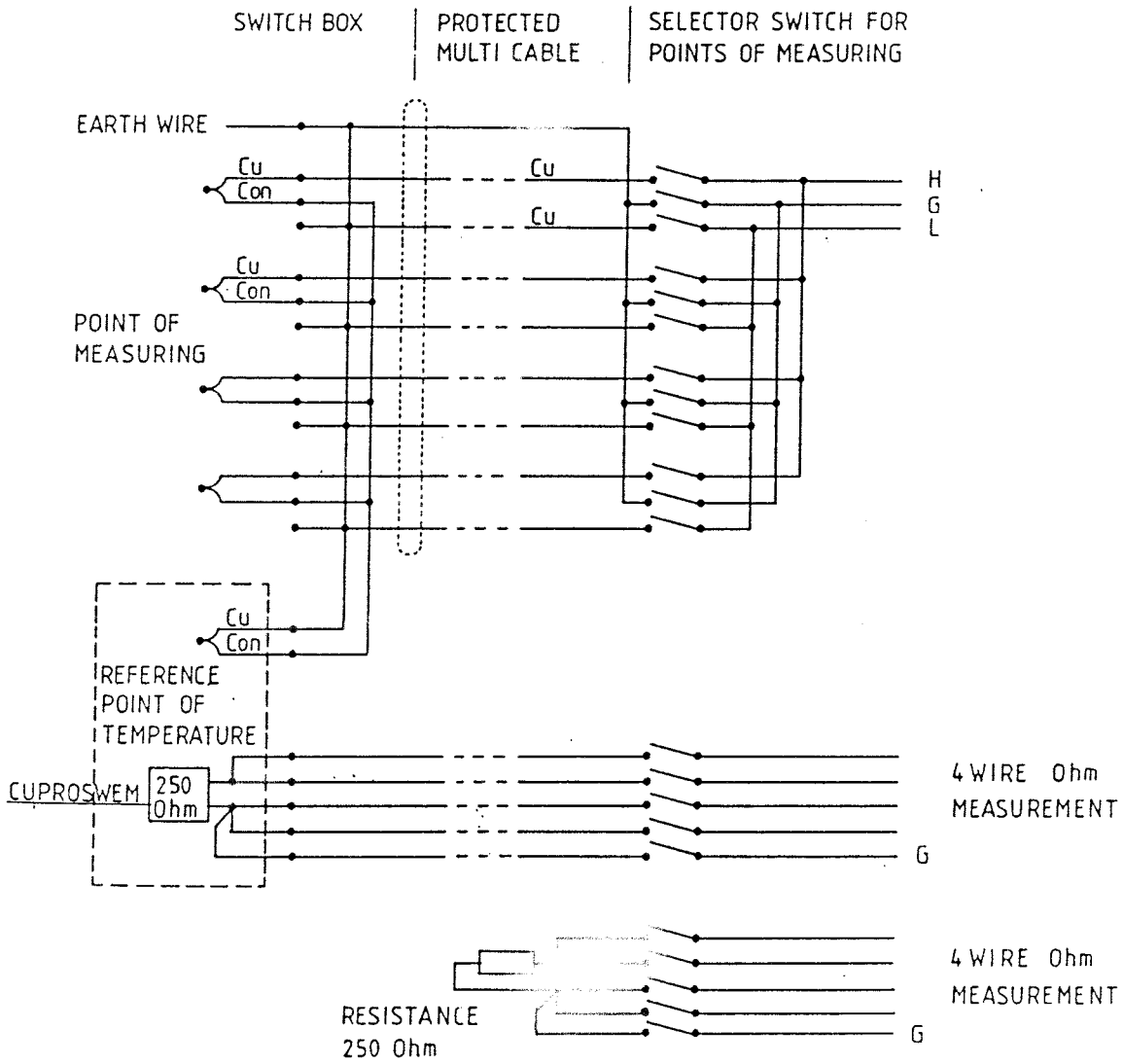

Figure 2-4 Measuring principle

2.2.3 Steel casings and heaters

2.2.3.1 Casings

The casings, which had outer and inner diameters of 51 and 35 mm, respectively, were prepared from ordinary steel with the following composition:

C	Si	Mn	P	S	Cr	Mo (%)
0.09	0.23	0.53	0.007	0.020	0	0

The casings were welded to permeable base plates on which the sets of clay blocks rested, the plates in turn resting on sand beds of about 100 mm thickness.

2.2.4 Heaters

The heaters were manufactured by the Swedish company Backer, Skåne. They were replaceable and had a built-in reserve capacity in the form of three elements of steel-encased, MgO-shielded heating wires designed so that the power interval was 0-2 kW (Fig.2-5).

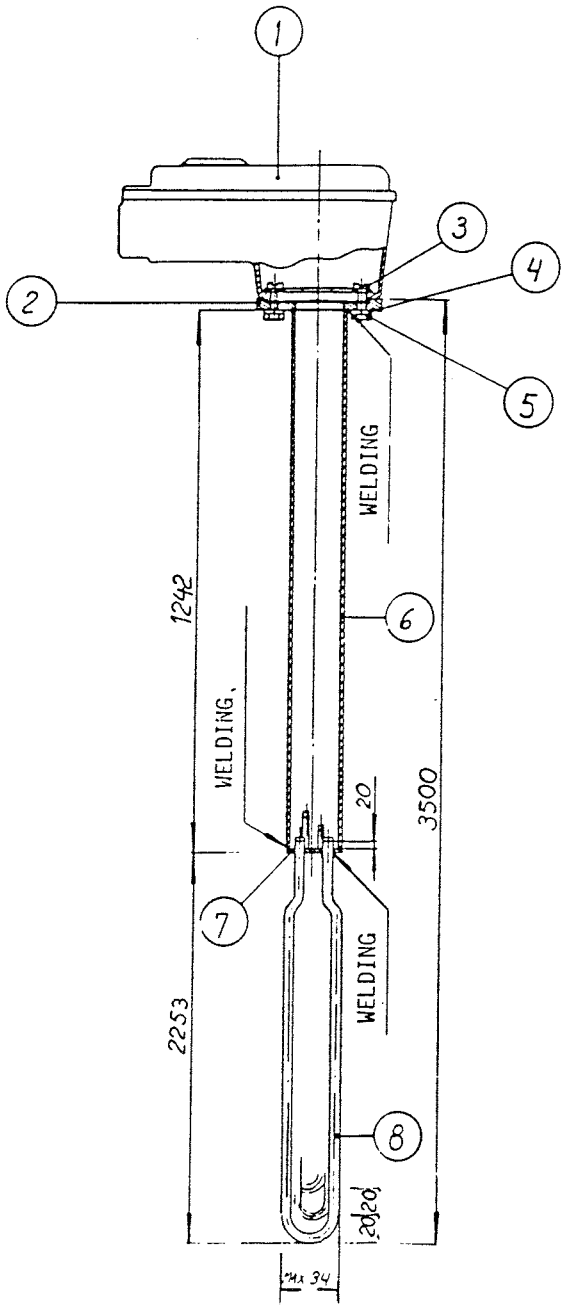

Figure 2-5 Heater design (Backer)

2.3 TEST SITE DATA

2.3.1 Groundwater composition

The groundwater at depth in Stripa is known to be of low salinity and water samples from the boreholes confirmed that. The major components were found to be the following:

Na^+	$= 4.13 \times 10^{-3}$ M	F^-	$= 0.13 \times 10^{-3}$ M
Ca^{2+}	$= 1.30 \times 10^{-3}$ M	Cl^-	$= 1.83 \times 10^{-3}$ M
Mg^{2+}	$= 0.14 \times 10^{-3}$ M	SO_4^{2-}	$= 0.55 \times 10^{-3}$ M
K^+	$= 0.10 \times 10^{-3}$ M		

HCO_3^- is probably the additional anion that is required for electroneutrality.

2.3.2 Rock structure

The location and orientation of open fractures in Holes I and II are given in Table 2-1 as evaluated from pilot holes, 147 and 56 mm in diameter. The small spacing of the fractures near the tunnel floor is due to neoformation of breaks by the blasting and to activation of previously sealed fractures by the excavation-induced stress release. Fig.2-6 shows the 200 mm drill core obtained by overcoring the 147 mm hole (Hole I). The presence of richly fractured rock at the base is obvious.

Table 2-1 Fractures in Holes I and II

Hole I		Hole II	
Dist. from floor, m	Orientation*	Dist. from floor, m	Orientation*
0.02	Incl.	0.07	Incl.
0.17	Incl.	0.13	Incl.
0.38	Flatlying	0.35	Incl.
0.47	Flatlying	0.48	Incl.
0.74	Flatlying	0.65	Incl.
1.00	Flatlying	0.83	Incl.
1.40	Flatlying	0.87	Incl.
1.50-2.40	Fracture zone	1.22	Incl.
		1.35	Incl.
		1.50	Incl.
		1.80	Flatlying
		1.97	Flatlying

* Dip in the range of 45-70°

At the end of the tests large samples of rock containing the clay-filled 200 mm holes were extracted by slot-drilling and this demonstrated that, except for the upper 1 m part of the holes, the rock contained only relatively few major, long-extending water-bearing fractures, which had a dip of around 70°. The general appearance of the rock structure was of the type indicated in Fig.2-7.

Upper end

0 1.0 m

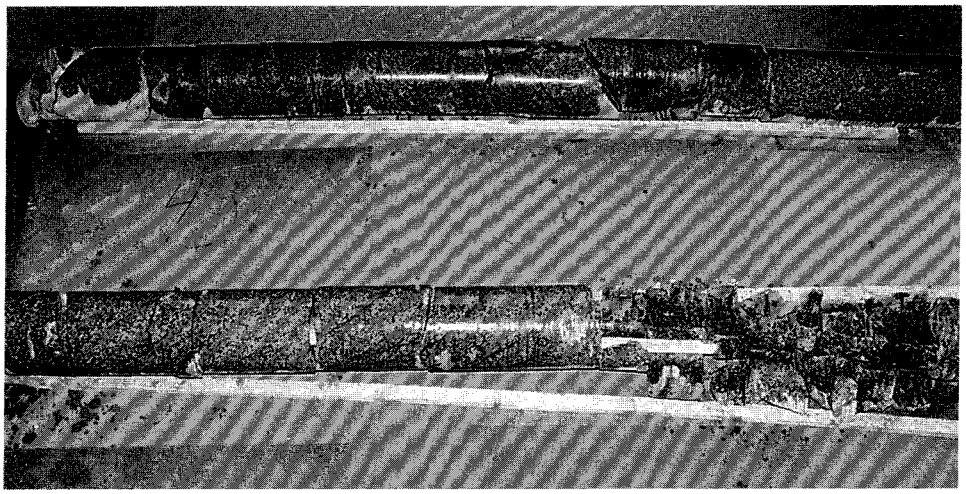

1.0 2.0 m

Figure 2-6 The hollow drill core from Hole I

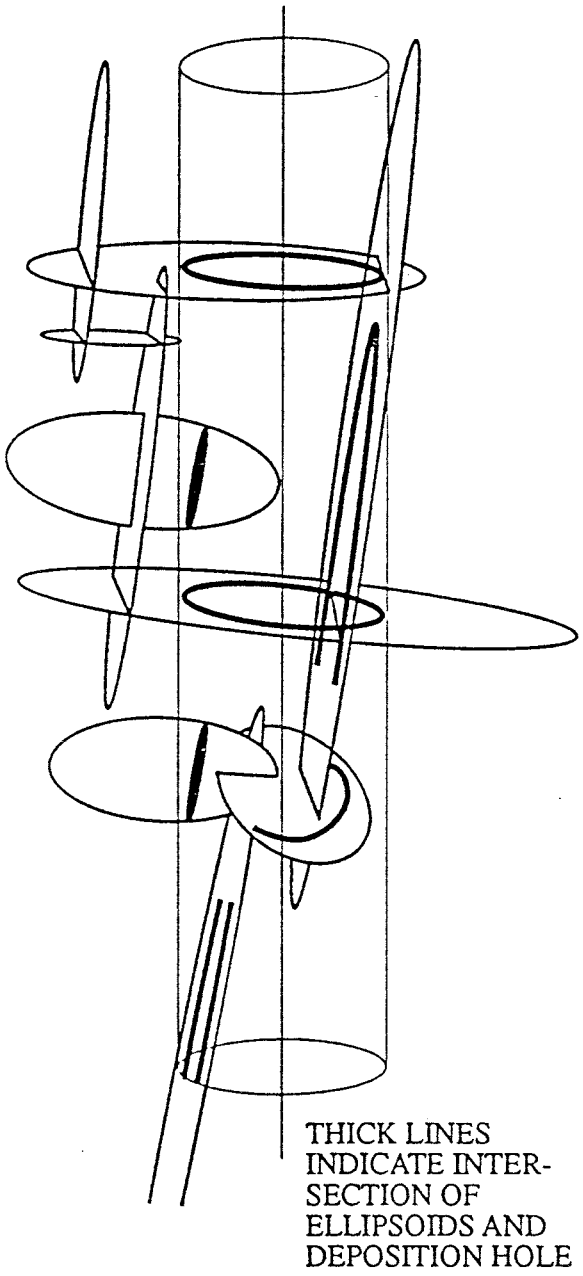

Figure 2-7 Schematic view of the general rock structure at the test site with typical orientation and spacing of fractures marked as ellipsoids

The bulk hydraulic conductivity of the rock was not determined but a number of investigations of tunnel floors at Stripa suggest that it was 10^{-8}-10^{-6} m/s in the upper meter, and 10^{-10} to 10^{-9} m/s deeper down (1).

2.3.3 Piezometric pressure

The general experience from tests at about 350 m depth at Stripa is that the water pressure stabilizes at about 1 MPa at about 3 m distance from the periphery of blasted tunnels at this depth. This was confirmed by recording the piezometric pressure at the base of the test holes, the measurements being made by use of filters connected to manometers at the tunnel floor. The expected and measured pressures were found to range between about 0.5 and 0.8 MPa at the bottom of the holes and it was assumed that the pressure at the clay/rock interface dropped linearly to zero at the tunnel floor. Hence, the water pressure at the uppermost part of the clay column was estimated to be about 0.2 MPa.

2.3.5 Temperature conditions

The temperature of the virgin rock at 350 m depth in the Stripa mine is in the interval 10-13°C as recorded in various tests (1). Heating experiments and ventilation have occasionally changed the rock temperature in many drifts, including the present one, to a few meters depth but the temperature has been brought back to ambient in a few months after termination of such tests by effective heat dissipation due to the high thermal conductivity of the rock (3.6 W/m,K) assisted by circulating groundwater. Hence the starting temperature in the test area was 10-13°C.

3 CLAY MATERIAL

The clay consists of alteration products of a Sparnacian marine limestone/flintstone sequence redeposited in shallow sea water. It originates from the western part of the Paris basin.

3.1 MINERALOGICAL AND CHEMICAL CHARACTERIZATION

3.1.1 Methods of analysis

XRD patterns were obtained using a Philips PW 1730 diffractometer (CoKα radiation) and entered into a microcomputer with DACO-MP (Socabim) system for analysis. A slow scanning speed (0.5 °2Θ/min) was applied for getting characteristic pattern profiles, using unoriented samples for the ensemble of mineral trains (5-80 °2Θ scan), and making separate runs with oriented air-dry and ethylene-glycol treated samples to identify clay minerals (2.5-16 °2Θ).

The estimation of the percentage of smectite in presumed mixed-layer minerals was made by comparing the data with the theoretical patterns calculated by use of the theoretical patterns calculated by use of Reynold's (2) NEWMOD program (Version 1, True Basic). The applied criteria were the positions of the (001) peaks and the value of the intensity ratios of the peaks at around 4 and 6 °2Θ of the patterns obtained from the oriented samples treated with ethylene glycol. This ratio is termed A/B in this report.

The swelling clay minerals (mixed-layer kaolinite/smectite termed K/S, and smectite termed S) contained in the samples after saturation with ethylene glycol are characterized by a (001) peak at around 17 Å that is difficult to discern clearly. The K/S (002) peak is at around 8.20 Å while that of smectite is at around 8.50 Å. For mixtures of these two minerals d(002) varies between these two values and for distinguishing between them an XRD pattern decomposition technique has been applied, namely the program DECOMPXR developed by Lanson et al (3,4,5). The major advantage of this program is that it was designed especially for handling the case of clay minerals which give X-ray peaks with large variations in width, i.e. from 0.1 °2Θ to several °2Θ. Its validity has been confirmed by studies carried out with mixed-layer illite/smectite (5,6).

The determination of the ratio of K/S and S was made by decomposing the (001) and (002) peaks. For the (002) peaks, the recording of the patterns in the appropriate angular field was carried out with a longer counting time (0.1 °2Θ/min). The data thus obtained were compared with those provided by the

simulation of patterns using the NEWMOD program.

Quantification of clay mineral contents of poly-mineral assemblages by XRD depends critically on several factors (7,8,9) and one requirement is to investigate artificially composed mixtures of pure constituents with defined mass proportions. Five mixtures of the clay used in Stripa (Fo-Ca 7) and the smectite that turned out to be formed in the experiment were prepared and analyzed.

The chemical composition of clay samples was determined by atomic absorption spectrometry after dissolving the samples (fusion and acid etching). The cation exchange capacity was measured by saturation with ammonium acetate (10).

Additional information was obtained by infrared spectroscopy using a Nicolet spectrometer and the KBr pellet method, and by Mössbauer spectroscopy (^{57}Co source) including decomposition for determination of the parameters of the characteristic doublets.

3.1.2 Mineralogical analysis

3.1.2.1 X-ray diffraction

X-ray diffraction has made it possible to make a detailed identification of the Fo-Ca 7 clay minerals. The complete results of this work were published by Proust et al. (11,12).

The minerals identified are:

* Random-ordered mixed-layer kaolinite/smectite (K/S)
* Kaolinite
* Quartz
* Hematite
* Gypsum
* Calcite

In the powder patterns, two (060) peaks at 1.490 and 1.494 Å characterize two dioctahedral phases, namely kaolinite and mixed-layer kaolinite/smectite. The absence of the (060) peak at about 1.53 Å shows that trioctahedral minerals are not present.

The patterns for the oriented sample of the <2 μm fraction of the Fo-Ca 7 clay were obtained using untreated material as well as magnesium- and potassium-saturated material, which allows identification of high- and low-charge smectite (13). For each treatment both air-dry samples and samples prepared

air-dry and then saturated with ethylene glycol were investigated.

The 7.19 Å peak is that of free kaolinite (Fig.3-1). The peak at 14.66 Å in the air-dry material shifted to 17.10 Å after saturation with ethylene glycol when also a new peak at 8.20 Å appeared. The latter value should be 8.50 at minimum if free smectite had been present and such minerals therefore appear to be present mainly in mixed-layer K/S.

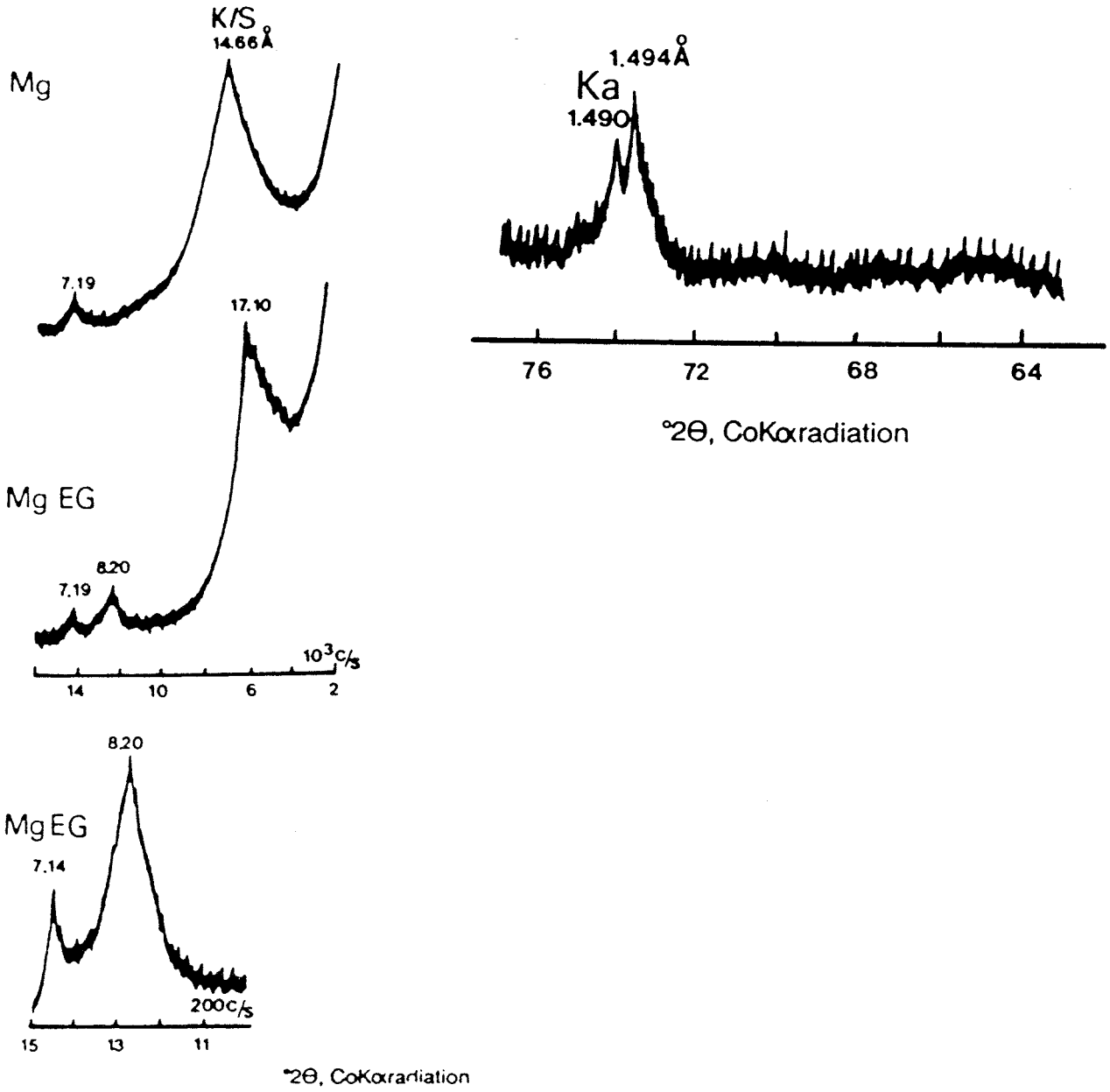

Figure 3-1 Left: X-ray powder diffraction patterns of the virgin Fo-Ca 7 material (oriented). Mg=magnesium-saturated; MgEG=magneisum-saturated and glycolated

Right: XRD pattern with K peaks. Virgin material, unoriented sample

It should be pointed out that the mixed-layer material cannot be of chlorite/smectite type since the (001) peak should then be 16.50 Å at maximum (2,14). The conclusion that it is at all of mixed-layer type is supported by the background level at around 4 °2Θ (15). Furthermore, the peak at 8.20 Å of the Fo-Ca 7 clay is a function of d/(001)$_{kaolinite}$/(002)$_{smectite}$/ which is fundamentally different from the pattern for a mechanical mixture of smectite and kaolinite. They would yield two distinct peaks; one at around 7.2 Å and the other at about 8.5 Å.

The simulations computed by use of the NEWMOD program showed that the best approximation is obtained for 50/50 random-ordered mixed-layer kaolinite/smectite with coherent stacks containing 10 layers.

The cationic saturation with Mg^{2+} and K^{+}, respectively, modified the patterns significantly as seen from Table 3-1. The position of the diagnostic peak illustrates the heterogeneity of the smectite layers, and it is concluded that of the total smectite content that makes up half the mineral mass, 30 % consists of low-charge layers and 70 % of high charge layers. Hence, these studies show that the Fo-Ca 7 clay consists of two phases: a random-ordered mixed-layer K/S swelling mineral (14) and free kaolinite.

Table 3-1 Estimation of the smectite content in virgin mixed-layer kaolinite/smectite using XRD data

Maximum expandability		Low-charge expandability		High-charge percentage: % HC. Sm.
d(001/002)	% Tot. Sm.	d(001/002)	% LC. Sm.	% Tot. Sm. – % LC. Sm.
8.20 Å	50%	7.75 Å	15%	35%

% Tot. Sm. = total percentage of smectite; % LC. Sm. = percentage of low-charge smectite; % HC. Sm. = percentage of high-charge smectite.

The relatively large amount of clay required for the Stripa field tests made it necessary to use a second batch of clay that turned out to have a slightly different composition, namely 90 % mixed-layer kaolinite/smectite, 5 % free kaolinite, and 5 % free smectite. The smectite turned out to be beidellite, i.e. the aluminum-bearing version.

3.1.2.2 Chemical analyses

The chemical analyses of the Fo-Ca 7 material are given in Table 3-2. They are provided as raw data and after correction by eliminating the contribution of other minerals than the clay minerals. Plotting of the corrected data in the $4Si\text{-}M^{+}\text{-}R^{2+}$ triangle of

Meunier and Velde (16) suggests that the composition of the smectite layers is intermediate to the two poles beidellite and montmorillonite (Fig.3-2). The cationic exchange capacity (CEC) of this material is 63.8 meq/100 g, which is lower than the value for pure smectites (17).

Table 3-2 Electron microprobe analyses (wt. %) of virgin material

Bulk chemical analyses												
												Mean
SiO_2	45.99	46.81	42.09	47.17	44.22	42.61	42.00	42.09	47.17	40.83	45.46	44.22
Al_2O_3	25.36	26.10	23.50	26.51	23.66	22.72	23.60	23.50	26.51	22.90	24.67	24.46
MnO	0.34	0.61	0.49	0.35	0.11	—	—	0.49	0.35	0.07	0.18	0.27
MgO	1.16	0.88	0.83	1.11	0.69	0.77	1.16	0.83	1.11	0.74	0.89	0.92
CaO	2.93	2.87	2.88	2.80	2.80	2.38	2.51	2.88	2.80	2.28	2.47	2.69
Na_2O	0.76	0.16	—	0.43	—	0.37	0.21	—	0.43	0.47	0.61	0.31
K_2O	0.40	0.44	0.70	0.14	—	0.40	0.27	0.70	0.14	0.06	0.07	0.30
TiO_2	2.20	1.75	2.79	2.90	1.32	1.40	1.59	1.49	1.66	1.27	1.54	1.81
Fe_2O_3	7.24	6.81	6.83	7.27	5.96	8.70	6.47	6.83	7.27	10.79	7.50	7.42
Chemical analyses corrected for quartz (6.7%), calcite (2%), goethite (% goet.), and hematite (% hem.)												
% Goet.	5.63	5.30	5.32	5.66	4.64	6.78	5.04	5.32	5.66	8.40	5.84	5.78
% Hem.	0.22	0.20	0.20	0.22	0.18	0.26	0.19	0.20	0.22	0.32	0.22	0.22
SiO_2	39.29	40.11	35.39	40.47	37.52	35.91	35.30	35.39	40.47	34.13	38.76	37.52
Al_2O_3	25.36	26.10	23.50	26.51	23.66	22.72	23.60	23.50	26.51	22.90	24.67	24.46
MnO	0.34	0.61	0.49	0.35	0.11	—	—	0.49	0.35	0.07	0.18	0.27
MgO	1.16	0.88	0.83	1.11	0.69	0.77	1.16	0.83	1.11	0.74	0.89	0.92
CaO	1.81	1.75	1.76	1.68	1.68	1.26	1.39	1.76	1.68	1.16	1.35	1.57
Na_2O	0.76	0.16	—	0.43	—	0.37	0.21	—	0.43	0.47	0.61	0.31
K_2O	0.40	0.44	0.70	0.14	—	0.40	0.27	0.70	0.14	0.06	0.07	0.30
TiO_2	2.20	1.75	2.79	2.90	1.32	1.40	1.59	1.49	1.66	1.27	1.54	1.81
Fe_2O_3	1.95	1.84	1.84	1.96	1.61	2.35	1.75	1.84	1.96	2.91	2.02	2.00

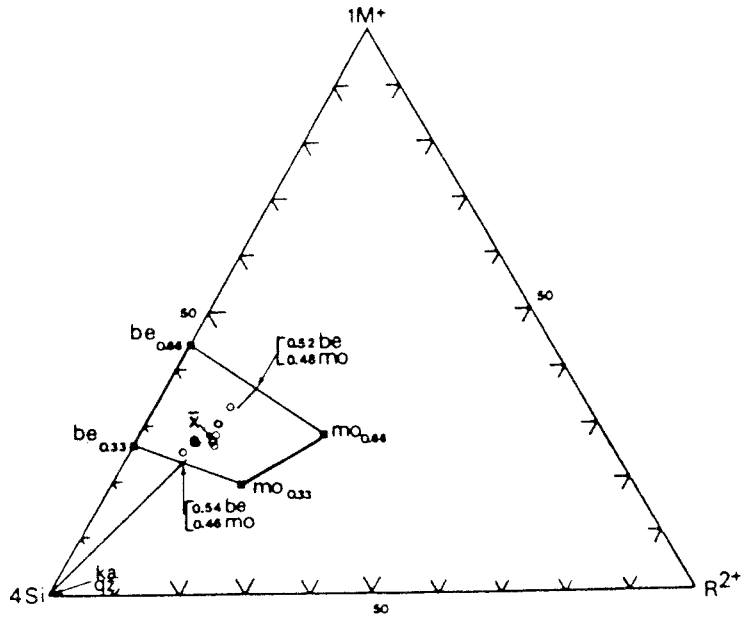

Figure 3-2 Plots of corrected microprobe analyses. be=beidellite, mo=montmorillonite, Ka=kaolinite, Qz=quartz. 0.52 be-0.48 mo=% of end members be and mo in the smectite component of the K/S. X=mean value

3.2 PHYSICAL PROPERTIES OF THE CLAY

The physical testing was made by use of samples that were compacted in air-dry powder form and then water saturated under confined conditions. 47 % of the powder passed the 63 μm sieve, 72 % the 250 μm sieve, and 87 % the 1000 μm sieve. The microstructure evolved by the applied preparation technique is characterized by a finely granular fabric with soft clay gel filling up the voids between granules (18).

The physical properties of the clay have been determined by laboratory experiments in Sweden and France. Table 3-3 gives swelling pressure, hydraulic and thermal conductivity data. Triaxial and direct shear tests of clay saturated with distilled water gave cohesion figures of around c'=50 kPa and ϕ=5° for normal pressures exceeding 200 kPa.

Table 3-3 Swelling pressure (p_s), hydraulic conductivity (k), and thermal conductivity (λ)

Dry density g/cm^3	p_s MPa	k m/s	λ W/m,K
1.40	0.9	$3x10^{-13}$	-
1.50	2.0	10^{-13}	1.6
1.60	4.5	$8x10^{-14}$	1.6
1.70	8.0	$5x10^{-14}$	-

The creep behavior, which is indicative of whether cementation has taken place or not, was investigated by use of shear tests with special respect to the shear stress distribution in the samples (19). The parameters A,B and t_o, evaluated from the initial part of plottings of strain and strain rate versus time, are measures of the shear strength and cementation effects (cf. Fig.3-3). They are evaluated from the curves that are adjusted to comply with the general creep equation:

$$\gamma = B \ln(t + t_o) + A \qquad (1)$$

where
- γ = angular strain
- A = constant; normally $-50x10^{-4}$ to $50x10^{-4}$
- B = constant, measure of shear strength. B usually ranges between 10^{-5} (stiff) to 10^{-2} (soft). The value increases with stress
- t_o= constant; negative values and values lower than 1000 indicate cementation

The creep tests of the presently investigated clay with the dry density 1.50 g/cm^3 gave A=$-12x10^{-4}$, B=$2x10^{-4}$, and t_o= 2800 s.

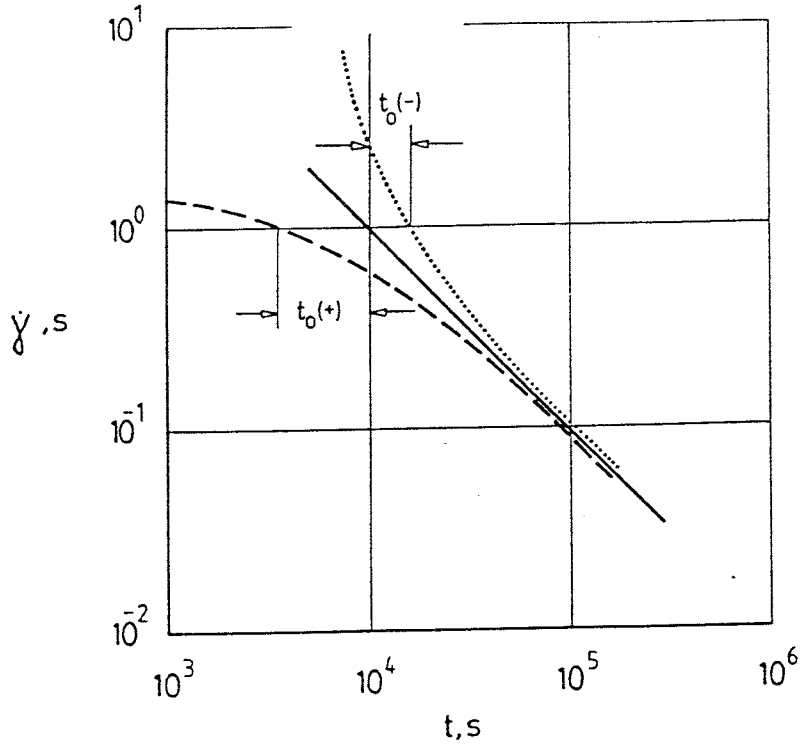

Figure 3-3 Creep curves plotted for evaluation of t_o. The full line corresponds to $t_o=0$. Broken line represents positive t_o:s, while t_o is negative for the dotted one

4 PREDICTIONS

4.1 GENERAL

Earlier field and laboratory tests as well as theoretical models derived for mineralogical changes formed the basis of the predictions, which concerned the latter type of changes as well as the evolution of temperature and swelling properties of the clay.

4.2 MINERALOGY

4.2.1 Experience from the Stripa BMT

At the time when the tests were planned, the data from the Buffer Mass Test were practically the only long-term hydrothermal test results that were available and they concerned MX-80 (Wyoming Bentonite clay) that had been heated to about 90°C for 2 years and up to 127°C for the subsequent third year (20). The chemical and mineralogical analyses from this experiment did not show changes in any respect, thus demonstrating that heating under the applied repository-like conditions for about 3 years does not yield any measurable change in smectite content or in physical properties (21).

4.2.2 Expectations

At the planning stage of the present experiment the idea of smectite conversion layer-by-layer to yield mixed layer minerals and ultimately hydrous mica was accepted by most investigators. Hence, two general types of reactions could be foreseen:

$$\text{Smectite} + \text{Al} + K^{+} \text{ ----> Hydrous mica} + Si^{4+}$$

$$\text{Smectite} + K^{+} \text{ ----> Hydrous mica} + Si^{4+}$$

The very low concentration of potassium in the Stripa groundwater suggested, in agreement with the finding from the BMT study, that only insignificant transformation to nonexpandable clay minerals would take place in a 4 year long field test, while the release and precipitation of silica might be significant and result in some cementation and loss in swelling power of the clay.

4.3 PHYSICAL PROCESSES

4.3.1 General

Predictions were made with respect to temperature evolution, swelling pressures and piezometric pressures. Also, the rate of water saturation, applying the model derived by Börgesson (20), was estimated and predicted to yield 90 % degree saturation after slightly more than 6 months for the laboratory-determined diffusion coefficient $2.3 \times 10^{-10} m^2/s$. This model, which is valid for water uptake under isothermal conditions, turns out to apply also when thermal gradients of up to $2^{\circ}C/cm$ prevail as demonstrated by the BMT test. It was assumed, however, that the higher gradient in the present test might imply a different rate and character of moistening.

4.3.2 Temperature

Using the laboratory-derived figures for the heat conductivity and specific heat of the unsaturated clay material, i.e. 1.6 W/m,K and 1200 Ws/kg,K, respectively, and the corresponding figures for the rock (3.60 W/m,K and 800 Ws/kg,K), the temperature rise was predicted by applying FEM analysis. The calculations showed that the power should be about 1 kW in the initial phase in order to arrive at the desired temperature of the clay/heater interface of about 170° over part of the column. Fig.4-1 shows the predicted temperature incease at midpoint heater at a constant heat conductivity of 1.6 W/m,K and 1 kW power. With an ambient rock temperature of $10\text{-}13^{\circ}C$ the maximum temperature would be around 175° after about 2 months. Since the heat conductivity was expected to change due to moisture redistribution and subsequent wetting of the clay, the heater power had to be variable. However, later in the test it was decided to keep the power constant in order to make it possible to record changes in the thermal field that could be caused by mineral alterations or unexpected behavior of any sort.

Calculations of the temperature evolution was made by applying different sets of thermal data, i.e. 2.6 W/m,K for the rock and 1.4 and 1.6 W/m,K for different parts of the clay, but the deviation from the curve in Fig.4-1 were insignificant.

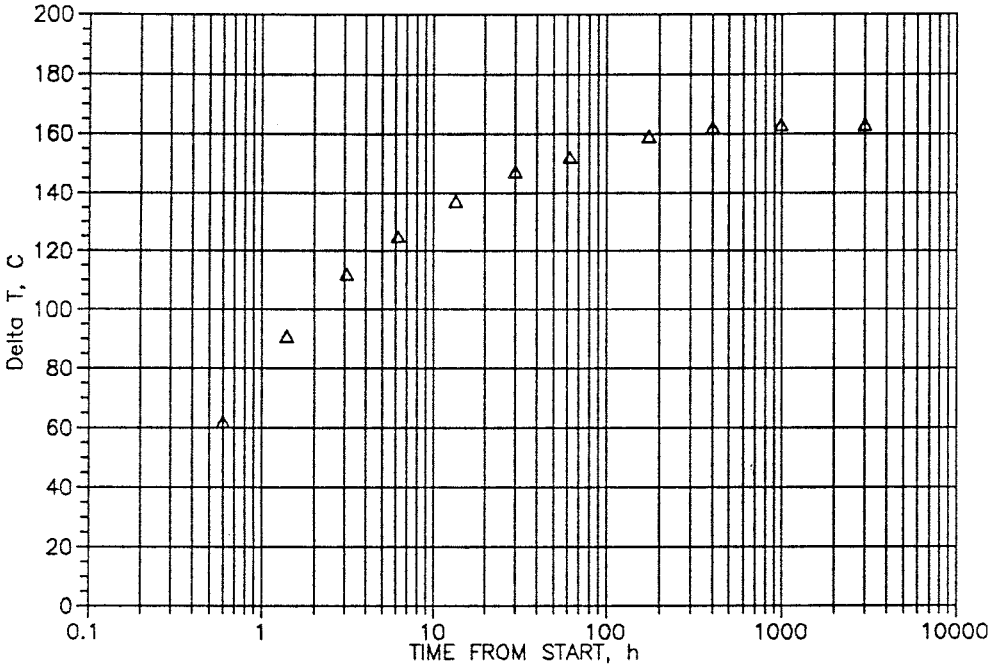

Figure 4-1 Predicted temperature development at the clay/heater interface

4.3.3 Swelling pressure

The laboratory data obtained from room temperature tests suggested that, neglecting the possible influence of heating, the swelling pressure in the larger part of the clay columns would become around 2 MPa in the lower and central parts if a very high degree of water saturation could be achieved. A pressure of around 1.5 MPa was expected at the clay/sand interface in the upper part of the hole because of the expansion of the clay associated by axial compression of the overlying sand layer.

Considering the influence of heat, no laboratory tests have been made at higher temperatures but ex-

periments with clays rich in Ca-smectite show that the swelling pressure drops by around 25 % at 130°C, which suggests that the swelling pressure of smectitic clay with a dry density of 1.53 g/cm^3 would be around 1.4-1.6 MPa at a high degree of saturation (22). Hence, in the lower part where pressure cells 6,7 and 8 were located (Fig.2-2), the swelling pressure would theoretically be in the interval 1.2-1.5 after about 6 months.

4.3.4 Piezometric pressures

The general experience from tests at about 350 m depth at Stripa is that the water pressure stabilizes at about 1 MPa at about 3 m distance from the periphery of blasted tunnels at this depth. This was confirmed by recording the piezometric pressure at the base of the test holes, the measurements being made by use of filters connected to manometers at the tunnel floor. The expected and measured pressures were found to range between about 0.5 and 0.8 MPa at the bottom of the holes and it was assumed that the pressure at the clay/rock interface dropped linearly to zero at the tunnel floor. Hence, the water pressure at the uppermost part of the clay column was estimated to be about 0.2 MPa.

The total pressure, recorded by the Gloetzl cells in the lowest part of the hole (No 6), was hence expected to be on the order of 1.8-2.0 MPa after about 6 months.

5 TEST RESULTS

5.1 FIELD OBSERVATIONS

5.1.1 Temperature

5.1.1.1 Hole I

Temperature recording in Hole I gave data in reasonable agreement with the predictions for the first week (cf. Fig.5-1) but strong variations then took place that were found to be caused by water leakage into the casing. After plugging the casing with a block of highly compacted bentonite the temperature development returned to normal and then proceeded in the way shown in Fig.5-2. In the hottest zone, termed "A" in this figure, the temperature successively dropped from around 185°C to somewhat less than 170°C, indicating that the heat conductivity increased.

A check was made of the heat conductivity in the early phase when the temperature had stabilized at about 186° in the hottest zone, using the expression in Eq.(2), which yielded λ=1.6 W/m,K. This value, which is equal to the laboratory-derived one, was increased to around 1.8 W/m,K which indicates considerable but not complete water saturation. In fact, a zone of a few millimeters thickness with the original water content preserved would account for the deviation from the value 2 W/m,K that is estimated to represent fully water saturated clay of the present type and density.

$$q = 2\pi\lambda k^{-1}(T_{inner} - T_{outer}) / \ln(r_{outer}/r_{inner}) \qquad (2)$$

where
- q = power transferred per meter length
- k = shape factor (0.9)
- λ = heat conductivity
- T = temperature
- r = radius

5.1.1.2 Hole II

After a very short initial period of low power for checking instrumentation and tightness, the power was set at 1000 W for about 2 months, and then at 900 W for about 4 months, while it was again raised to 1000 W and kept constant at that level for the remaining 38 months. The temperature development at the clay/-casing interface and the clay/rock contact is given

in Fig.5-3, temperatures being recorded also at two intermediate distances between these two boundaries.

The diagram shows two important features for the hottest zone, namely that the temperature first dropped from around 182°C to 173°C as in Hole I, but then increased to 183°C in a jerky fashion, indicating intermittent changes in heat transfer from the hot casing. The initial trend of dropping temperature was interpreted as an increased heat conductivity caused by water uptake and improved heat transfer capacity due to establishment of a firm clay/steel contact by swelling of the clay, while the subsequent rise is ascribed to gas formation, yielding a drop in heat conductivity. Weekly, irregular changes in temperature at the perfectly stable power, were most probably caused by production of water vapor or hydrogen gas, yielding "peristaltic" effects.

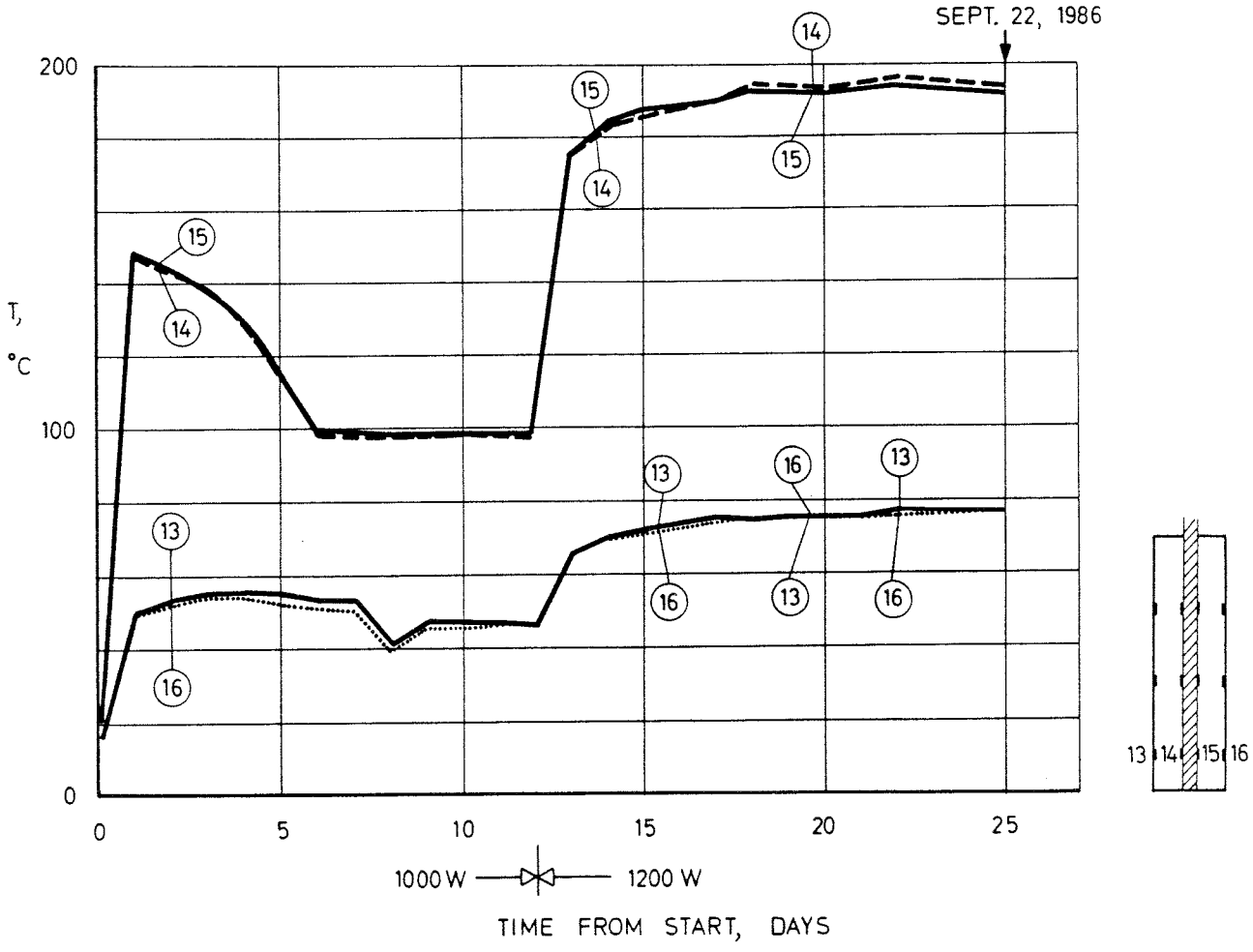

Figure 5-1 Temperature evolution in the lower part of Hole I early in the test

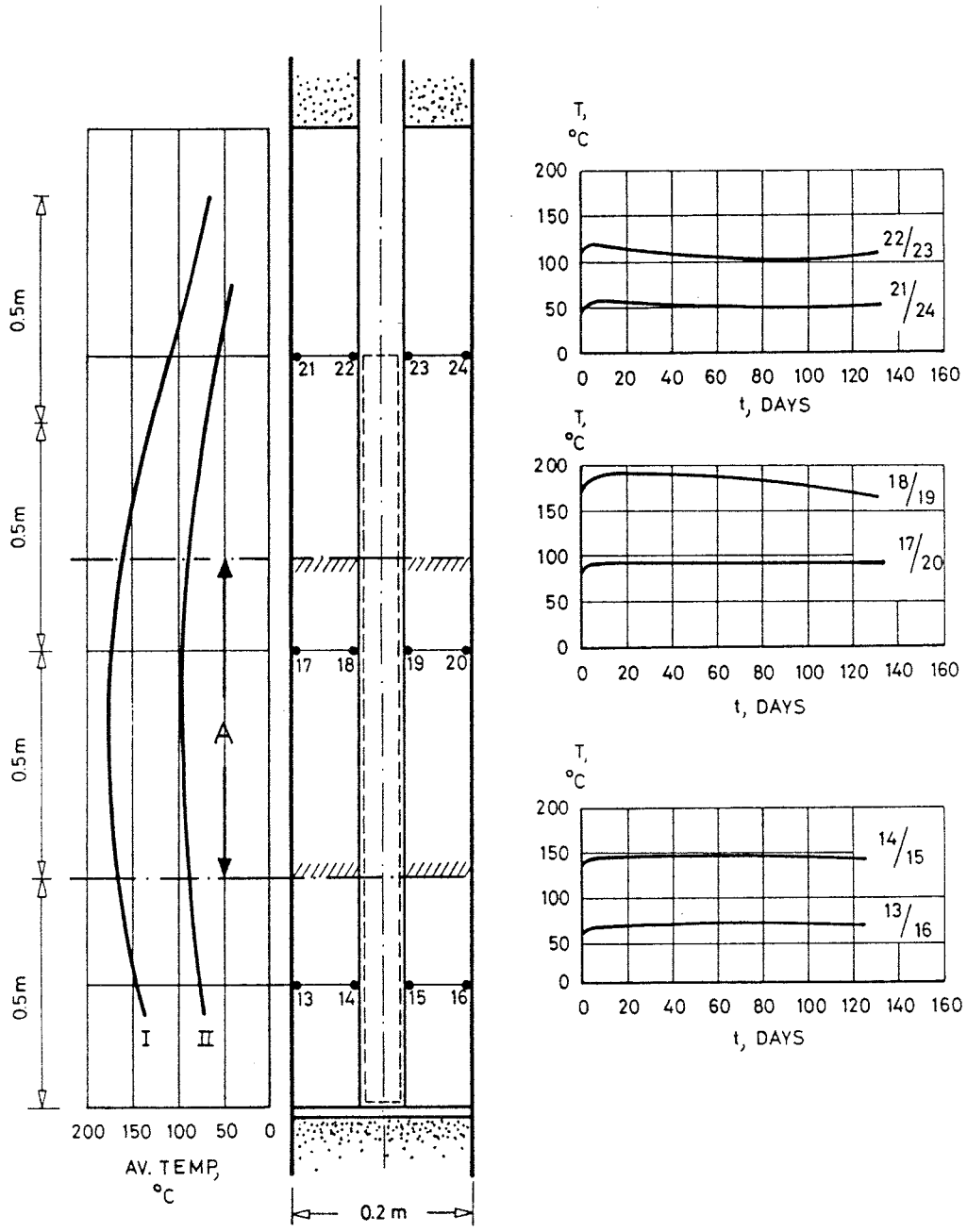

Figure 5-2 Temperature evolution after the intial period, the power being changed from 1200 to 1000 W after about 2 months

Applying the same way of deriving heat conductivities as for Hole I, one finds that the average heat conductivity of the clay in Hole II was initially around 1.6 W/m,K and that it dropped to between 1.5 W/m,K and 1.6 W/m,K after about 32 months. The temperature drop at the very end of the test was due to power failures.

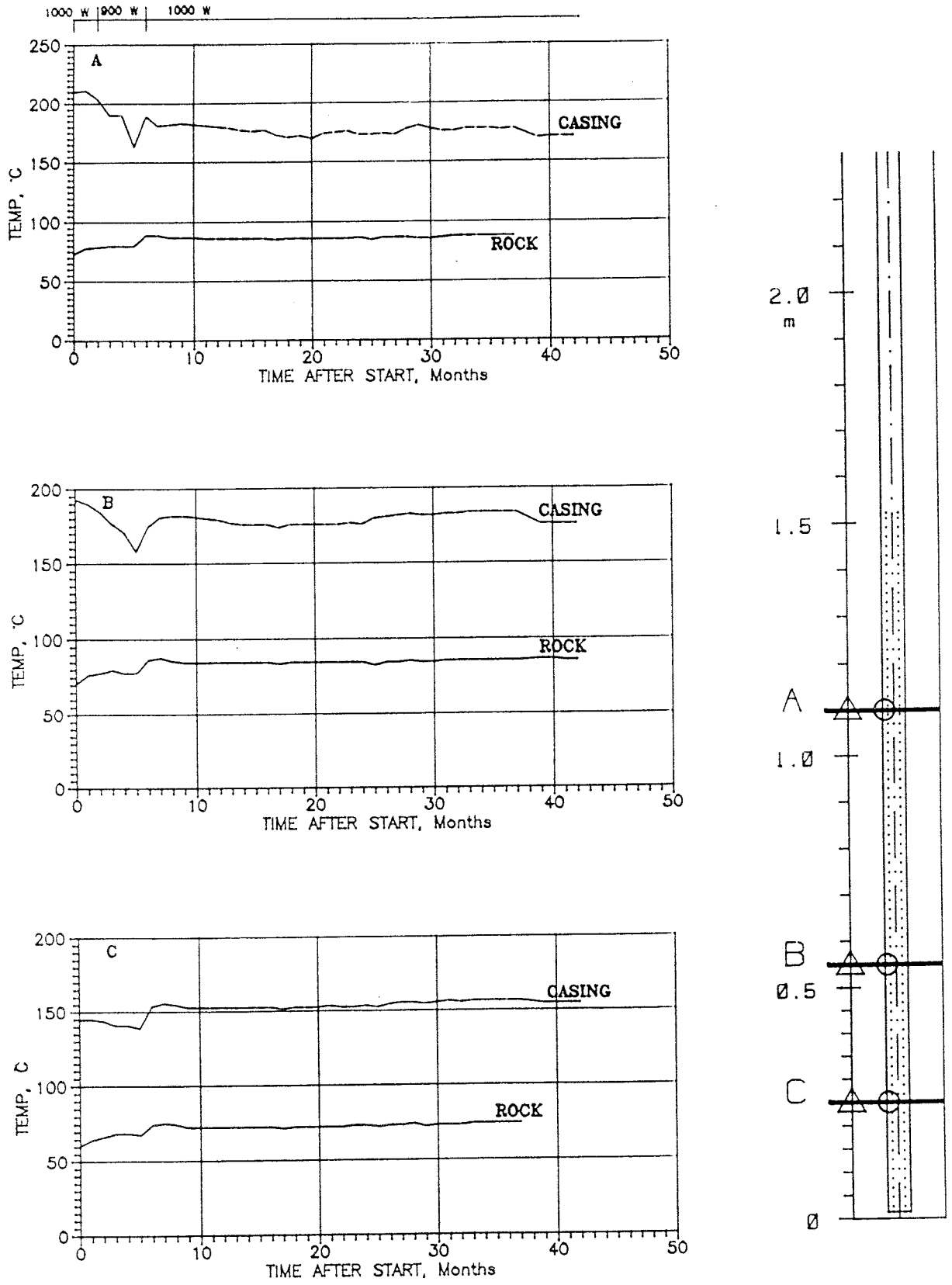

Figure 5-3 Temperature evolution in Hole II

5.1.2 Swelling pressure

5.1.2.1 Hole I

The total pressure (p) at the instrumented levels varied strongly in the initial phase due to relative clay block movements, but a clear pattern could be seen after opening the valve to the drainage pipe from the filter at the base of the hole 9 days after test start (Fig.5-4). It had to be opened in conjunction with sealing the casing with bentonite, and recording under drained conditions showed that the swelling pressure at cell 3 had reached about 1.2 MPa after 3 weeks, while it had become 0.7 MPa at the upper clay/sand contact (Cell 4). Cells 1 and 2 had ceased functioning after two weeks.

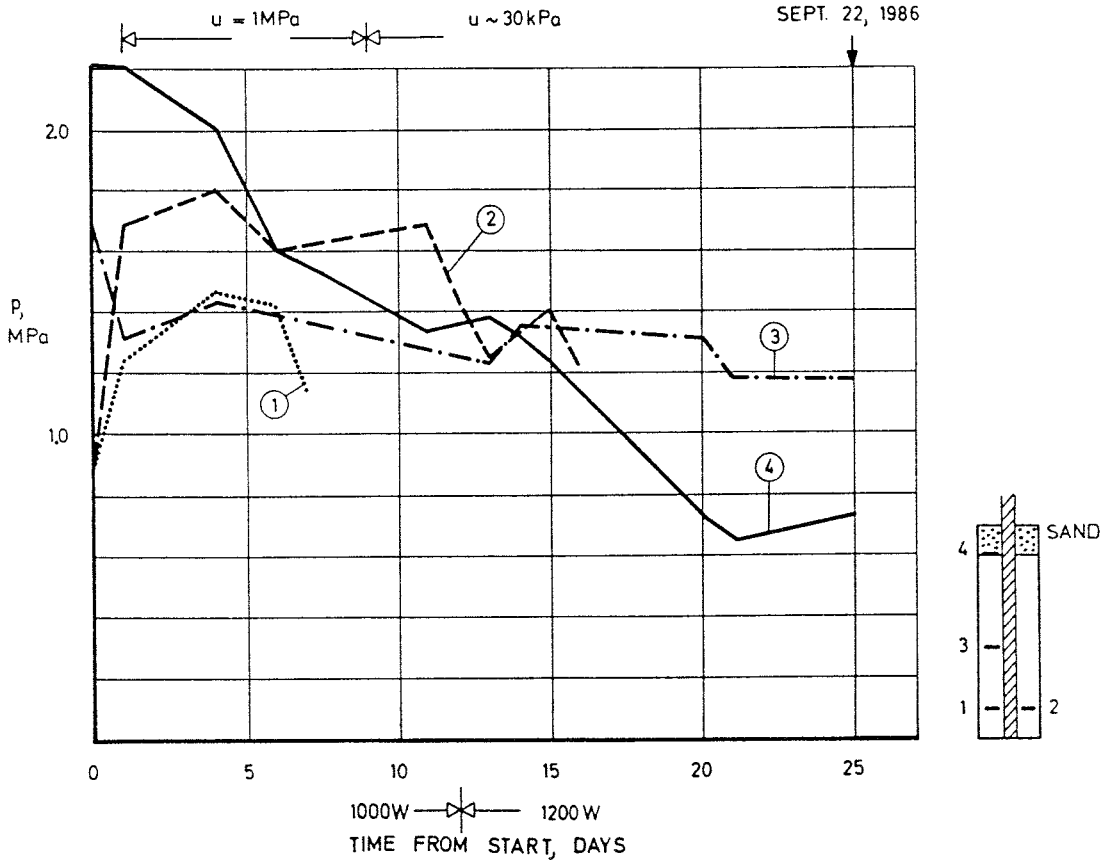

Figure 5-4 Total pressures in Hole I

Cell 3 failed after one month and the remaining Cell 4, at the top, gave a swelling pressure that increased to 0.8 MPa after 3 months and to 1.1 MPa at the end of the test, i.e. after about 8 months. This figure suggests that although the degree of water saturation had not become complete, it had still become as high as about 85 % as concluded from the fact that the expected final value after expansion to an equilibrium state with complete homogenization was 1.3 MPa.

5.1.2.2 Hole II

The total pressure increased steadily to about 1.6 MPa in the first 48 days in the lower part of the hole, after which the cells 6 and 7 (cf. Fig.2-2) broke down. Since the piezometer pressure was around 0.5 MPa at this stage, the swelling pressure in that part of the hole was around 1.1 MPa, or about the same as in Hole I. In the upper part of the hot zone (Cell 8), the swelling pressure rose to 1.4 MPa after 6 months and the cell then ceased to work. Cell 9 at the sand/bentonite contact high up in the hole gave a swelling pressure of 0.8 MPa after 0.5 years and 1.0 MPa after 1 year, and the ultimate pressure became 1.3 MPa after 1.5 years. Fig.5-5 shows the evaluated swelling pressures in the first 50 days, the irregularities being due to slight, relative block movements in conjunction with the expansion due to water uptake.

These observations indicate that the water uptake, expansion and homogenization of the clay were largely completed in about 8 months in the lower part, while it took a longer time in the uppermost part of the column due to slow upward expansion of the clay associated with compression of the upper sandfill. All these findings are in complete agreement with the actually observed maturation of the clay at excavation half a year after start of the experiment in Hole I.

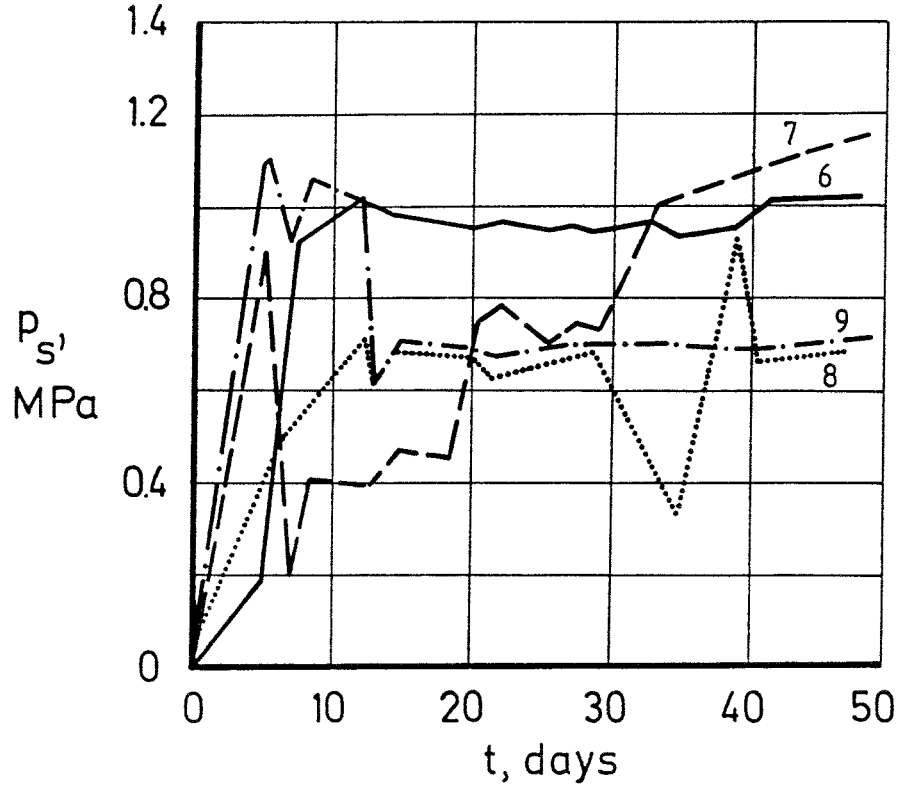

Figure 5-5 Evaluated swelling pressures in the first phase of the test in Hole II

5.1.3 Piezometric pressures

The water pressure was recorded at the base of the two holes, i.e. at slightly less than 3 m depth, and it was found to be approximately in the predicted range, i.e. between 0.5 MPa and 0.9 MPa, the lower pressure prevailing in the first few months before pressure equilibrium occurred. In the later phase the average pressure was about 0.75 MPa.

5.1.4 Extraction of clay from the rock

The power was turned off less than 1 day before the extraction of the clay by which the temperature dropped sufficiently much to avoid evaporation and drying in the sampling stage, but not more than would be required to retain the moisture distribution.

For Hole I, the plan was to extract the clay by coring such that a coherent, undisturbed clay body with about 19 cm diameter could be obtained. This operation was successful down to about 1.5 m depth but further coring was considered to be too slow to bring the clay up with preserved water content distribution. Since the theoretically required pulling force in order to overcome the wall friction was less than 3 tons, i.e. the maximum load that could be applied, an attempt was made to pull out the entire clay body and this turned out to be successful.

For Hole II it was required to apply overcoring technique in order to bring up the clay body as well as a confining monolithic rock body with about 0.5 m diameter. This was made by using slot-drilling with 56 mm core drilling to 4 m depth and by breaking the rock column at the base by use of "silent dynamite" (Demex). The rock column, which was assumed to be easily broken up along some major fractures as predicted by the scetch in Fig.5-6, had approximately the shape of Greek or Roman temple columns, the detachment being illustrated by the photographs in Figs.5-7 and 5-8. Like in Hole I, samples were taken for immediate determination of the water content in the underground laboratory at Stripa, as well as for subsequent testing in Clay Technology's and CEA's laboratories.

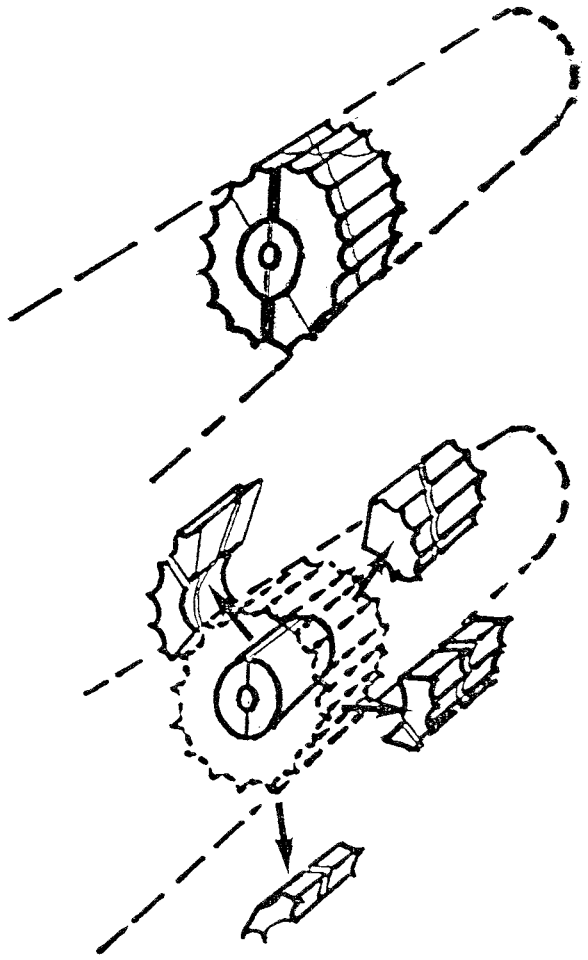

Figure 5-6 Expected appearance of extracted core and detachment procedure

5.2 PHYSICAL CONSTITUTION AND PROPERTIES

5.2.1 Water content distribution

5.2.1.1 Hole I

The water content distribution of the clay in Hole I is shown in Fig.5-9, from which one finds that the large majority of the clay was completely water saturated. Close to the casing in part of the hottest zone, i.e. within less than 1 cm from its surface, the degree of saturation was around 60 %, and between this zone and the fully saturated surrounding clay there was an intermediate zone with an average degree of water saturation of 85 %.

Figure 5-7 Upper: Sectioned core from Hole II. The lower half shows black precipitations on the clay in the hottest, right part. Lower: Splitting of rock column

Figure 5-8 Upper: Appearance of clay core. The clay, which exhibited a slightly brittle character, was in tight contact with the rock. Lower: Sampling parallel to splitting of rock column

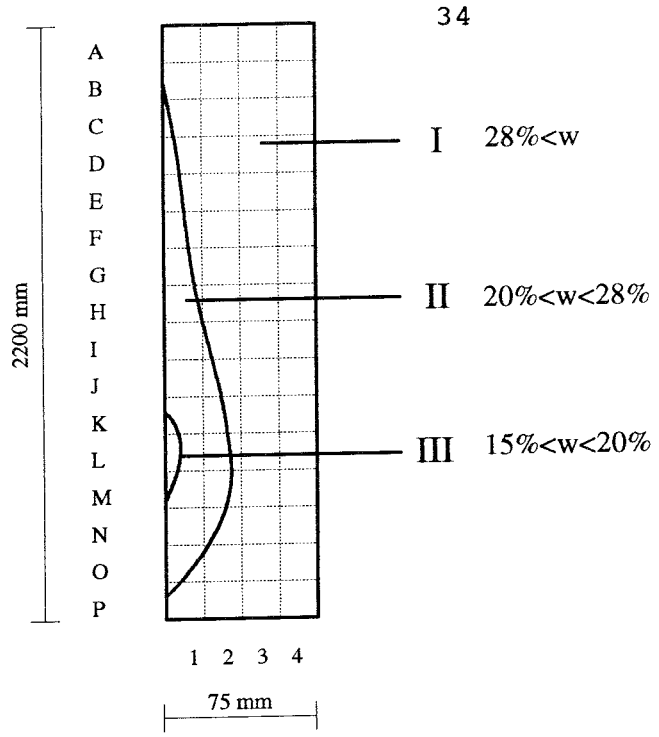

Figure 5-9 Zones of different degrees of water saturation in Hole I (Left vertical boundary of the diagram represents the clay/casing interface). The fully saturated zone I had a water content of at least 28 %. Zone II had a water content of 20-28 %, while it was 15-20 % in zone III

The high degree of water saturation of the clay in Hole I is in good agreement with the measured swelling pressures and recorded temperature in the clay column.

5.2.2.2 **Hole II**

The water content distribution of the clay in Hole II is given by Fig.5-10, from which it is seen that significant drying had taken place. The outermost zone I represents about 100 % water saturation, while zone II had about 85 % degree of water saturation and zone III about 60 %. In contrast to the conditions in Hole I there was also an inner zone IV with an average degree of water saturation of 35 %, i.e. considerably lower than in Hole I. The temperature evolution is an evidence of that drying succeeded wetting in Hole II.

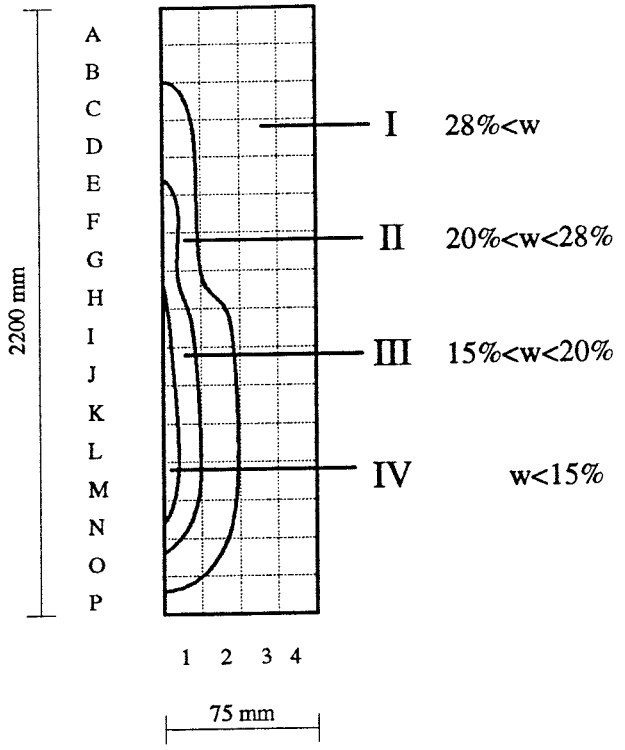

Figure 5-10 Zones of different degrees of water saturation in Hole II. The fully saturated zone I had a water content of at least 28 %. In zone IV, not present in Hole I, the water content was appreciably less than 15 % and the average degree of water saturation of 35 %

It is concluded from the measurements that while the clay was largely water saturated in Hole I, that was opened for about 8 months, considerable drying had taken place in the almost 4 year long test in Hole II. The drying implies that water was expelled from the hottest part of the clay core by gas with a pressure that must have been high enough to overcome the capillary pressure.

5.2.2 Physical properties

5.2.2.1 Hole I

The clay appeared slightly drier close to the hot casing but was otherwise homogeneous and undisturbed samples could be extracted without difficulty for determination of the rheological properties, as well as for the microstructural and mineralogical examinations (Table 5-1). The latter served as a general checking of whether major changes had taken place or not, leaving more detailed analyses for Hole II.

Table 5-1 Location of samples and specification of tests

Sample No	Location	Temperature	Test*
A1	Top of clay core clay/steel interface	60°C	EM, XRD
A4	Top of clay core clay/rock interface	40°C	C, EM, XRD
E1	Mid-height heater clay/steel interface	170°C	C, EM, XRD
E4	Mid-height heater clay/rock interface	90°C	EM, XRD

* C = Creep tests, EM = Electron microscopy, XRD = X-ray diffractometry

Creep properties

20 mm shear box-samples were prepared and left to homogenize for 1-3 weeks under drained conditions (distilled water), carefully adjusting the normal pressure to compensate for swelling or compression. The equilibrium pressure turned out to be 1.6 MPa for both the 40°C and the 170°C samples, indicating that no significant change in mineral constitution had taken place. The fact that the pressure turned out to be slightly lower than the one obtained in the testing of virgin clay material at room temperature (2.0 MPa) is explained by some slight expansion in the preparation of the creep tests.

The creep curves are given in Figs.5-11 and 5-12 from which it is concluded that the rheological properties were practically the same for the two samples and that they are very similar to those of virgin material. A slightly softer behavior of the most heat-exposed sample is noticed for the highest load step and it may be explained by some slight increase in smectite content or by homogenization.

XRD tests

The study, which was conducted on oriented specimens, was only intended to give a quick estimate on possible major changes in smectite content. The diffractograms exhibited the same pattern, indicating that no significant alteration had taken place. Table 5-2 shows the lamellar spacing given by (001) reflexions for samples representing 40, 60, 90 and 170°C.

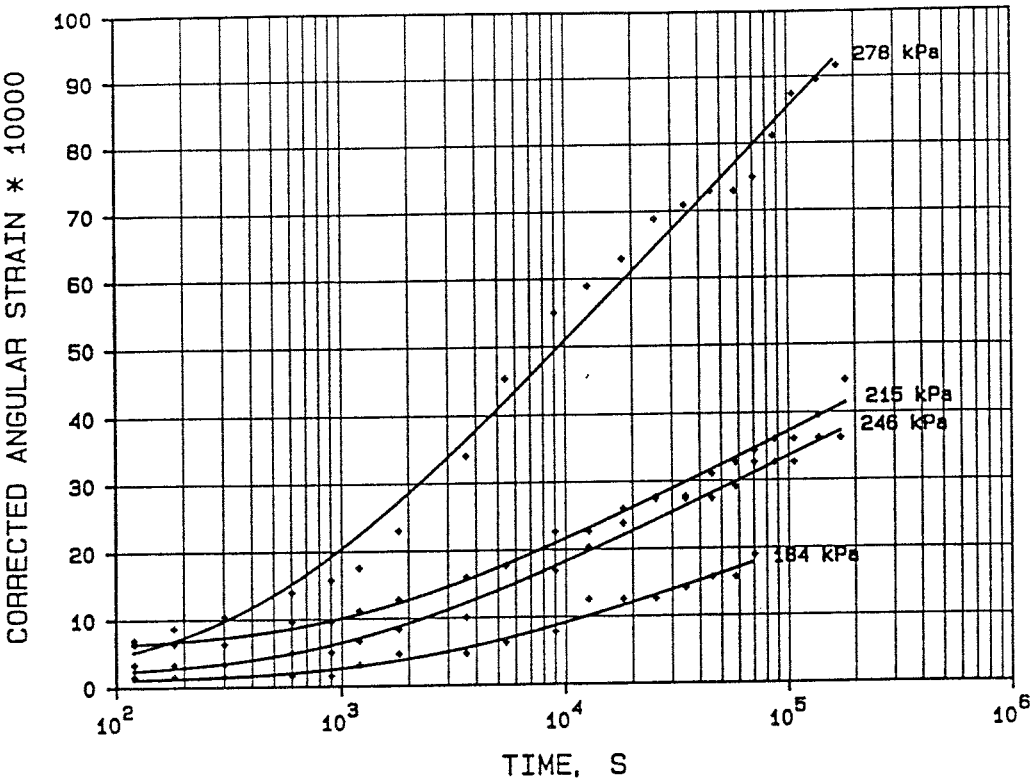

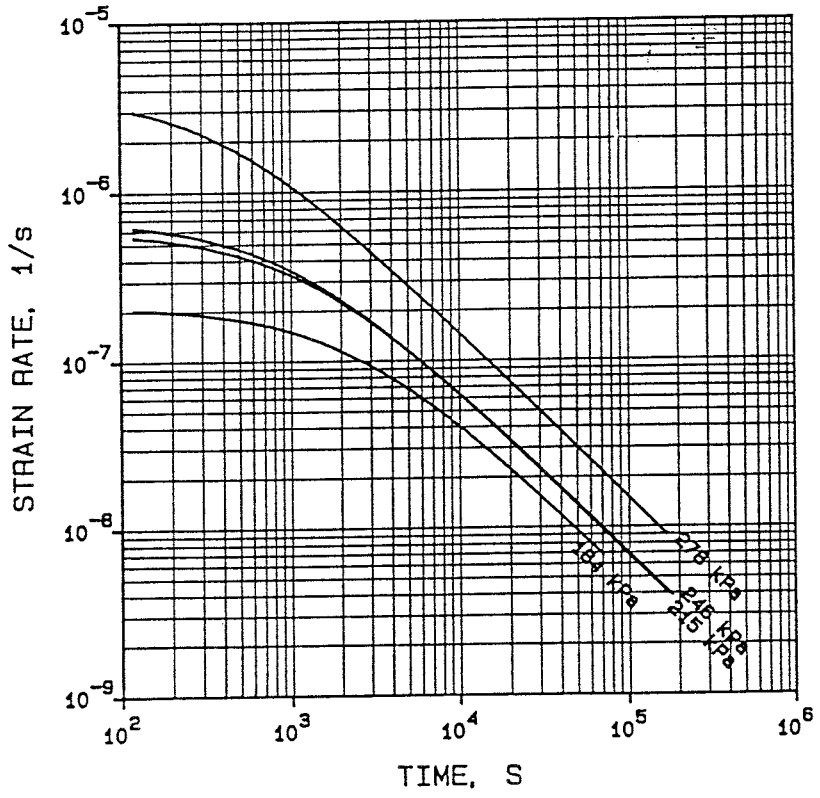

Figure 5-11 Upper: Creep strain versus time of sample A4 (40°C). Lower: Strain versus time of sample A4 (40°C)

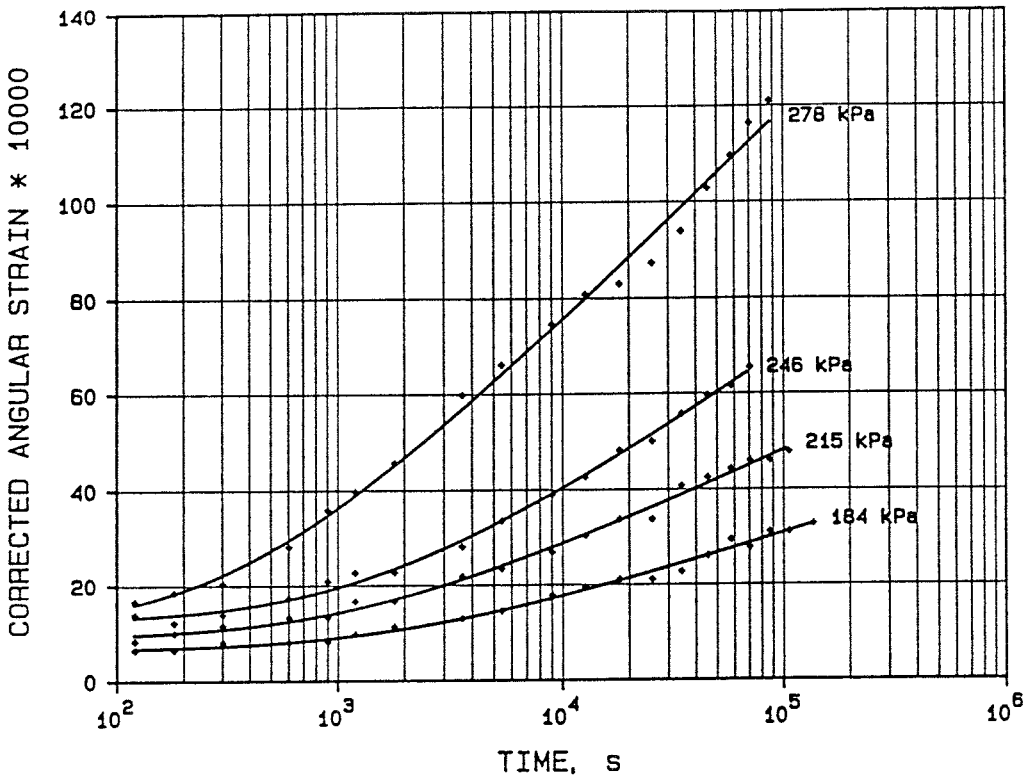

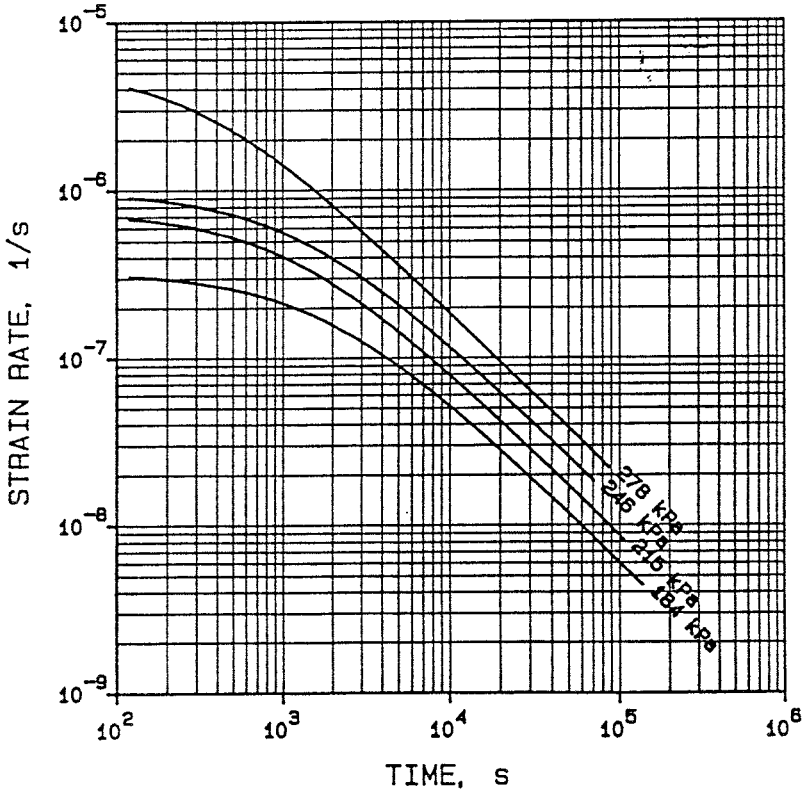

Figure 5-12 Upper: Creep strain versus time of sample E1 (170°C). Lower: Strain rate versus time of sample E1 (170°C)

Table 5-2 XRD data for the clay in Hole I

Sample No	Temperature °C	EG-treated material Å
A1	60	16.99
A4	40	16.67
E1	170	16.99
E4	90	17.15

Electron microscopy

Low voltage scanning microscopy (Philips SEM 515) of uncoated specimens extracted from freeze-dried samples was applied to avoid artifacts from metal coating. Representative micrographs are shown in Figs.5-13 to 5-15, from which one can draw the following conclusions:

* The 40°C samples show the typical appearance of smectite clay, meaning that many of the smectite components serve as coatings of kaolinite stacks. This is in agreement with the finding that (001) smectite peaks are very dominant (Table 5-2)

* The 90°C samples show some heterogeneity, in the form of aggregation or formation of large stacks probably induced by the temperature and possibly by dissolution and loss of material

* The 170°C samples show very clear evidence of neoformation of large crystals (10 μm) of gypsum or anhydrate and small nodules of amorphous silica gel. The typical network of fluffy stacks of smectite flakes is not seen in these samples

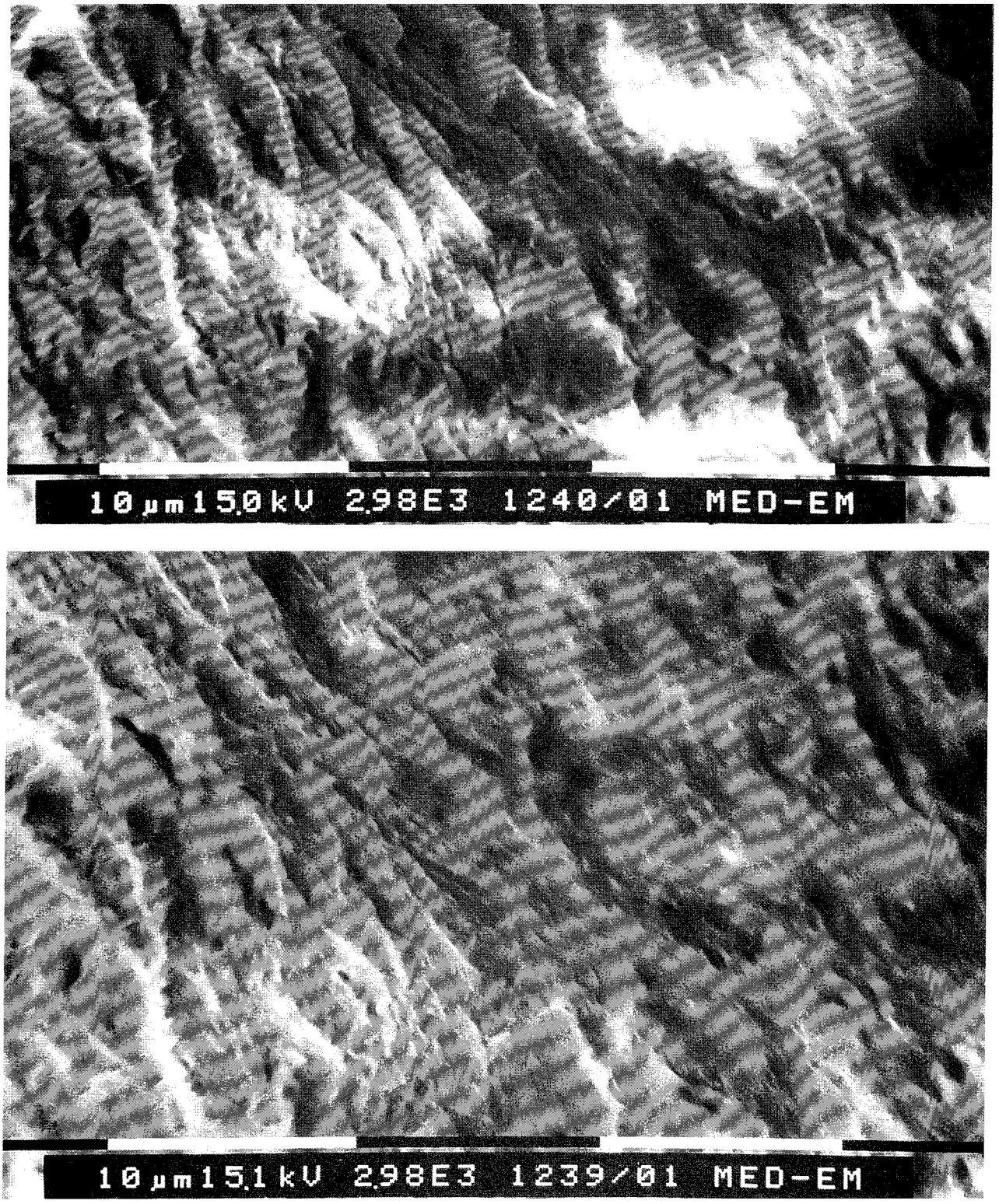

Figure 5-13 Scanning micrographs of sample A4 (40°C), showing the typical fluffy network of flakes of smectite clay. Kaolinite particles appear to embedded in or coated by smectite

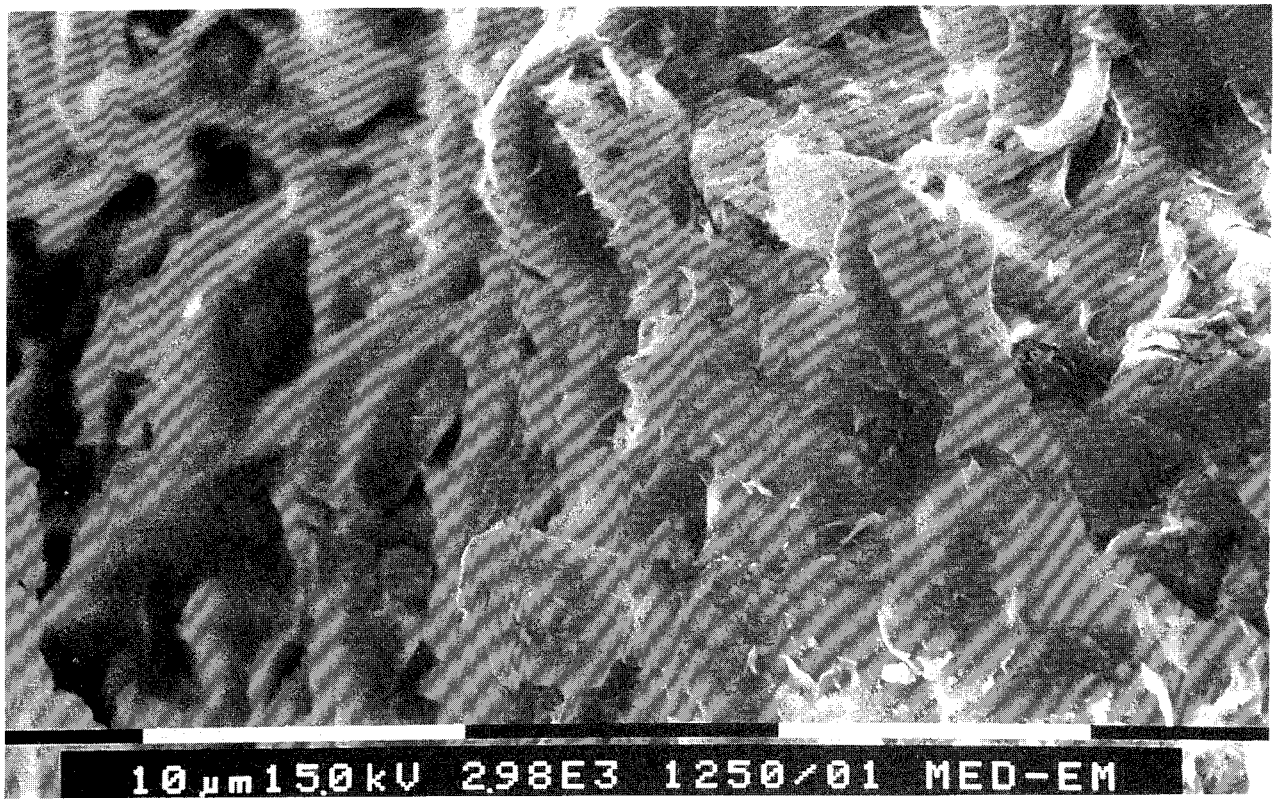

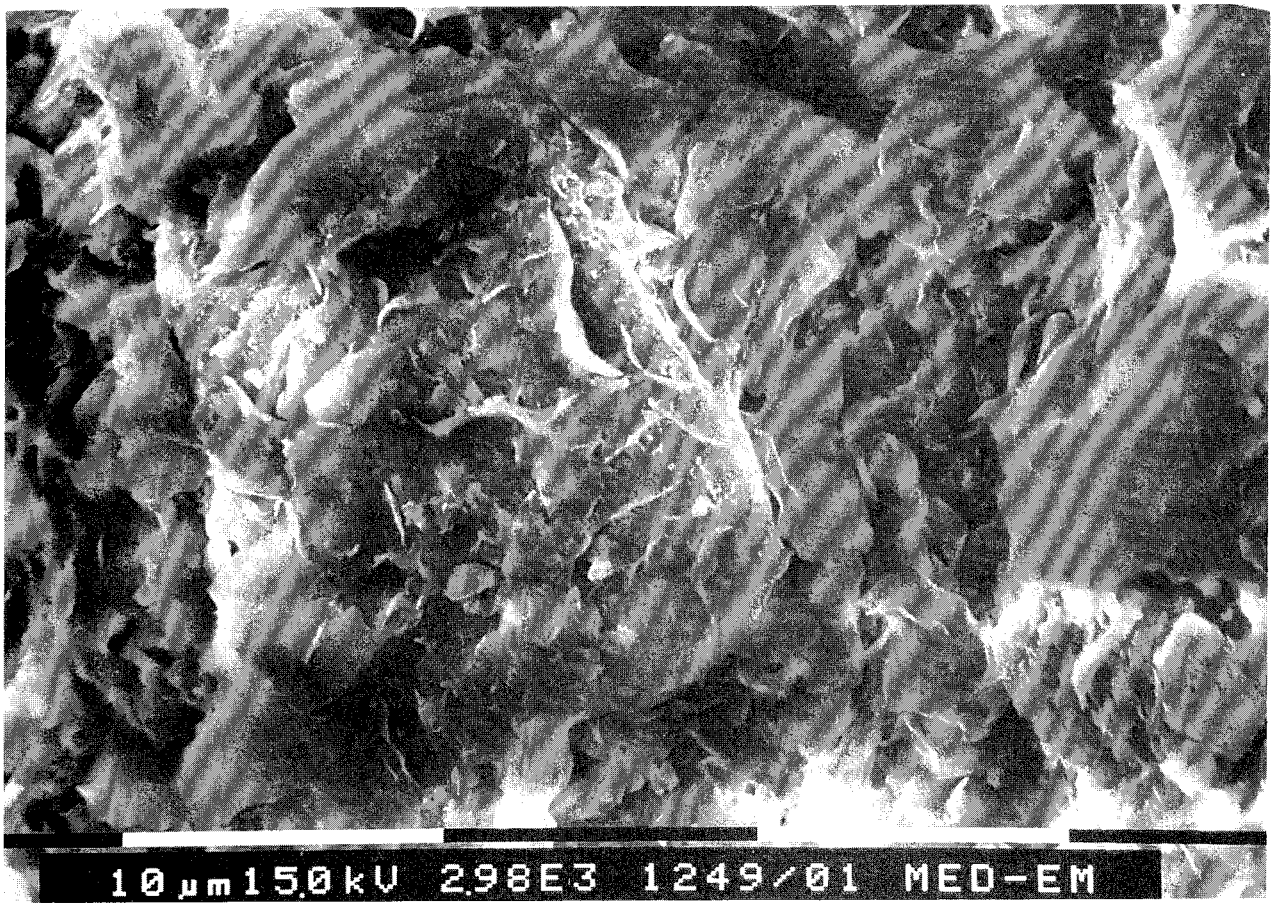

Figure 5-14 Scanning micrographs of sample E4 (90°C), showing a heterogeneous "aggregated" pattern, still without the diagnostic morphology of kaolinite particles

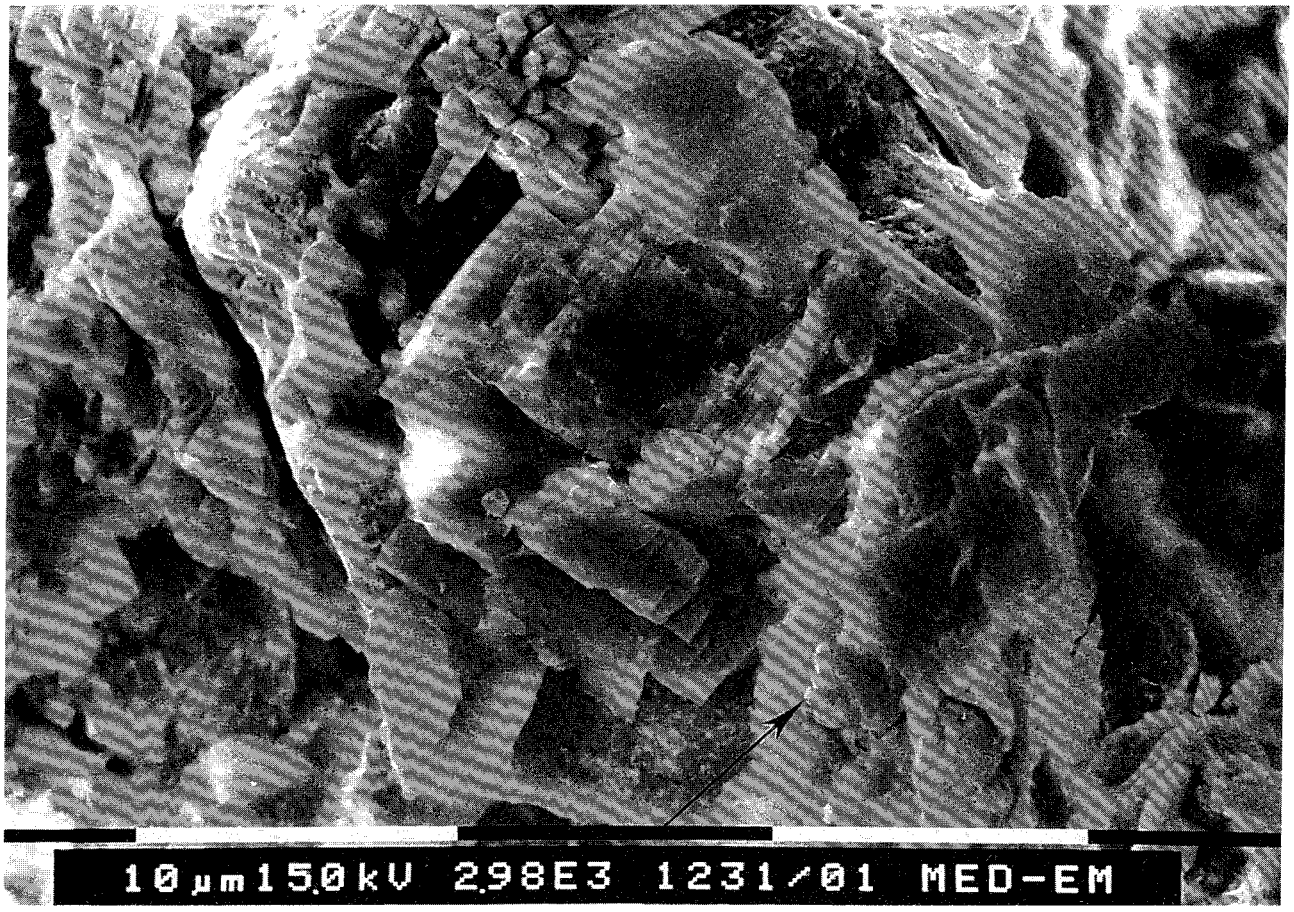

Figure 5-15 Scanning micrograph of sample E1 (170°C), exhibiting numerous large sulphate crystals and small rounded nodules of presumably amorphous silica gel (arrow)

Transmission electron microscopy of samples embedded in acrylate plastic (23) gave substantial additional information on the microstructure of samples exposed to moderate temperature (90°C). This is illustrated by Figs.5-16 and 5-17, of which the first one demonstrates that kaolinite forms a separate phase. Both pictures suggest that smectite stacks containing around 5 flakes actually appear as coatings of kaolinite stacks holding some 50-100 flakes. This demonstrates that at least some of the kaolinite and smectite form separate (free) phases representing more or less regular grouping of stacks of flakes.

Figure 5-16 Transmission micrograph of sample E4 (90°C) showing large kaolinite aggregate. The lower part of the picture exhibits dense kaolinite stacks separated or coated by thin smectite stacks (Magnification 10^5 x)

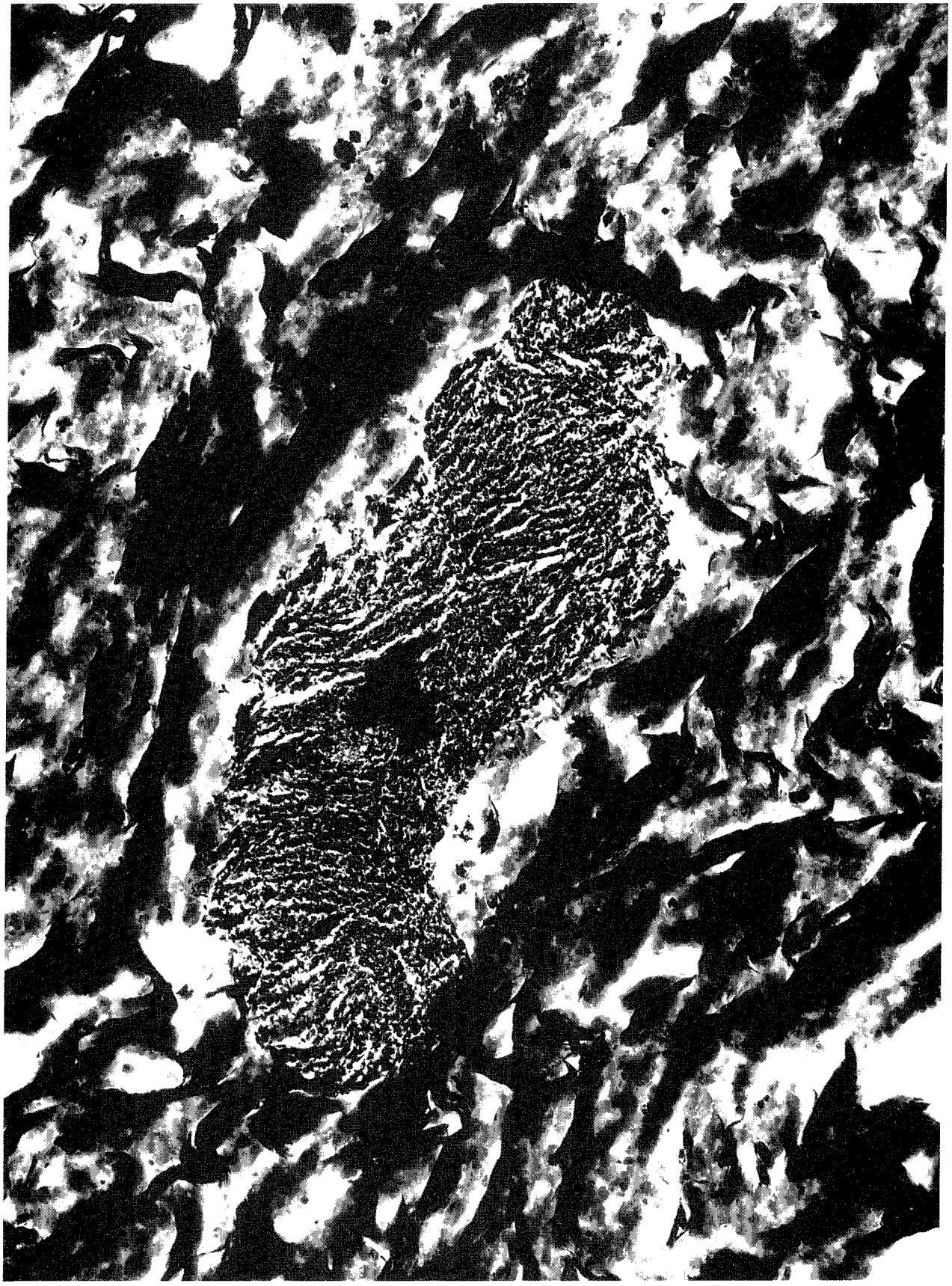

Figure 5-17 Transmission micrograph of sample E4 (90°C) showing integrated networks of dense kaolinite stacks and fluffy smectite aggregates, surrounding a large crystal of unknown composition cut by the microtome knife (Magnification 60 000 x)

It is concluded from the determination of the rheological properties, the checking of key mineral features, and the electron microscopy, that no significant changes in mineral constitution and physical properties had been caused in the 8 month period of testing except for a zone extending a few millimeters from the steel casing. In this zone anhydrite and gypsum were found to be neoformed.

5.2.2.2 Hole II

General

While the clay in zones I and II (Fig.5-10) gave the same visual impression as in the corresponding zones in Hole I, the material in zones III and IV was very clearly altered. Thus, over approximately 1 m axial length of the hottest zone, i.e. where the temperature had been around 170°C at the clay/casing interface for almost 4 years, one could identify 5 zones specified in Fig.5-18. L0 had the form of a solid crust of 8 mm thickness, i.e. 10 % of the total clay annulus, the innermost 2-3 mm being very dark. L1, extending to 20 mm from the steel surface and comprising L0, was clearly coarsely aggregated. L2, L3, and L4 showed successively less alteration.

The hard and brittle character of zone L0 made it impossible to test the clay in oedometers or shear equipments and only chemical and mineralogical tests could be made. Samples from the other zones could be prepared and tested without difficulty. The test program, also giving evaluated hydraulic conductivity and swelling pressure data, is shown in Table 5-3. The L-samples were taken about 70 cm from the base of the clay column, while the B-samples were extracted about 200 cm from the base. B1 was located at the same distance from the casing as L1, B2 as L2 etc.(cf. Fig.5-18).

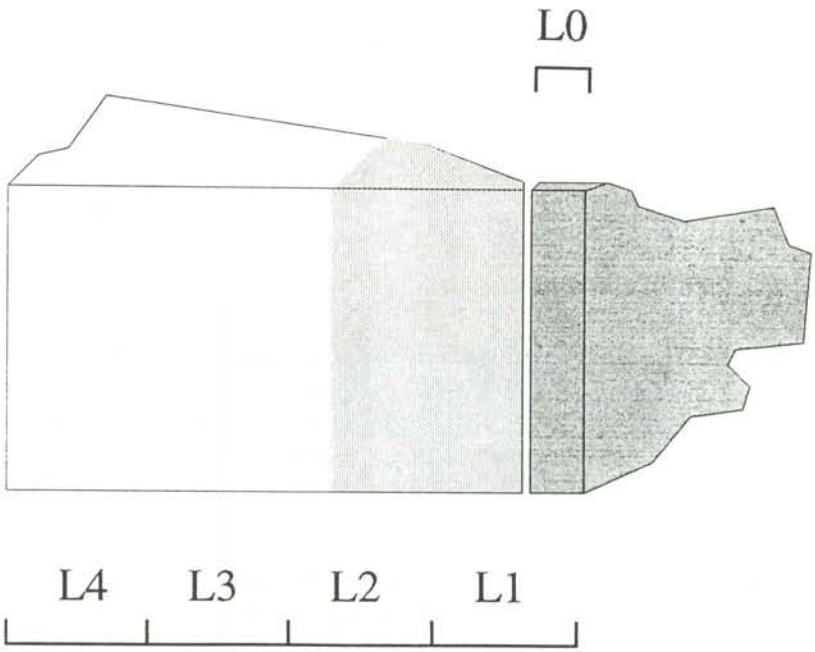

Figure 5-18 Appearance of the clay with zone division. Zones L1-L4 were all 19 mm thick. The darkened part was 25-30 mm thick and the inner "claystone" L0 zone 8 mm

Table 5-3 Test program. p_s = swelling pressure, k = hydraulic conductivity, w_L = liquid limit, CEC = cation exchange capacity, E.A. = element analysis

Sample	Temp. °C	p_s MPa	k m/s	w_L %	XRD	CEC	SEM	E.A.
L0	150-180	0	-	-	X	-	X	X
L1	130-150	0.2	$2x10^{-10}$	77	-	-	X	X
L2	110-130	-	-	-	X	78	X	X
L3	95-110	-	-	-	-	-	X	X
L4	80-95	0.8	$7x10^{-13}$	115	X	74	X	X
B1	25-30	-	-	-	-	-	-	X
B2	25-30	-	-	-	-	-	-	X
B3	25-30	-	-	-	X	78	X	-
B4	20-25	1.2	$3x10^{-13}$	-	-	-	-	-

Physical properties

The swelling process leading to the finally recorded values given in Table 5-3 is indicated in Fig.5-19, from which it is obvious that the samples, which were trimmed to fit 20 mm diameter oedometers and prevented from expanding more than about 2 % on taking up a small amount of distilled water, behaved differently depending on their location in the temperature field.

Sample B4, that had been exposed to only 20-30°C, behaved normally and gave a swelling pressure (1.2 MPa) that was almost the same as that measured in the field test.

Sample L1, having been exposed to 130-150°C, showed very little expansivity and gave a final swelling pressure of only 0.2 MPa. This demonstrates that cementation through precipitation had taken place and the same effect, although less severe, was also exhibited by the outermost sample L4. For this sample the finally recorded swelling pressure was 0.8 MPa, which is around 50 % of the highest swelling pressure that was recorded in the deeper parts of the hole.

The fact that the liquid limit had dropped by about 50 % in sample L1 shows that the hydration power of the clay had decreased, the most probable mechanism being that heat-contracted stacks of smectite flakes were prevented from taking up water and expanding by cementing or coating agents. This effect was even stronger in sample L0 leading to its claystone-like appearance. The liquid limit of sample L4 was as high as that of virgin material (cf. sample B4), which shows that the cementation bonds that caused the reduced swelling potential were only weak and that they were broken down by the preparation of the samp-

le for the liquid limit testing. The same explanation is valid for the CEC values of samples L2 and L4, which are very near that of the undisturbed sample B4.

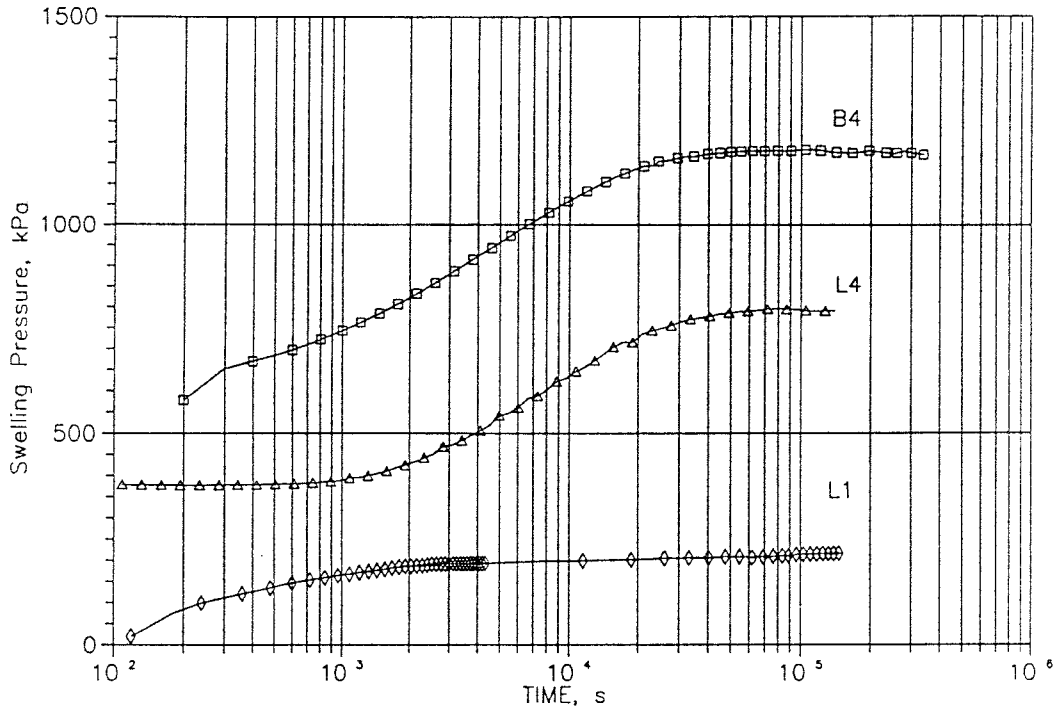

Figure 5-19 Evolution of swelling pressure

Creep properties

The same preparation and testing technique was applied as for the samples from Hole I. Plottings of strain versus time are given in Fig.5-20 and the evaluated creep parameters are specified in Table 5-4. The parameters represent averages of the second and third load steps. One finds that the data from testing samples L4 and B1 are almost identical and that they are similar to those of virgin material prepared in the laboratory.

The more ductile behavior of the laboratory-prepared sample manifested by the higher t_o, and the slightly higher strength demonstrated by the lower B-value, as compared to the data of the B1-sample, can be explained by less homogenization than was produced at enhanced temperature in the field experiment.

The drop in B-value of sample L1 to about one seventh of that of virgin clay indicates that strong stiffening took place by cementation and the strong drop in t_o, leading to a negative value, verifies this.

Table 5-4 Rheological data from creep tests

Sample	Temperature °C	A	B	t_o s
L1	130-150	$2x10^{-4}$	$3x10^{-5}$	-7
L4	80- 95	$-18x10^{-4}$	$3x10^{-4}$	1700
B1	25- 35	$-17x10^{-4}$	$3x10^{-4}$	1500
Lab (p.15)	20	$-12x10^{-4}$	$2x10^{-4}$	2800

The swelling tests and the creep experiments demonstrated that very significant changes in physical properties had taken place in the clay within about 20 mm distance from the hot surface. The visual impression of transformation to claystone was hence verified: the material had become brittle and had completely lost its swelling ability.

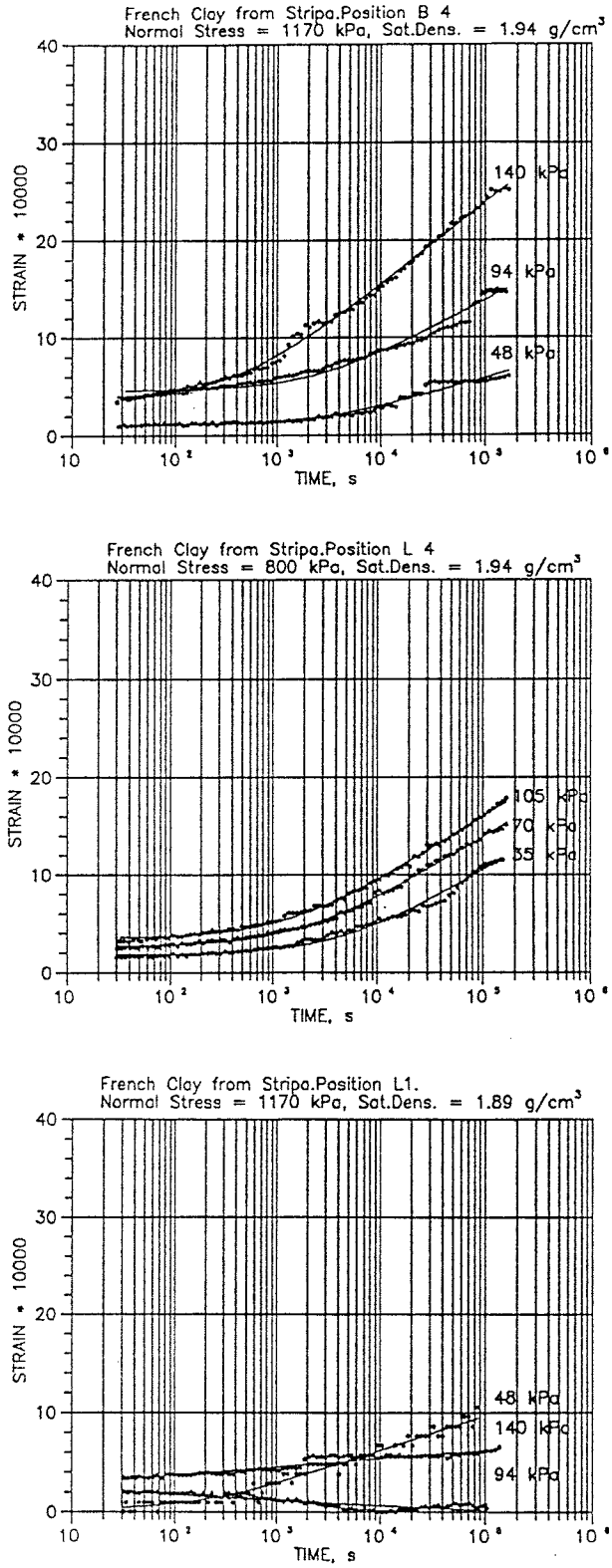

Figure 5-20 Creep curves

5.3 MINERALOGICAL AND CHEMICAL CONSTITUTIONS

5.3.1 Introduction

Mineralogical and chemical investigations of the extracted clay samples were conducted both by CEA and Clay Technology AB, the latter study being carried out as a general overview of major changes without aiming at identifying the detailed alteration mechanisms. The nearfield rock and the steel metal were investigated as well but only the most essential results will be presented in the present report.

5.3.2 Sampling

The big semi-circular core of clay from Hole II that was transported to CEA was sampled for mineralogical and chemical analyses in the following way:

* at 0.25 m from the base of the core (T_{max}=150°C)
* at 0.50 m from the base of the core (T_{max})=175°C)
* at 0.75 m from the base of the core (T_{max}=175°C)
* at maximum distance from the heater ("reference" sample, T_{max}=40°C)

From each of the levels 7 samples were taken close to the heater (samples termed xx-1) and at the rock (samples termed xx-7), xx denoting the distance in centimeters from the base. Each sample had the shape of a slice with 10 mm thickness and a volume of 1 ml. Samples were also taken from the dark, hard claystone (sample termed 75-0).

"Aggregate" material and the fraction <0.2 μm from 12 selected samples were investigated. The particle size separation was made in two steps: sedimentation followed by ultracentrifugation using a Beckman J2-21 machine equipped with a rotor for continuous fluid flow.

5.3.3 Mineralogical analyses (CEA)

5.3.1.1 XRD, Qualitative estimates

The "reference" sample showed the same general pattern as the virgin Fo-Ca 7 clay, i.e. the sets of peaks that were interpreted as kaolinite/smectite - d(001)>17 Å, d(002)< 8.5 Å - and kaolinite, with some smectite (5 %).

In samples 75-1 and 50-1 located next to the heater, the swelling material turned out to be almost pure smectite (Fig.5-21) while the rest of the XRD peaks closely resemble those of the "reference" clay. The differences in d(002) and in A/B (ratio of the intensities of peaks at 6 and 4°2Θ).

The decomposition was concluded to have yielded two swelling phases with closely located diffraction peaks. One of the peaks is narrow and representing smect
ite, the other is wider and contributed by the K/S. The recorded peaks are therefore the *sums* of the two individual components.

The kaolinite had disappeared in the samples exposed to the highest temperatures (75-1 and 50-1) and the amount of this mineral had decreased in all the other samples. Calcite and iron oxides, which are present at low concentrations in Fo-Ca 7 were not consistently found, while anhydrite ($CaSO_4$) appeared in the hardened zone.

In the hardened zone the patterns of oriented specimens were found to be similar to those of samples 75-1 and 50-1 (smectite). However, in the powder pattern there is a (060) peak at around 1.52-1.53 Å that is characteristic of trioctahedral clay minerals. In the aggregate sample smectite and anhydrate were identified and also quartz although at lower concentration than in the virgin clay. The cementation prevents the swelling components to expand spontaneously but grinding breaks down some of the strong bonds. Scanning microscopy has shown amorphous quartz (opal-A) and calcium silicate as cementitious agents in the clay. Iron oxy-hydroxides are probably present as well but they do not make up a significant fraction of the cement.

5.3.1.2 XRD, Quantitative estimates, temperature influence

While the 75-1 and 50-1 samples taken close to the heater show peaks that confirm that the swelling clay minerals are pure smectites, the decomposition of the clay that had taken place in the other samples had to be evaluated by using peaks in the range of 10-16°2Θ, a broad peak around 12°2Θ with d between 8.00 and 8.15 Å, and a narrow peak <10°2Θ with d between 8.20 and 8.40 Å. The relative intensity of the narrow peak was found to increase towards the heater. Using the data obtained from the artificial mixtures it is concluded that the ratio smectite/mixed layers is between 0.1 and 0.5, while it is 1.0 for the 75-1 and 50-1 samples. The main results of the decomposition are summarized in Figs.5-22 to 5-24.

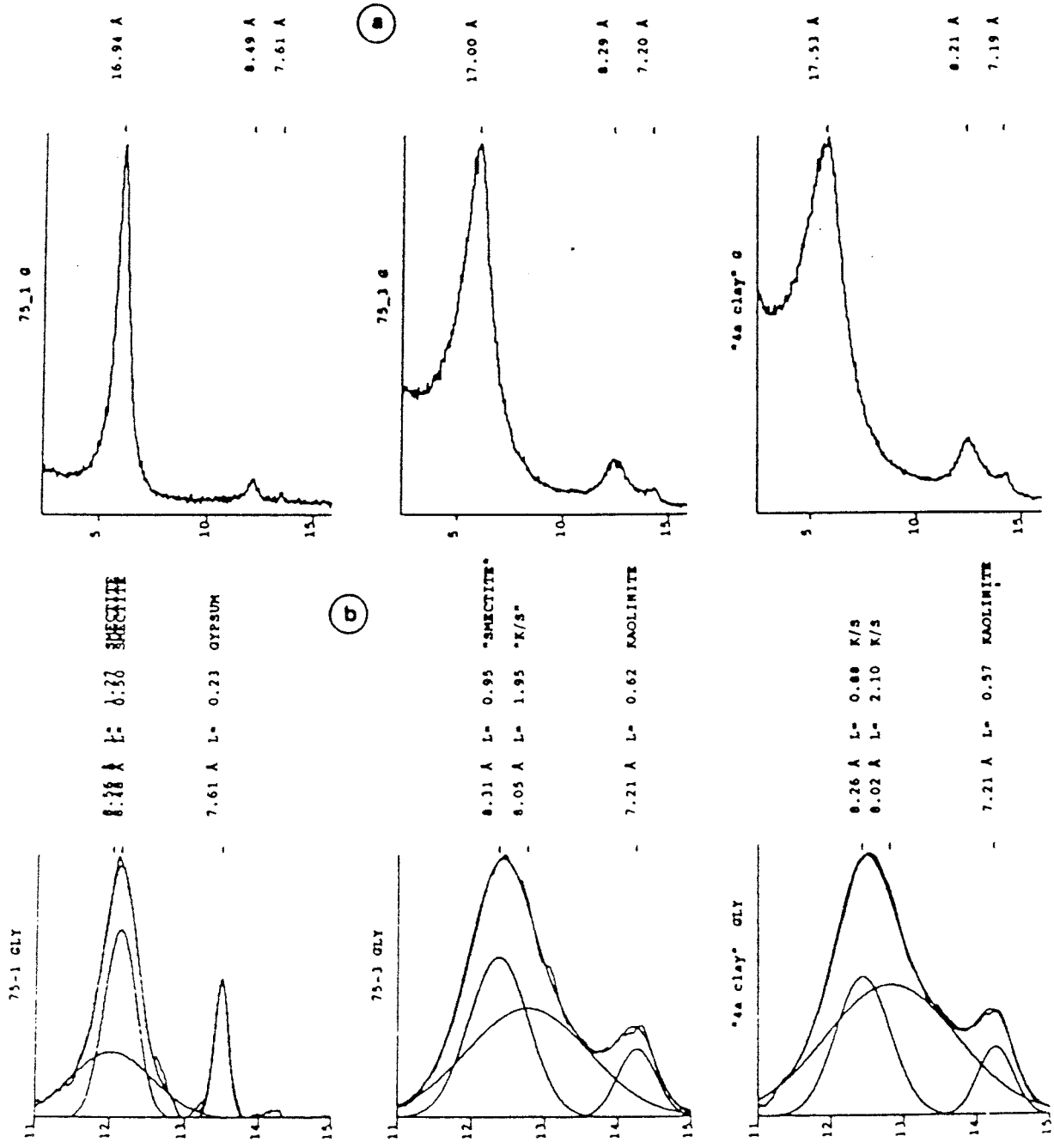

Figure 5-21 a) XRD patterns of oriented EG-treated bulk samples. Temp: 75-1: 175°C, 75-3: 90°C, 4a is virgin clay
b) Interpretation of decomposed (002) peaks

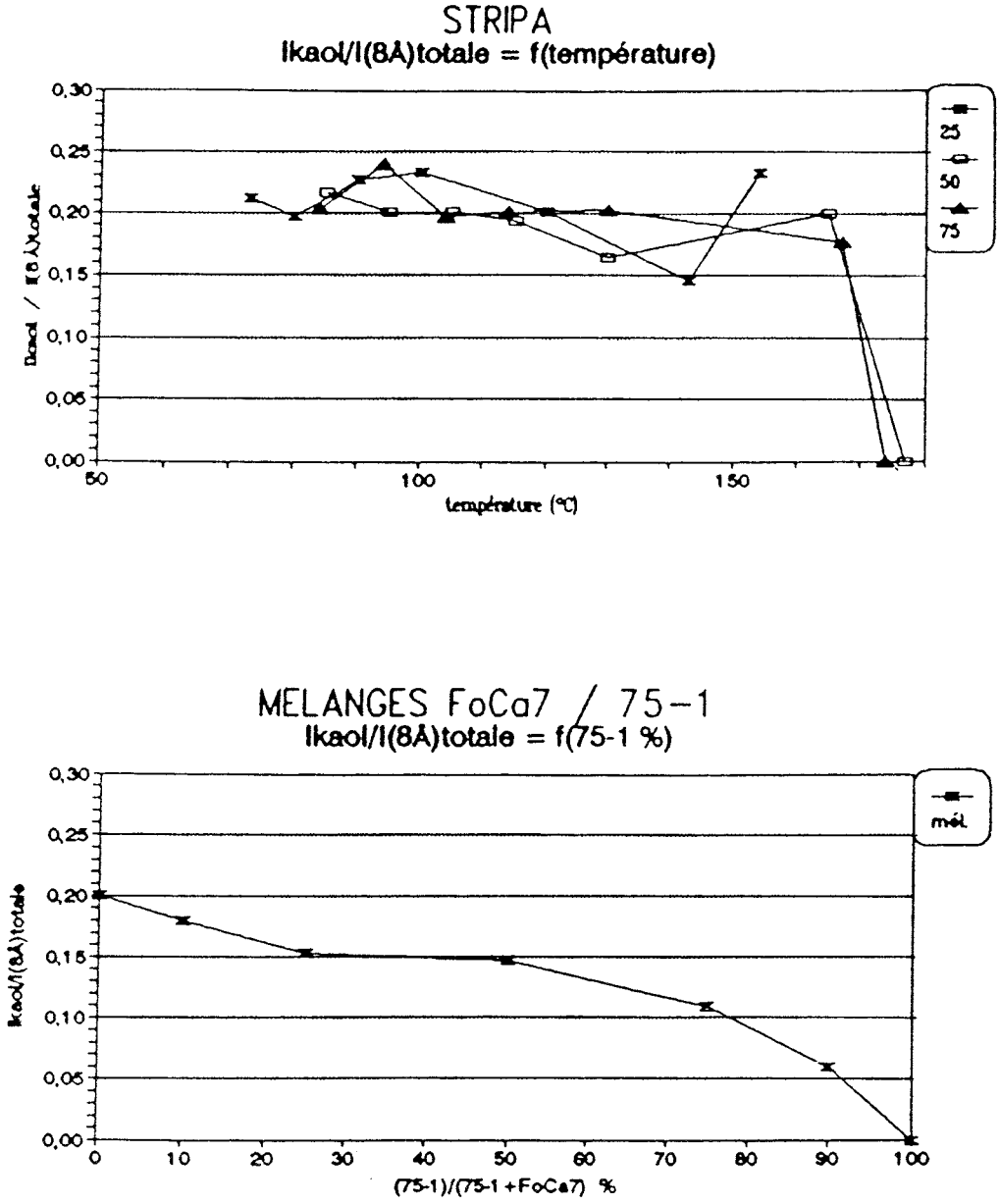

Figure 5-22 Variation of the intensity ratio of K/Swelling minerals. Upper: Stripa data. Lower: Data from artificial mixtures of Fo-Ca 7 and 75-1

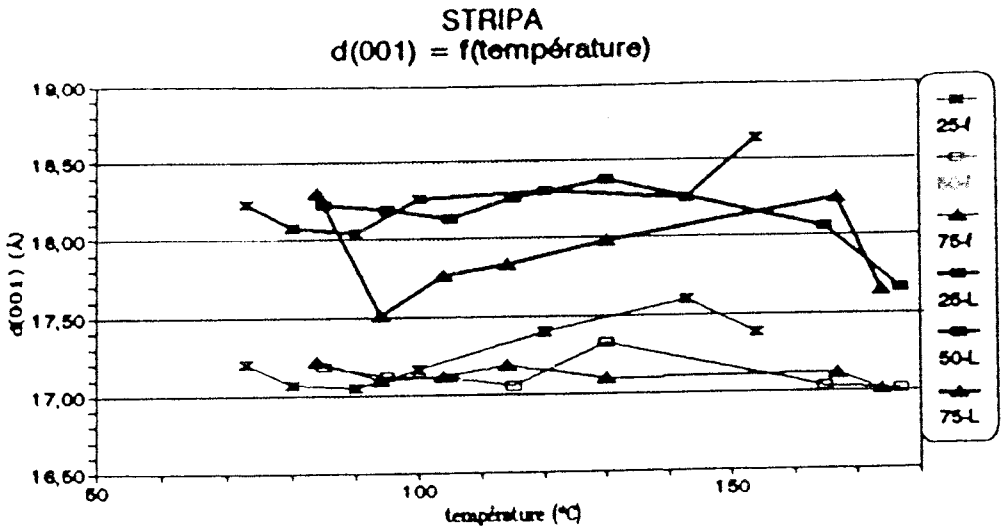

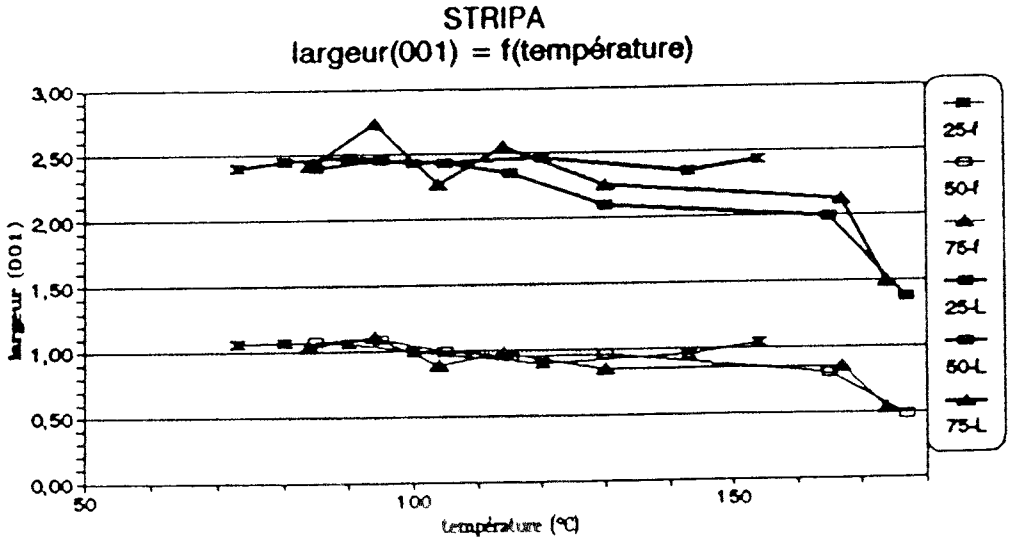

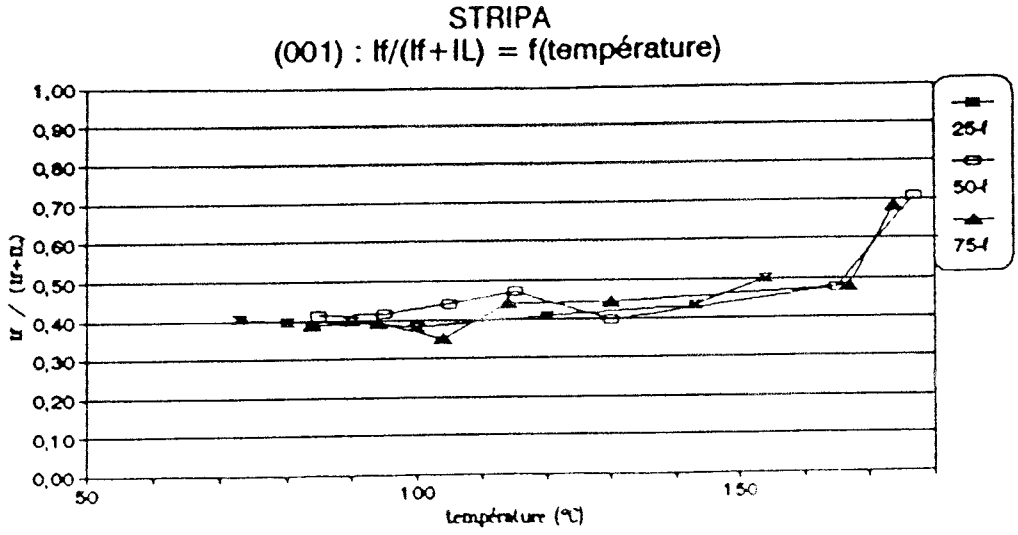

Figure 5-23 Decomposition of the (001) peaks of Stripa clay. Upper: d-values, Central: Peak width at half height, Lower: Relative intensity of the narrow peak and the sum of intensities

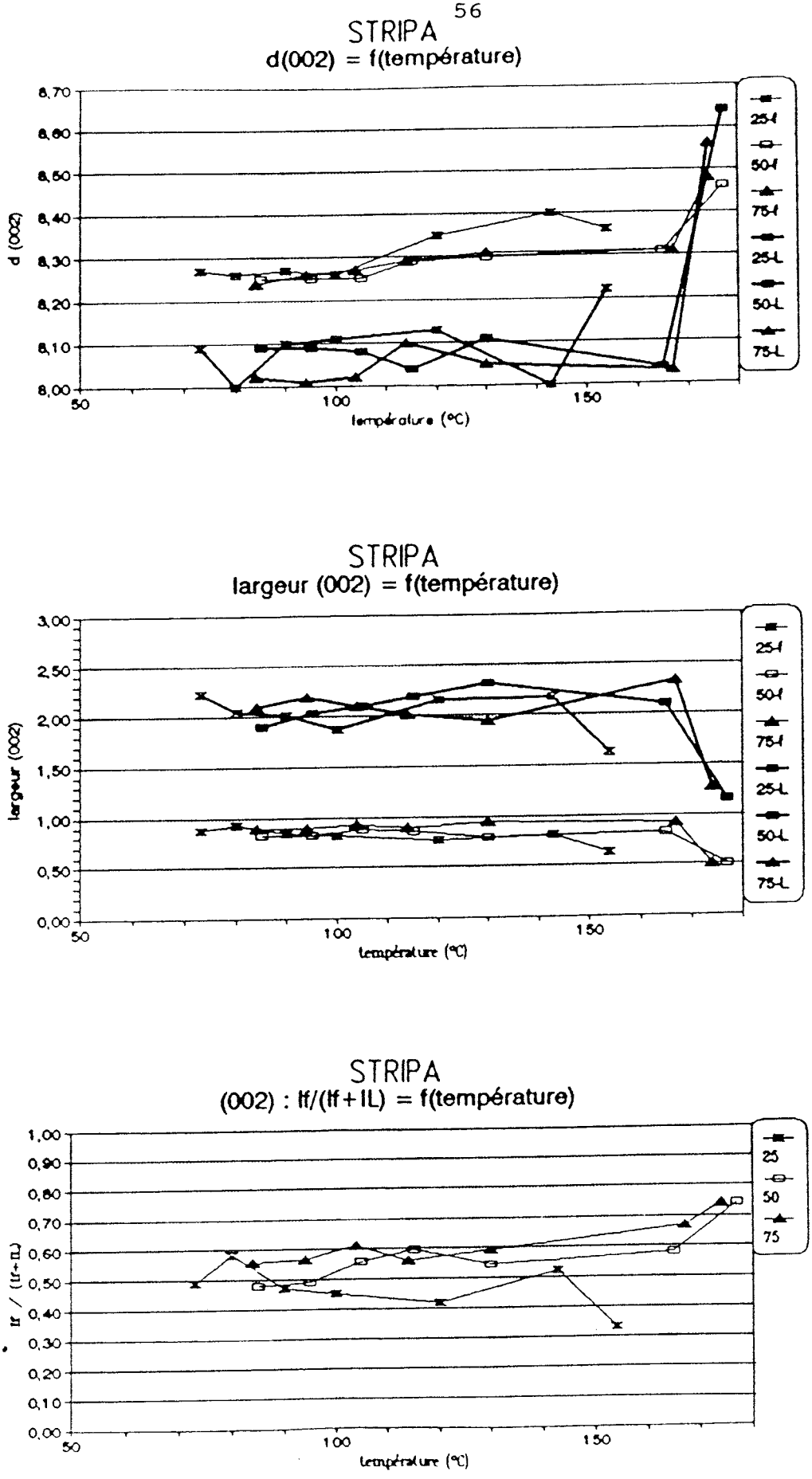

Figure 5-24 Decomposition of the (002) peaks of the Stripa clay. Upper: d-values, Central: Peak width at half height, Lower: Relative intensity of the narrow peak and the sum of intensities

Further conclusions from the analysis illustrated by Figs.5-22 to 5-24 are that the decomposition of kaolinite started at about 120°C, and that the narrow peaks underwent only little change below 100°C but that significant alteration started in the interval up to 170°C, above which the 50/50 KS/S was altered yielding pure smectite, probably according to a different mechanism than at lower temperatures.

It should be noted that the lower content of water close to the heater at 50 and 75 levels (0.5 and 0.75 m from the base, respectively) may have led to the different results obtained for the 25 level (0.25 m from the base).

Finally, the 3.34 Å quartz peak, peaks at 4.4-4.5 Å, and clay mineral peaks in general have been analyzed and this has led to the following conclusions:

* The quartz concentration decreased with increased temperature; very little up to 120-130°C but to a considerable extent above 150°C
* Anhydrite appeared at 120°C at the 25 level and was very obvious above 170°C
* Several temperatures may represent limits of mineral transformations. A most important fact is that changes in the peaks of clay minerals did not appear below 100°C

5.3.4 Mineralogical analyses (Clay Technology AB)

XRD analyses were made by use of a Philips PW 1730 machine with CuKα radiation. The purpose of the tests was to check if significant changes had taken place with respect to the presence of swelling minerals and of accessory minerals in the clay fraction and bulk material. For this purpose only packed samples were used, typical diffractograms being shown in Fig.5-25. They represent the three samples L0, L2, and B3 (cf. Fig.5-18, Table 5-3), exposed to the temperatures 150-180°C, 110-130°C, and 25-30°C, respectively, and one finds from comparing the diffractograms that samples L2 and B3 were practically identical except for some very slight reduction in calcite in sample L2. Sample L0 had undergone very significant changes, the most obvious ones being neoformation of anhydrite, decrease in quartz, feldspars and kaolinite, and complete loss of calcite. Although no quantitative information on changes in the content of swelling minerals of this sample is offered by the diffractograms, the peak at a about 7.5° 2Θ suggests neoformation of smectite. Still, the fact that the typical ductile behavior of smectitic clay had completely gone shows

that smectite minerals did no longer control the physical properties of the sample.

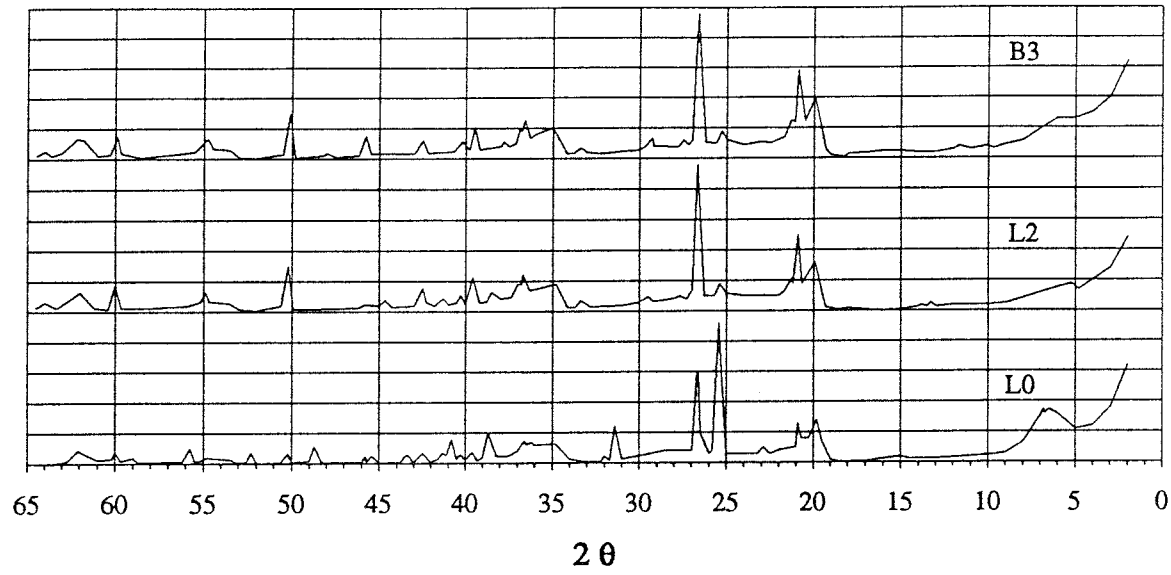

Figure 5-25 X-ray diffractograms of packed samples

5.3.5 Chemical analyses (CEA)

5.3.5.1 Element distribution, CEC

The outcome of the chemical analyses of the clay from Hole II is compiled in Table 5-5, the contents being expressed in terms of % of oxides.

Table 5-5 Chemical composition and CEC (meq/100 g) of 4 bulk samples and of their <0.2 μm fractions

	BULK SAMPLE				<0.2 μm FRACTION			
	75 - 1	75 - 2	75 - 3	75 - 4	75 - 1	75 - 2	75 - 3	75 - 4
SiO2	50.81	54.94	56.29	52.07	49.36	46.39	49.12	49.19
Al2O3	14.92	21.17	20.23	20.89	18.11	23.17	24.46	25.34
MnO	0.04	0.02	0.02	0.00	0.05	0.02	0.02	0.02
MgO	3.51	0.76	0.66	0.69	3.85	1.01	1.02	0.96
CaO	6.59	3.18	2.24	2.12	3.37	2.43	2.50	2.29
Na2O	1.27	0.63	0.75	0.91	0.36	0.30	0.39	0.19
K2O	0.65	0.23	0.30	0.34	0.38	0.29	0.29	0.20
TiO2	1.09	1.18	1.21	1.26	0.89	1.43	1.37	1.19
Fe2O3	7.24	7.35	7.47	7.65	8.21	8.14	8.38	8.09
LI1000°C	15.30	11.28	11.49	13.90	15.09	18.14	14.41	14.09
TOTAL	101.43	100.74	100.65	99.83	99.68	101.32	101.97	101.57
CEC	88.17	76.61	71.86	69.84	102.76	86.21	86.65	84.52

"Aggregate" material

One concludes from the analyses that the concentrations of MnO, Na_2O, K_2O, TiO_2 and Fe_2O_3 were not changed by the heat treatment. The samples richest in smectite (75-1 and 50-1) showed significant depletion in SiO_2 and Al_2O_3 while their MgO and CaO contents increased. This is in good agreement with the mineralogical analyses applying the following reasonings:

* Decrease in quartz content leads to reduction in SiO_2
* Decrease in kaolinite content leads to reduction in Al_2O_3
* Formation of anhydrite leads to increase in CaO
* Enrichment of smectite leads to increase in MgO and CaO

The CEC values turned out to be almost unchanged up to 150°C (65-80 meq/100 g) but they rose for the sample 75-1 with neoformed smectite to 88 meq/100 g.

<0.2 μm fraction

The same general conclusions can be drawn as for the "aggregate" material but the changes are more obvious. Thus, the samples 75-1 and 50-1 had lower Al_2O_3 contents (18 %) than the less heated clay (23-25 %) and they were richer in MgO (>3 %) than the less heated ones (1 %). The variation in SiO_2 is less consistent, probably because of the presence of opal-A. The CEC values were around 80 meq/100 g for the less heated sample, i.e. almost the same as for the virgin material, while those located in the claystone had 100 meq/100 g, which is characteristic of pure smectite.

5.3.5.2 Infrared spectroscopy

The infrared spectra were obtained in the 3000-400 cm^{-1} and 400-1200 cm^{-1} regions. The <0.2 μm fractions of four samples were studied: 50-7, 75-3 and 75-1, forming a series with increasing smectite content, and 75-0 from the claystone at the heater surface.

The spectra are rather similar: bands at around 426, 470, 534, 696, 754, 879, 912, 1007, 1037, 1100 (shoulder), 3628, 3658 and 3700 cm^{-1} characteristic of kaolinite (24,25) and/or kaolinite/smectite (26).

A weak band at 798 cm^{-1} may be due to quartz, the other bands of this mineral being masked by the bands of other minerals. In these three spectra the intensity of the kaolinite bands - free or mixed-layered - is found to decrease towards the heater.

The spectra of the claystone sample show bands at 470, 526, 792, 875, 918, 1031, 3630 and 3654 cm^{-1} corresponding to alumium smectites (montmorillonite and beidellite). The strong bands which characterize kaolinite have disappeared, thus confirming that this mineral had been completely transformed. The broad band at around 792 cm^{-1} may indicate quartz. The band at around 671 cm^{-1} has not been identified; it probably corresponds to the Mg-OH vibration of a trioctahedral clay mineral, like saponite, stevensite or talc (24,25). Nontronite was not present since the characteristic bands at 1020 and 490 cm^{-1} were not found.

5.3.5.3 Mössbauer spectroscopy

Mössbauer spectra of the <0.2 μm fractions of three samples, i.e. 50-7, 75-3 and 75-0 were obtained and the results from the latter were again different. Decomposition of the spectra of samples 50-7 and 75-3 indicated, by comparison with data provided by Coey (27), the presence of Fe^{3+} in octahedral positions and the absence of tetrahedral Fe^{3+}. There were broad bands characteristic of magnetic or paramagnetic substances like ferriferous phases or iron oxy-hydroxides with very small XRD-amorphous crystal size. The area of the bands could be used for deriving an approximate distribution of iron (28) and it was concluded that 70 to 80 % of the Fe^{3+} in these two samples was in octahedral positions.

The spectrum of the claystone sample 75-0 was different. It could be decomposed into two doublets with lines thinner than 1 mm/s, corresponding to Fe^{3+} and Fe^{2+} in octahedral positions. It should be noted that the virgin material did not contain Fe^{2+} and that it, hence, seems to originate from the heater steel. The decomposition did not show the broad bands that would indicate other minerals than phyllosilicates.

5.3.5.4 Aspects of the kinetics

The available data were assumed to allow for estimation of the activation energy of the reaction involving transformation of 50/50 kaolinite/smectite to smectite, although there were only data for one particular reaction time, i.e. 4 years. The order of the reaction could therefore not be determined and hence not the reaction constant (29).

Similar derivations have shown that mineral reactions of the type "low-charge smectite converted to high-

charge smectite" or "smectite to illite" are of first order (13,30,31). An attempt was made to make the evaluation by use of 21 experimental temperatures for which the ratio of kaolinite/smectite and smectite minerals was known, assuming that the first-mentioned component was the only one present from start. This gave a slope of the log $k/1000\ T^{-1}$ line that would give the activation energy E_a according to Lasaga's expression:

$$E_a = - R \times 2.3 \times s$$

where R = 2 kcal/K,mole
2.3 = ratio of ln to $^{10}\log$

A premlinary evaluation indicated that the reaction took place in several steps and that only a restricted number of mineral species were involved at each temperature. Thus, the disappearance of kaolinite and quartz and the formation of anhydrite took place at 120°C, while the change in kaolinite/smectite ratio was initiated at around 100°C and enhanced above 120°C. This would suggest that the transformation of kaolinite/smectite to smectite becomes effective above 120°C and that both quartz and free kaolinite take part in the reaction (11,12). If no quartz had been present the reaction would have stopped rather soon (32).

The uncertainties involved in the evaluation of the activation energy for transformation of kaolinite to smectite was concluded to be too high to yield a definite value. For comparison, transformation of smectite to illite are generally reported to be in the range of 20-30 kcal/mole (30,31,32,33,34).

At higher temperatures than 120°C the general reaction is concluded to be:

K/S + K + Q + ε ---> S + A + ε'

where K/S = kaolinite/smectite
K = kaolinite (free)
Q = Quartz
S = Smectite
A = Anhydrite
ε = Possible non-identified reactant
ε'= Possible non-identified reaction product

At temperatures below 120°C the material is interpreted as a mixture of mixed-layer K/S and smectite, with a ratio of S/KS of 0.1.

5.3.6 Chemical analyses, Clay Technology AB

5.3.6.1 CEC

CEC-analyses were made by Clay Technology by use of the Chapman ammonium acetate method. The accuracy of this technique is only sufficient to detect clear changes in exchange properties (>10 meq/100g). Data are given in Table 5-3. An approximate theoretical CEC value of a virgin clay mixture of the present sort, i.e. with 50 % kaolinite and 50 % smectite, would be in the range 65-75 meq/100 g, the higher figure corresponding to the actually recorded values. The data are concluded to be in reasonable agreement with those obtained by CEA.

5.3.6.2 Element analysis

Chemical analyses were made on bulk material and on the clay fraction, the main data being collected in Table 5-6. The investigations were made by SGAB, Luleå, using multicomponent spectrometer analysis technique (ICP-AES) of samples melted in lithium metaborate and dissolved in nitric acid. The table gives the main elements in the form of oxides, the accuracy being 1.5 % RDS. The ignition loss (LOI) shows the relative amounts of volatile components (950°C) and for making a direct comparison of the results possible, the element values are corrected with respect to LOI.

It is concluded that no significant change took place in the clay fraction of any of the samples L1, L2, L3, and L4 as compared to the unheated B1 sample, except for an increase in SiO_2 by 5 % in the coldest sample L4 (80-95°C).

The bulk analyses show that there was a significant loss in silica and aluminum and a strong increase in calcium, magnesium and sulphur in the L0 sample (150-180°C). The loss in Si and Al is explained by the dissolution of quartz, feldspars and kaolinite that was observed by the XRD analysis of the material in the hottest zone, and by the precipitation of anhydrite and possibly magnesium sulphate indicated by the XRD study. It is estimated that calcium, sulphate and magnesium cannot have been supplied by the confining rock and groundwater but that they originated from accessory minerals in the clay. Thus, it is anticipated that calcium stemmed from dissolved calcite and feldspar, while magnesium may have originated from ions in exchange positions - being replaced by calcium or protons - and sulphate ions emanating from degraded silt-sized sulphide minerals like pyrite.

Table 5-6 Chemical composition

ELEMENT ANALYSES FROM CLAY FRACTION

Main Elements (%)

Sample	SiO2	Al2O3	Fe2O3	TiO2	MgO	CaO	K2O	Na2O	P2O5	LOI	Total
L1	53.5	28.4	9.4	1.4	1.1	2.7	0.3	1.6	0.1	10.2	98.53
L2	54.7	29.0	9.5	1.4	1.0	2.4	0.2	0.8	0.1	9.8	99.05
L3	54.8	28.3	9.9	1.5	1.0	2.4	0.2	0.9	0.1	9.6	99.04
L4	56.4	26.7	9.9	1.6	1.0	2.3	0.2	1.1	0.1	11.1	99.09
B1	53.2	29.6	9.9	2.0	0.9	2.3	0.2	1.1	0.1	10.5	99.28

Trace Elements (ppm)

Sample	Ba	Co	Cr	Cu	Sr
L1	56	17	153	62	105
L2	85	14	174	59	102
L3	95	17	168	75	95
L4	94	13	224	87	87
B1	59	21	173	184	83

ELEMENT ANALYSES FROM BULK

Main Elements (%)

Sample	SiO2	Al2O3	Fe2O3	TiO2	MgO	CaO	K2O	Na2O	P2O5	S	LOI	Total
L0	55.6	15.7	7.78	0.97	4.61	8.90	0.11	0.31	0.03	3.29	5.7	97.25
L1	60.0	24.1	9.57	1.53	0.88	2.30	0.14	0.29	0.09	0.00	7.3	98.83
L2	60.8	23.5	9.34	1.49	0.79	2.44	0.19	0.33	0.09	0.00	0.7	98.95
L3	60.9	23.6	9.25	1.50	0.80	2.40	0.21	0.36	0.08	0.00	0.4	99.14
L4	60.7	23.6	9.45	1.49	0.83	2.33	0.19	0.37	0.09	0.00	20.7	98.98
B1	61.0	24.1	9.54	1.50	1.03	2.70	0.22	0.35	0.11	0.11	8.3	100.6
B2	61.5	23.7	9.21	1.48	1.04	2.90	0.20	0.35	0.10	0.22	8.3	100.7

Trace Elements (ppm)

Sample	Ba	Co	Cr	Cu	Sr
L0	63	<8	88	14	197
L1	47	18	136	70	79
L2	815	12	141	67	94
L3	692	12	128	65	95
L4	736	15	137	66	96
B1	632	15	150	64	94
B2	686	16	137	63	98

In general, these chemical analyses are in agreement with those carried out by CEA.

5.4 MICROSTRUCTURAL CONSTITUTION

5.4.1 CEA

Thin sections of the clay were prepared after impregnation with resins for microscopic studies. These made it possible to provide details of the claystone of samples 25-1 and 75-1, which could be compared with those of the reference sample. One observation was that the reference sample showed considerable heterogeneity with millimeter-sized dark grains embedded in a more transparent matrix.

Optical microscopy gave the following conclusions:

* Discrete grains of dense, layered clay were oriented at random. A few quartz and iron oxide grains could be identified
* The clay grains appeared to be cemented together by very small quartz and calcite grains
* The quartz content was clearly diminished in the claystone next to the heater

The heterogeneous composition of small entities can be expected to yield different reactions resulting in somewhat incompatible data.

Scanning electron microscopy using EDX showed that the magnesium content was higher in the cement of the claystone than in the clay grains and this was concluded to be due to the formation of trioctahedral phases in the claystone. The enhanced magnesium content was generally found to be associated with an increase in iron content, probably yielding trioctahedral clay minerals of smectite type (35).

5.4.2 Clay Technology

5.4.2.1 Microstructural appearance

The electron microscopy was focussed on finding major structural changes and identifying mineral changes by use of energy dispersive X-ray analysis. The instrument was a Philips 515 SEM equipped with a Link 2000. The X-ray detector was equipped with a beryllium window which limited the analyses to elements with Z>11 (Na).

Comprehensive SEM analyses showed clear changes in microstructure and mineral composition in the L0 (150-180 ^{o}C) and L1 (130-150^{o}C) samples. In the L0 sample it was observed that the clay formed a co-

herent mass without the typical wavy structure that is typical of virgin material. This is illustrated by the micrographs in Fig.5-26, which also show local regions rich in amorphous silica. They were much more frequent than in the clay close to the hot casing in Hole I (Fig.5-27) and are concluded to be the major cementing substance. Similar significant microstructural changes were seen also in sample L1 (Fig.5-27), while sample L3 showed the typical wavy structure of smectite forming a continuous mass (Fig.5-28).

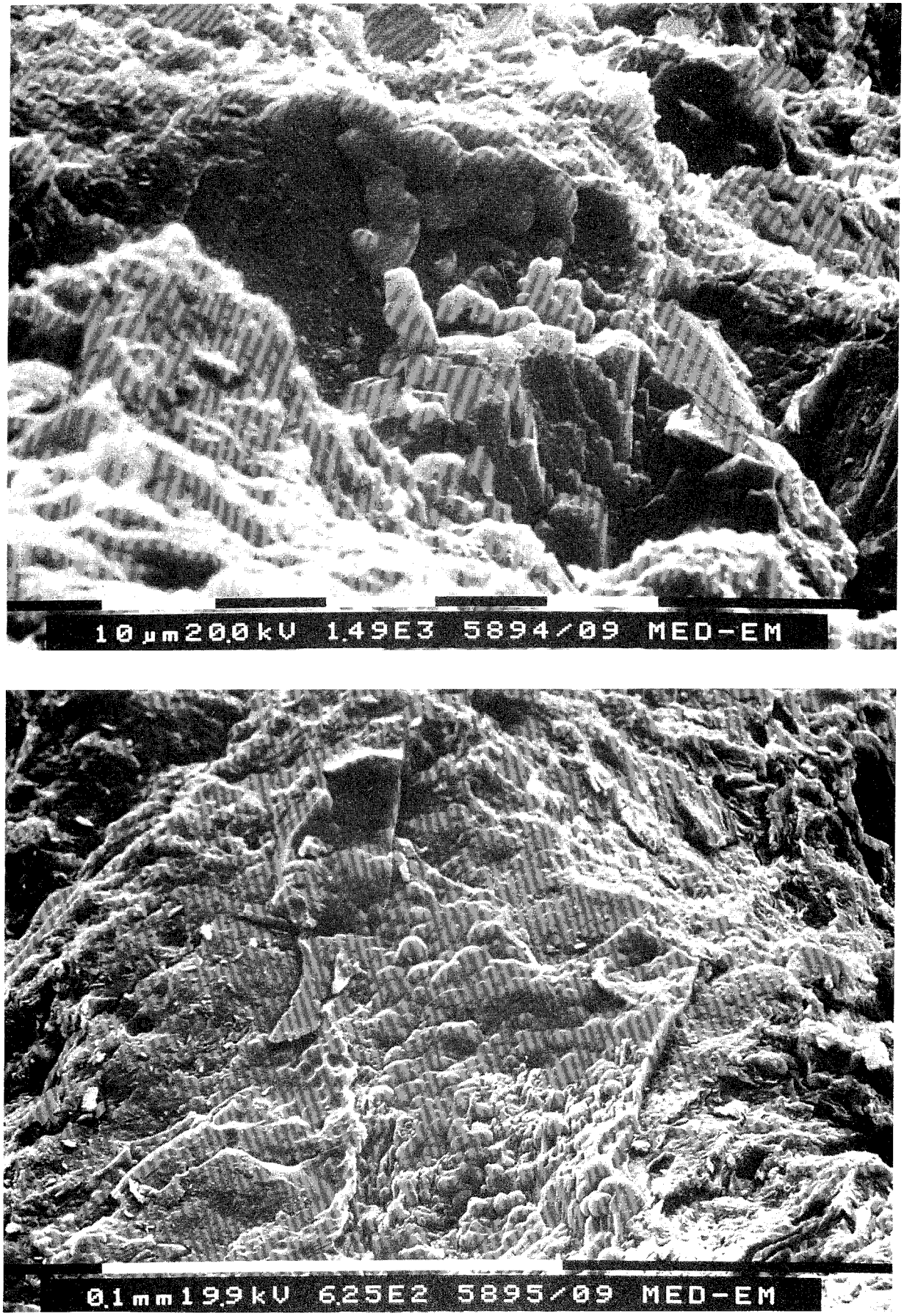

Figure 5-26 Scanning micrographs of sample L0 (150-180^{o}C)

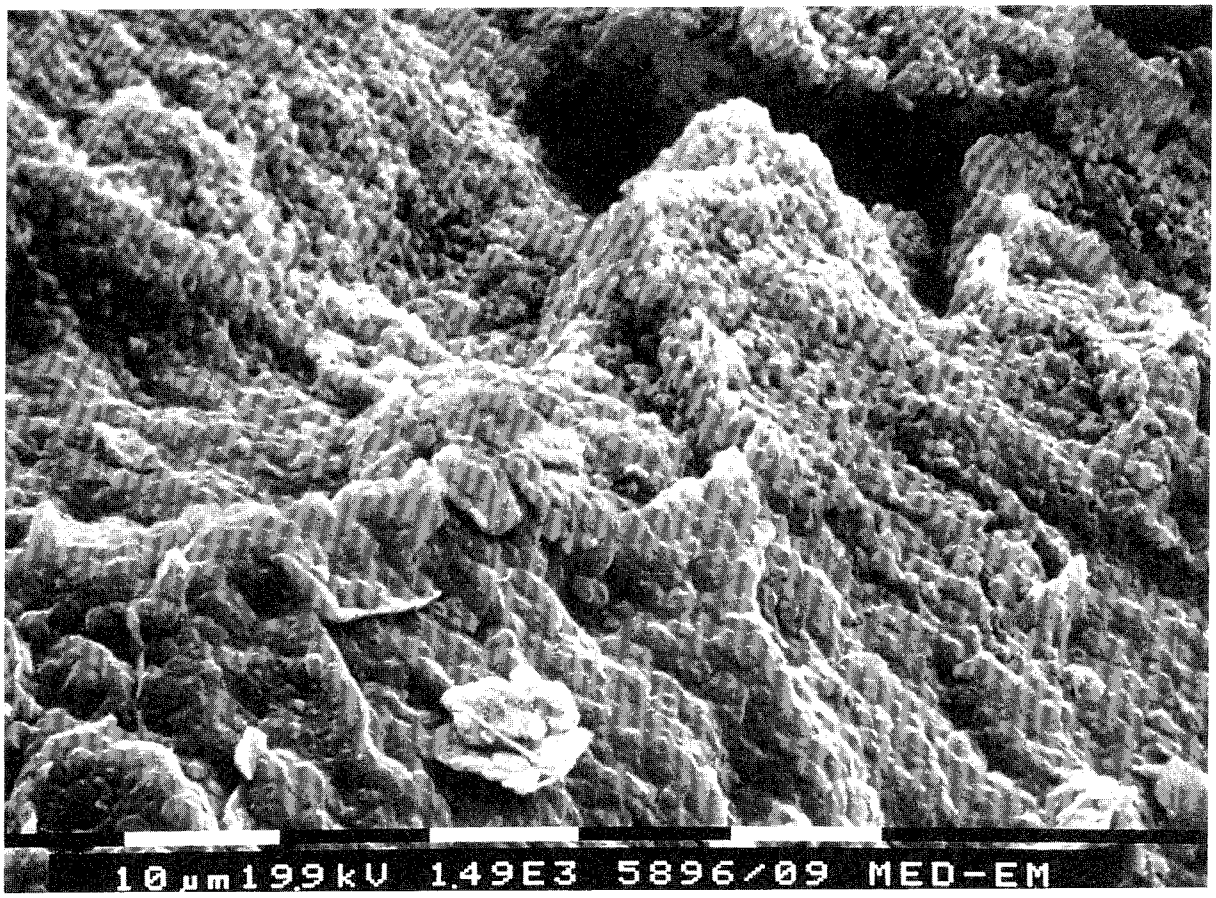

Figure 5-27 Scanning micrograph of sample L1 (130-150^{o}C)

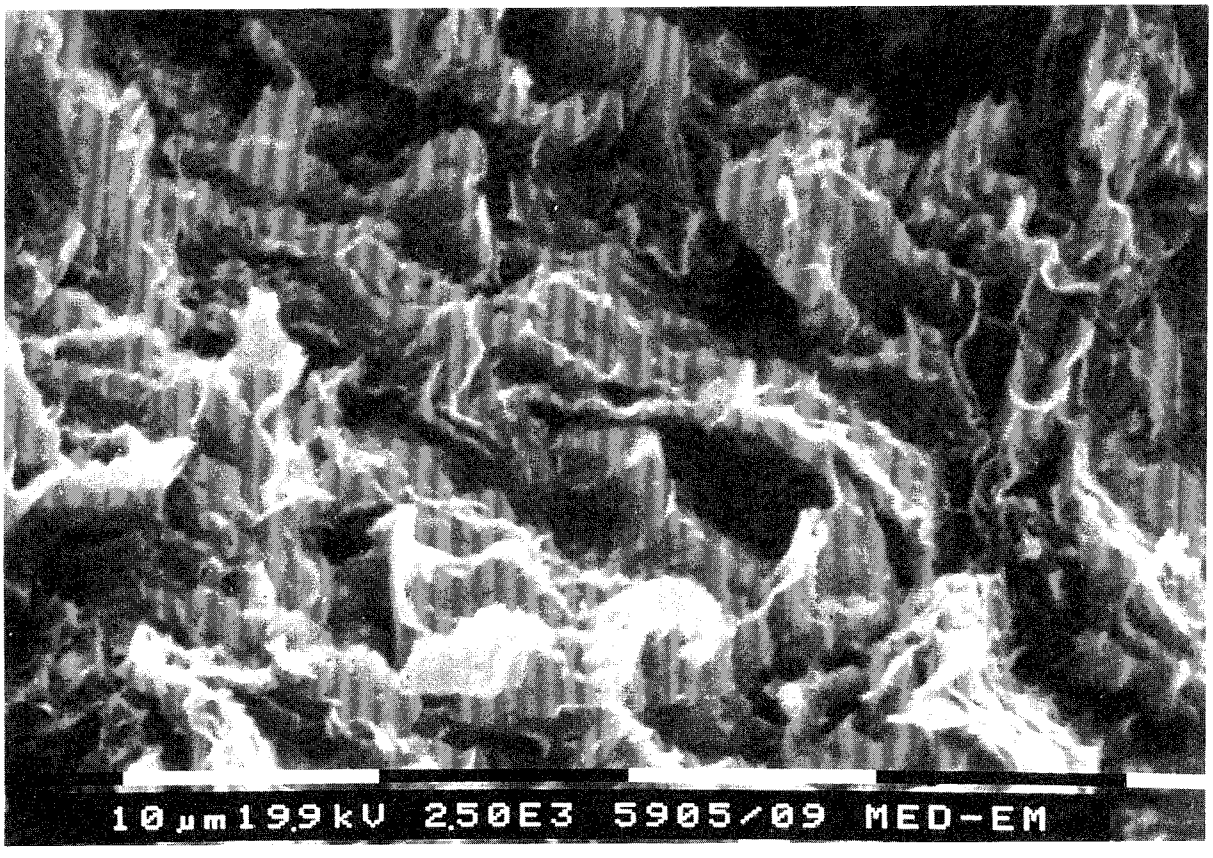

Figure 5-28 Scanning micrograph of sample L3 (95-110^{o}C)

5.4.2.2 Element analyses

The element analyses clearly showed that calcium and sulphate were closely associated forming anhydrite crystals in sample L0 (150-180°C) as illustrated by the good fitting of Ca and S in Fig.5-29. This figure also demonstrates the typical phenomenon of depletion of aluminum and relative enrichment in silica in the coherent clay matrix, the silica probably being precipitated in the form of an amorphous silica gel with strongly cementing properties. Iron was not identified in quantities that exceeded those of the virgin clay, which means that hardly any iron was released from the steel casing into the clay and that amorphous silica precipitates therefore were largely responsible for the cementation.

Aluminum appeared to dominate over silica in sample L1 (Fig.5-30) and in this sample pyrite particles that were partly disintegrated giving off sulphate and iron could be identified. Fig.5-31 shows the typical distribution of silica and aluminum in virgin smectite of montmorillonite type.

A possible mechanism leading to the enrichment of anhydrite at the hot boundary is that it has a lower solubility at higher temperatures. Precipitation at the hot end hence caused a sink that created a concentration gradient yielding successive migration of calcium and sulphur to the hot zone.

The micrographs represent typical element distributions and were selected in the course of the comprehensive scanning that was made for chemical and microstructural characterization of the clay.

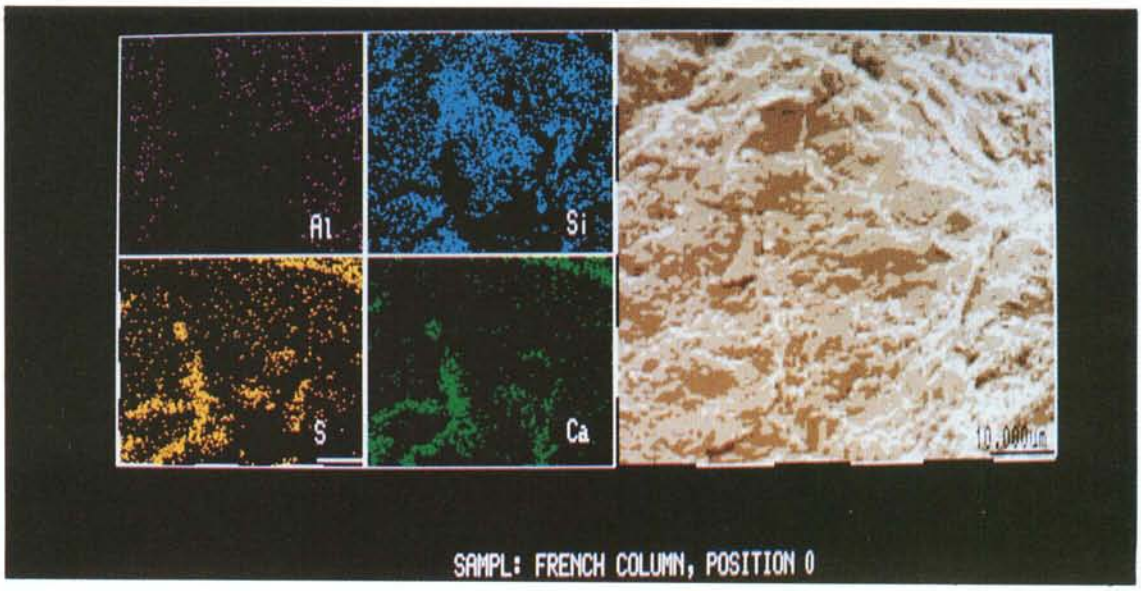

Figure 5-29 Element distribution in sample L0 (150-180°)

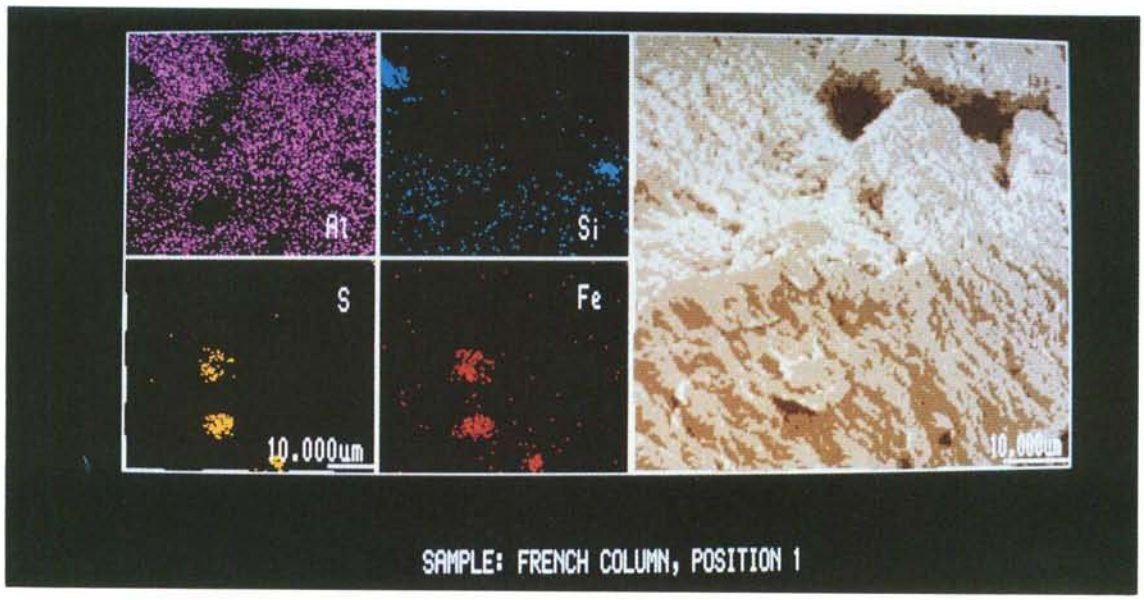

Figure 5-30 Element distribution in sample L1 (130-150^{o}C)

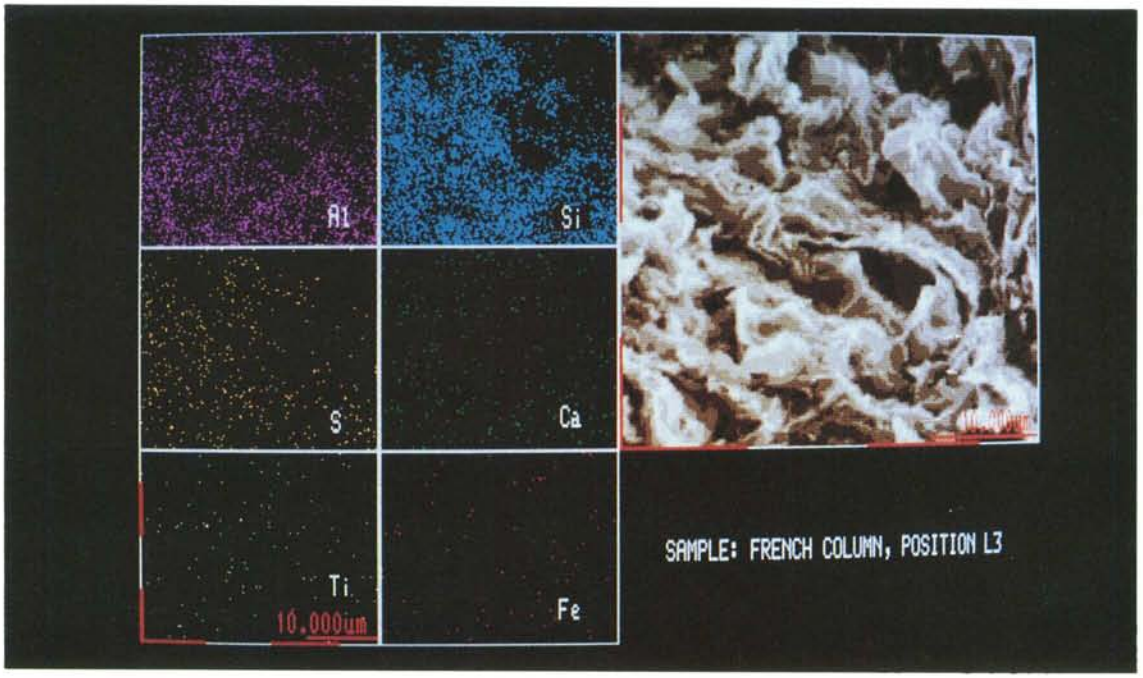

Figure 5-31 Element distribution in sample L3 (95-110^{o}C)

5.5 STEEL/CLAY INTERACTION

5.5.1 General

The visual impression of the clay next to the heater, i.e. the blackish color, suggested that iron had migrated and precipitated in the form of oxy-hydroxide components to a distance of several millimeters from the heater surface. Also, the obvious pitting-type corrosion of the steel suggested that considerable amounts of iron could have been released into the clay. Special care was therefore taken to analyse the clay with respect to the presence and form of iron, and some preliminary study of the clay/steel contact and of the shallow steel surface were made.

5.5.2 Iron in the clay

It follows from the reported chemical analyses in the preceding text that the iron content in the clay and claystone was in fact not significantly higher than in virgin Fo-Ca 7 clay and that the dark color was partly due to the strong reduction of the quartz content in the black part of the claystone. However, it was also obvious from the CEA study that ferromagnesium minerals in the form of trioctahedral smectite containing Fe^{2+} had been created in the black zone and contributed to the dark color. The whole reaction appears to be comparable to those observed around basalt intrusions where one finds hardening of the clay phase to be associated with darkening (36,37).

5.5.3 Clay/steel interface

5.5.3.1 Techniques

While the examination of the L0 sample (cf. Fig.5-18) showed that iron had not entered the clay in significant amounts, the study was extended to cover also the steel surface in order to investigate what chemical interaction between clay and steel that may have taken place at the interface. For this purpose the steel surface at the hottest part of the casing exposed at the removal of the surrounding stiff clay (L0) was investigated by SEM, and material scraped from the surface down to where unaltered steel appeared, was investigated by XRD. Also the steel was very carefully sawed and the section depicted by SEM in order to identify the depth of corrosion.

5.5.3.2 Electron microscopy

Fig.5-32 is an overview normal to the steel surface at very low magnification, showing areas with thin clay coatings and areas where the steel is exposed, indicating that no pitting had occurred. Fig.5-33 shows a

coated part where a few kaolinite flakes and some fibrous minerals appear in a mass of amorphous silica of the same type as in sample L0.

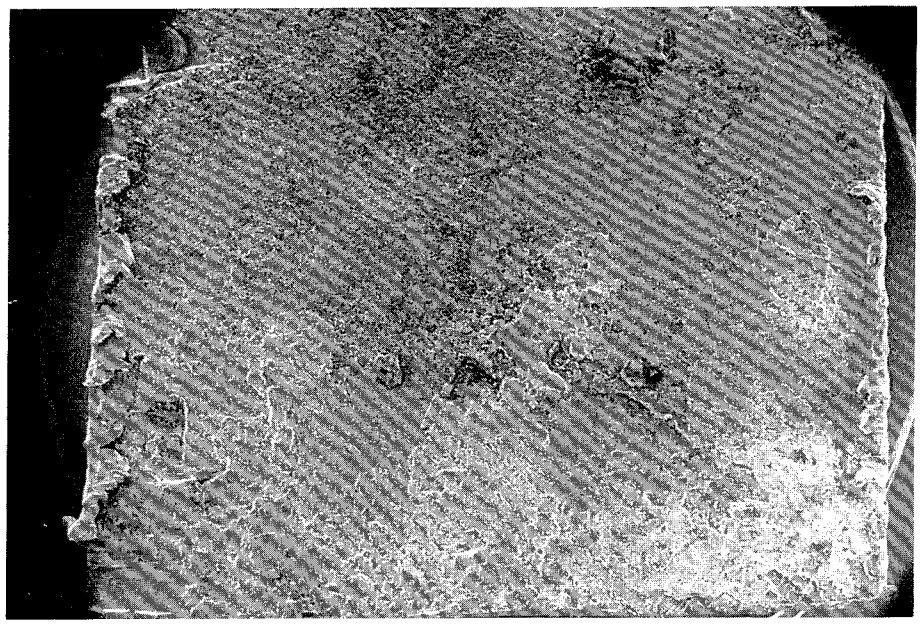

Figure 5-32 Scanning micrograph of steel surface with local clay coatings. 10x magnification

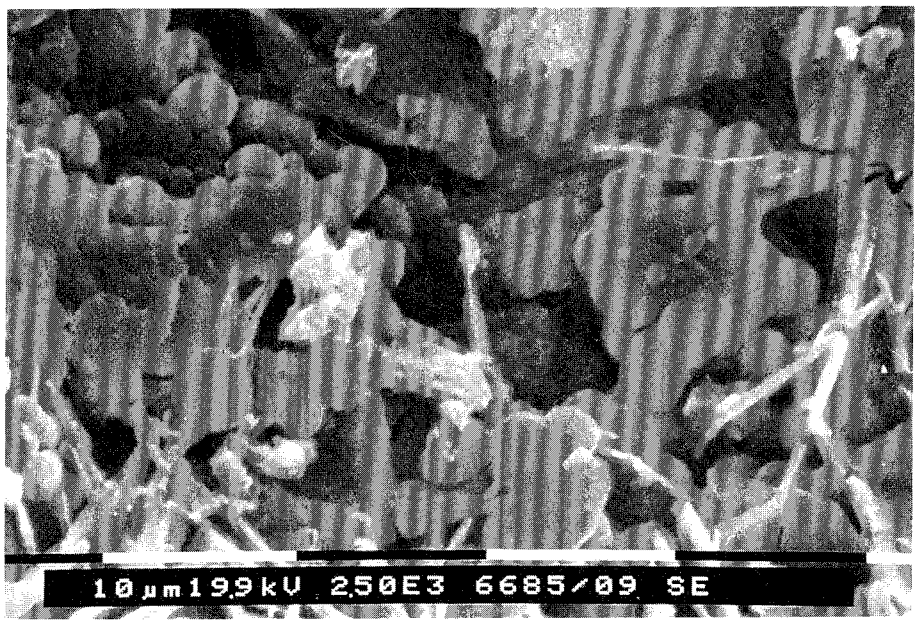

Figure 5-33 Scanning micrograph of clay coating rich in amorphous silica

Fig.5-34 shows the boundary of a clay coating "continent" with no clearly discernible kaolinite particles and with the rather smooth steel surface exposed at the bottom.

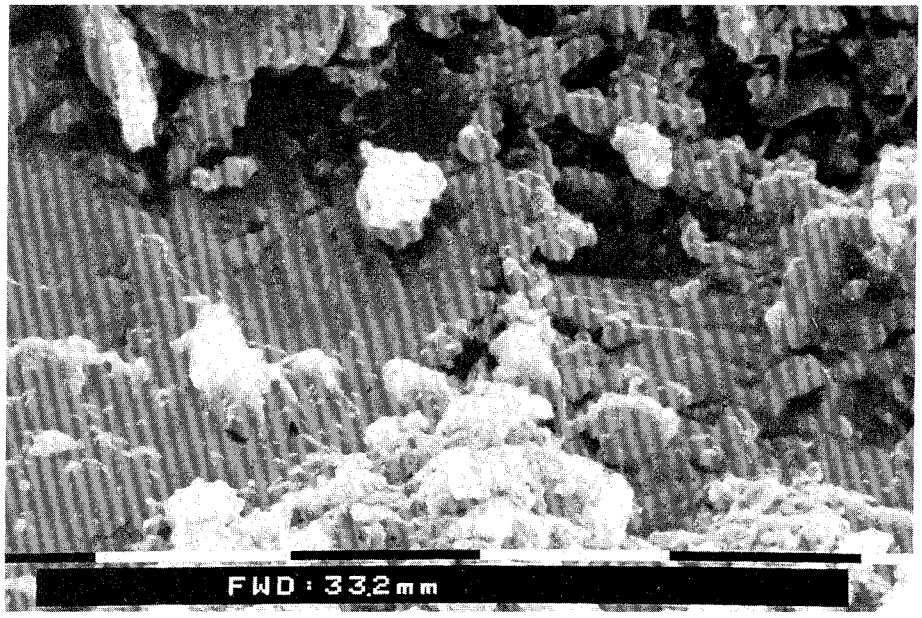

Figure 5-34 Scanning micrograph taken normal to the steel surface

5.5.3.3 **XRD**

The material scraped from the steel surface was prepared by packing and examined in the same way as the clay samples, giving the diagram shown in Fig.5-35. One finds that magnetite is not present and that hematite is the only iron-bearing component that can be identified with certainty. Quartz, tridymite, smectite and anhydrite are present like in the L0 sample, while the kaolinite content is insignificant. In addition to these minerals there are also 10 Å minerals which are probably of paragonite-type. The fact that magnetite, i.e. the major reaction product that one could expect because of the reducing conditions, was not identified does not mean that it was not formed. Thus, it may have escaped identification due to a very small crystal size and it may also be that it is not well crystallized or has the form of hydromagnetite, representing a spectrum of Fe^{2+} Fe^{3+} hydroxy compounds.

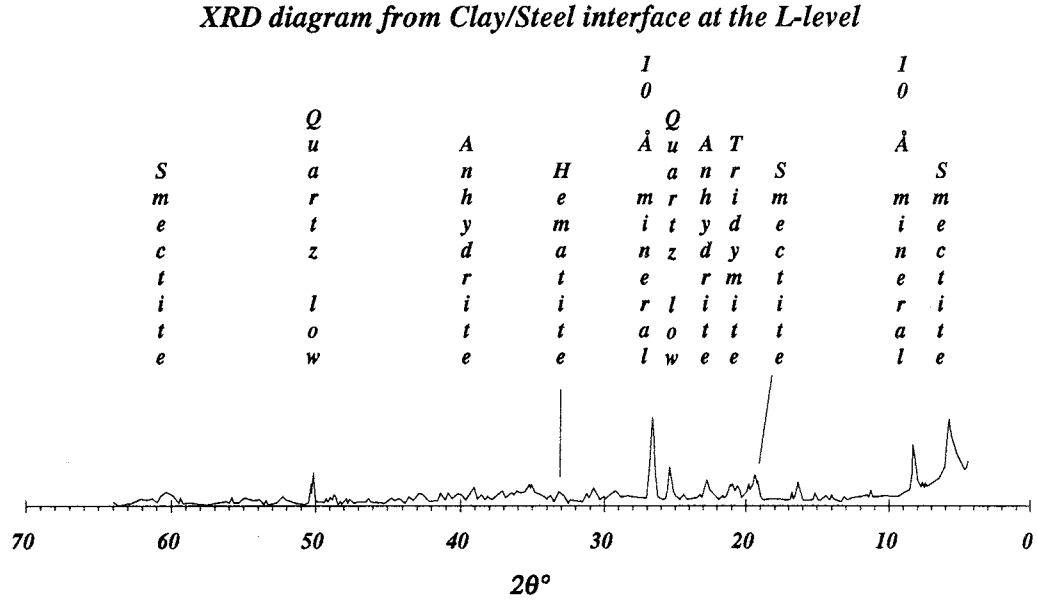

Figure 5-35 XRD diagram of material scraped off the steel surface

5.5.4 Shallow steel

5.5.4.1 General

Corrosion of steel in contact with smectitic clay has been experimentally investigated in reported studies that have indicated strong pitting and migration of iron to considerable depths in the clay (38,39). Thus, it was found that iron migrated to about 10 mm depth in 37 days but then stopped in experiments with steel in contact fully saturated highly compacted Na bentonite at room temperature. Air environment gave quicker reaction than nitrogen gas environment.

5.5.4.2 Electron microscopy

A close-up of the steel surface in tilted position for showing both the surface and the conditions at shallow depth, is given by Fig.5-36. This picture shows the character of the steel surface and it was concluded from examining a number of such pictures that the steel had a porous and disintegrated character down to 20 or maximum 30 μm depth. This is verified also by Fig.5-37, showing the profile of a sectioned part of the casing. While the accuracy of evaluating corrosion depth from scanning microscopy of the type that gave Fig.5-36 is rather good, samples prepared by sectioning and examined in the way that gave the picture in Fig.5-37 did not yield a very accurate corrosion depth.

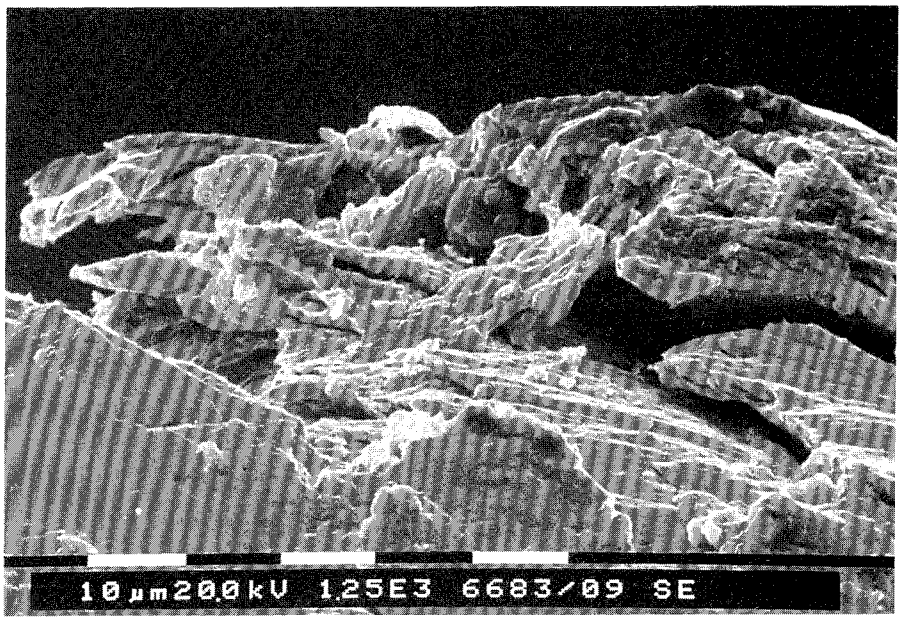

Figure 5-36 Scanning micrograph of inclined steel surface showing disintegration to 20-30 µm depth.

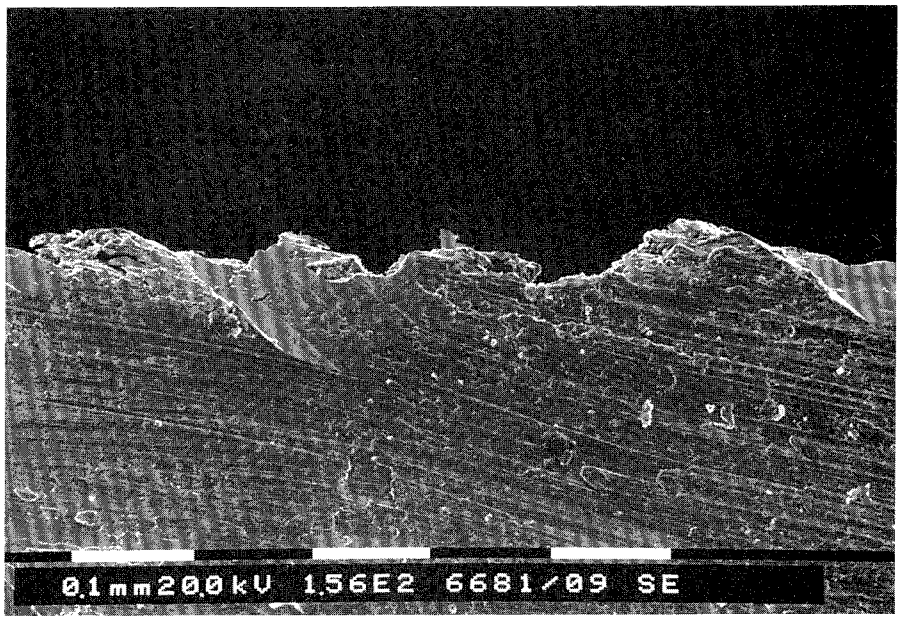

Figure 5-37 Section of steel casing showing the porous and disintegrated character of the surface down to an average depth of about 30 µm

6 DISCUSSION AND CONCLUSIONS

6.1 PHYSICAL PROCESSES

6.1.1 Dehydration mechanisms

It is clear from the fact that the 8 months long test in Hole I showed a much higher degree of water saturation than the 4 year test in Hole II, that time-dependent dehydration and expulsion of water from the hottest part of the clay core took place in the latter and that it became important rather late. In fact, a closer examination of the temperature evolution summarized in Fig.5-3 reveals that these processes became important after about 18 months. The expulsion of water must have been caused by gas production, either vapor produced by evaporation of water that was released from collapsed smectite stacks, or hydrogen gas formed from corrosion of the steel casing under the prevailing reducing conditions.

Using the evaluated data on the degree of water saturation it is concluded that the total gas-filled space was 2.2 liters over 1 m length of the innermost 22 mm thick clay annulus. The gas pressure must have caused expulsion of water upwards/sideways through the clay, for which the capillary pressure had to be overcome. The capillary pressure is close to the swelling pressure for high clay densities and it was hence on the order of 1.4-1.5 MPa at the upper end of the hot zone, well below the sand/clay interface (40). Higher gas pressures would imply that a critical level had been reached by which both gas and water could have left in a piping-like process without creating a uniform dry zone.

If the gas consisted of water vapor the pressure 1.5 MPa would correspond to about 170°C, which was the actual temperature and this therefore speaks in favor of the vapor hypothesis. However, the fact that dehydration and expulsion of gas did not become obvious until after around 18 months implies that considerable mineralogical or microstructural changes leading to a reduction in hydration potential must have taken place after this period. Complete collapse of the smectite stacks to form paragonite-type minerals would yield conversion of about 0.7 liters of "internal" water to "external", free water that could be moved out by the vapor pressure and this can possibly account for part of the dehydration. This assumption as well as that of illitization due to uptake of potassium from the surrounding clay, which is in fact excluded as evidenced by XRD and element analyses, are counter-evidenced by the recorded neoformation of smectite in the hottest zone. There remains a possibility that the time-

dependent dissolution of kaolinite resulted in such an increase in void space that the capillary retention and thereby the hydration potential would drop successively, but this could hardly yield the recorded loss of water.

An alternative and highly probable explanation is that hydrogen gas was formed by steel corrosion under reducing conditions and at enhanced pH, the basic reaction being the following:

$$3Fe + 4H_2O > Fe_3O_4 + 4H_2$$

It is equally possible that hydromagnetite was formed yielding $Fe_3(OH)_8$, which represents a spectrum of $Fe^{2+}Fe^{3+}$ hydroxy compounds. Both would contribute to the black color of the steel casing and of the clay contacting it.

Back-calculating[1)] the amount of steel that would have taken part in such a reaction, producing all the 2.2 liter gas at 1.5 MPa, gives the figure 50 μm of shallow corrosion over 1 m length of the casing. Estimating that some of the gas was air, emanating from the initial partly air-filled voids in the clay, and some was water vapor, leaving the hydrogen gas volume to be 50 %, it is estimated that the corrosion depth would be around 25 μm, which is in fact in very good agreement with the actual observations in this study.

6.1.2 Ion migration mechanisms

The accumulation of sulphates in the hot zone close to the casing, which could be identified in the 8 months long test and which was comprehensive in the 4 year test, was basically due to the concentration gradient in dissolved sulphur, calcium and magnesium that was created when precipitation of sulphates was initiated at the wetting front of the hot zone. However, a second mechanism may well have contributed to the migration and that is the process of cyclic moisture transport in partially water saturated soil (1,41).

This mechanism involves evaporation in the hot region and moisture movement in vapor form through interconnected, wider passages towards and into the colder region where it condensates and moves back by film transport along external stack surfaces exposed in fine void systems. The main force that drives water back towards the hot end is assumed to be osmosis. Dissolved ions are thereby dragged from the colder parts towards the hot end where precipitation takes place.

---

1) Pers. comm. Lars Werme, SKB

As indicated by the 8 month test, salt precipitation was initiated rather early, the rate of accumulation being a function of the temperature gradient and of the wetting rate.

6.2 MINERAL ALTERATIONS

6.2.1 Conditions for changes

One condition for mineral alteration by dissolution and precipitation is that water is present in sufficient amounts. This seems to have been the case in both experiments except for the close vicinity of the steel canister in the last two and a half years. Here, mineral transformations may have been strongly retarded after this period of time, which is estimated to have a significant influence on the interpretation of recorded data and on the derivation of activation energies.

A major fact is that all the reactions took place under a temperature gradient that must have involved transport of dissolved species towards the hot end or towards the cold end, depending on the solubility of the various compounds as well as on ion exchange and dehydration processes in the clay.

6.2.2 Transformation and conversion of clay minerals

The study of the hardened, claystone-part of the clay core has given evidence of neoformation of a few phases that can allow us to characterize the reactions and identify the alteration mechanisms.

A major finding is that trioctahedral, swelling clay minerals of the saponite or stevensite types were formed in the claystone. In hydrothermal experiments using the Fo-Ca 7 clay it was observed that appreciable amounts of magnesium were released which was available for neoformation of various phases as observed at Stripa (12).

The steel heater may have had the important function of representing an oxidized cathodic zone with high pH that is known to be a preferred location for the formation of magnesium-rich clay minerals (35,42). The involved kinetics are very fast and crystallization occurs readily even under unfavorable conditions (43), which may have made the formation of trioctahedral Fe^{2+}-bearing smectites possible at Stripa where the water pressure was low and dehydration must have retarded all reactions close to the heater.

Summarizing the reactions involving clay minerals one finds the reactants and reaction products to be as follows:

REACTANTS	REACTION PRODUCTS
* Mixed-layer 50/50 kaolinite/smectite	* Dioctah. smectite
* Kaolinite	* Anhydrite
* Quartz	* Opal-A
* Calcite	* Trioctah. smectite
* Gypsum	* Calcium silicates
* Pyrite	* ε′
* Goethite	
* Hematite	
* ε	

where ε and ε′ are possible reactants and reaction products, respectively, which could not be identified. One species corresponding to ε that was found in one of the mineralogical analyses was feldspar, which underwent strong dissolution within the claystone, thereby providing the hot reaction zone with silica and aluminum.

It is concluded that all the reactants where not involved simultaneously at any given temperature, and more work, in particular further analysis of the core from the 8 months long test in Hole I, is required for clarifying the entire chain of reactions.

6.3 LONG-TERM STABILITY

6.3.1 What would the ultimate product be in repository environment and what is the reaction rate?

Since no geochemical modelling has been performed the ultimate reaction products are not known but the fact that the overall smectite content increases in the hydrothermal period with Fo-Ca 7 clay in a repository suggests that the ultimate clay mineral reaction product will be hydrous mica ("illite"). Amorphous and crystalline silicates precipitated as cements will persist for very long periods of time.

The rate of conversion of the original clay minerals to the end product hydrous mica is determined primarily by the rate of neoformation of the di- and trioctahedral smectites, and ultimately by the access to dissolved potassium. The first process appears to be a quick one as concluded from the present Stripa experiment, while the other is entirely determined by the rate at which potassium is supplied by the environment through groundwater flow or diffusion.

No safe conclusion respecting the activation energy and the rate of dissolution/precipitation involved in the creation of di- and trioctahedral smectites can be drawn from the present experiments because of the time-dependent rate of moistening and subsequent dehydration of the clay close to the heater.

It is estimated that if the potassium content of the porewater had been higher or if potassium feldspars had been abundant, an appreciable part of the beidellite component would have been converted to hydrous mica.

6.4 CHEMICAL AND MINERALOGICAL PROCESSES THAT AFFECT THE PHYSICAL PROPERTIES OF THE CLAY

6.4.1 Microstructural changes

The porosity of the clay exposed to higher temperatures than about 130°C increased due to loss of solid substance and the pore size distribution was changed to yield larger voids in conjunction with aggregation. This was found to yield an increase in hydraulic conductivity by at least 3 orders of magnitude within 1 cm distance from the hot boundary. Changes of the microstructure, probably associated with partly permanent heat-induced collapse of the smectite stacks, occurred also in the clay exposed to about 110-130°C, the process being aggregation in conjunction with creation of wider voids in a syneresis-type fashion, yielding an increase in hydraulic conductivity by at least 100 %. Even the outermost part, where the temperature did not exceed 95°C, a net increase in hydraulic conductivity by 100 % was recorded.

6.4.2 Precipitation processes that affected the physical properties

Cementation by precipitation of amorphous silica occurred in all parts of the clay annulus, very weakly in the outer parts where the temperature was lower than about 110°C, and very strongly where the temperature exceeded 150°C. The precipitation of silica caused stiffening of the clay and a drop in swelling potential which were both very substantial in the parts exposed to more 130°C and which were significant also in the part where the temperature had not exceeded 80-95°C.

6.5 GENERAL CONCLUSIONS

It is concluded from the determination of the rheological properties, the mineralogical and chemical analyses, as well as from the microstructural investigations, that significant changes had taken place in the 4 year experiment, primarily in the hottest zone close to the casing but also to some extent all the way to the clay/rock interface.

The major findings are:

* In the hottest part, i.e. where the temperature was in the range of 150-180 °C, the clay within about 6-8 mm distance from the steel casing had been dehydrated and turned into claystone due to cementation. A possible reason for the dehydration was formation of hydrogen gas by corrosion of the steel.

  The original ductility and swelling capacity were completely lost in this zone, in which neoformation of anhydrite and cementing silicates but also of smectite was very obvious. The amounts of originally present kaolinite and quartz in this zone had been strongly reduced. The hydraulic conductivity of the claystone was found to be three orders of magnitude higher than in the virgin clay

* The steel had interfered very little with the clay and the cementation is concluded to be independent of the access to steel and instead due to precipitation of silica compounds in amorphous and crystalline form in this inner zone as well as in the rest of the clay core. The silica emanated from dissolved quartz, kaolinite and feldspars. Still, the steel may have served as "catalyst" in the formation of trioctahedral smectite in the claystone

* The entire clay annulus - not only the innermost claystone-like part contacting the heater had undergone cementation due to precipitation of silica compounds. This involved significant changes in the rheological behavior of the clay and is undesired if the clay had represented a real canister embedment, both because of the loss of the self-sealing ability of smectite clay and because tectonically induced shearing would generate high shear stresses in the canister.

* The kinetics in the various processes are not clear since the hydration/dehydration probably affected both the dissolution and precipitation mechanisms. Hence, the rate and true mode of silification of the clay is not well understood and since it strongly affects the ductility and self-sealing properties of the peripheral parts of canister-embedding clay in a repository, further investigations at different temperatures over longer periods of time are required in order to make it possible to develop a physico/chemical model that can be used for extrapolation over repository lifetimes.

7 REFERENCES

1 **Pusch,R., Börgesson,L. & Ramqvist,G.** Final Report of the Buffer Mass Test - Volume II: test results. Stripa Project Technical Report 85-12, SKB, Stockholm, 1985

2 **Reynolds R.C.** Description of Program NEWMOD for the Calculation of the one-dimensional X-ray diffraction Patterns of Mixed-layered Clays. Manual for Practical Use. 1985

3 **Lanson,B.** Mise en Evidence des Mecanismes Reactionneles des Interstratifies illite/smectite au Course de la Diagenese. These, Univ. de Paris VI, 1990 (366 p)

4 **Lanson,B.** Application de la Composition des Diffractogrammes de Rayons X a l'identification des Mineraux Argileux. Rayons X Siemens (In press), 1992

5 **Lanson,B. & Besson,G.** Characterization of the End of the smectite-to-illite Transformation: Decomposition of XRD Patterns. Clays & Clay Minerals, 1992 (In press)

6 **Lanson,B. & Champion,D.** The I/S-to Illite Reaction in the Late Stage Diagenesis. Amer. J. Sci., Vol. 291, 1991 (pp.473-506)

7 **Brindley,G.W.** Quantitative X-ray Mineral Analysis of Clays. In: Crystal Structures of Clay Minerals and their X-ray Identification. Brindley,G.W. & Brown,G. Ed. Miner. Soc., London, 1980 (pp.411-438)

8 **Moore,D.M. & Reynolds,R.C.** X-ray Diffraction and the Identification and Analysis of Clay Minerals. Oxford Univ. Press, New York, 1989 (332 p)

9 **McManus,D.A.** Suggestions for Authors Whose Manuscripts Include Quantitative Clay Mineral Analysis by X-ray Diffraction. Mar. Geol., Vol.98, 1991 (pp.1-5)

10 **Jackson,M.L.** Soil Chemistry Analysis. Prentice Hall Inc., New Jersey, 1964

11 **Proust,D., Lechelle,J., Meunier,A. & Lajudie,A.** Hydrothermal Reactivity of Mixed-layer Kaolinite/smectite and Implications for Radioactive Waste Disposal. Eur. J. Mineral., Vol.2, 1990 a (pp.313-325)

12 **Proust,D., Lechelle,J. Lajudie,A. & Meunier.A.** Hydrothermal Reactivity of Mixed-layer Kaolinite/smectite: Experimental Transformation of High-charge to Low-charge Smectite. Clays & Clay Minerals. Vol.38, 1990 b (pp.415-425)

13 **Howard,J.J. & Roy,D.M.** Development of Layer Charge and Kinetics of Experimental Smectite Alteration. Clays & Clay Minerals. Vol.33, 1985 (pp.81-88)

14 **Reynolds,R.C.** Interstratified Clay Minerals. In: Crystal Structure od Clay Minerals and their X-ray Identification. Brindley,G.W. & Brown,G. Eds., Min. Soc., London, 1980 (pp.249-303)

15 **Inoue,A., Bouchet,A., Velde,B. & Meunier,A.** Convenient Technique for Estimating Smectite Layer Percentage in Randomly Interstratified Illite/-smectite Minerals. Clays & Clay Minerals. Vol.37, 1989 (pp.227-234)

16 **Meunier,A. & Velde,B.** Solid Solutions in I/S Mixed-layer Minerals and Illite. Am. Miner. Vol.74, 1989 (pp.1106-1112)

17 **Hower,J. & Mowatt,T.C.** The Mineralogy of Illites and Mixed-layer Illite/montmorillonite. Am. Miner. Vol.55, 1966 (pp.825-854)

18 **Pusch,R. & Hökmark,H.** GMM - A General Microstructural Model for Qualitative and Quantitative Studies of Smectite Clays. SKB Technical Report 90-43, SKB, Stockholm, 1990

19 **Pusch,R., Börgesson,L. & Erlström,M.** Alteration of Isolating Properties of Dense Smectite Clay in Repository Environment as Examplified by Seven Pre-Quaternary Clays. SKB Technical Report 87-29, SKB, Stockholm, 1987

20 **Börgesson, L.** Water Flow and Swelling Pressure in Non-Saturated Bentonite-based Clay Barriers. Eng. Geol., Vol. 21, 1985 (pp. 229-237)

21 **Pusch,R.** Final Report of the Buffer Mass Test - Volume III: Chemical and Physical Stability of the Buffer Materials. Stripa Project Technical Report 85-14, SKB, Stockholm, 1985

22 **Börgesson, L. & Pusch, R.** Rheological Properties of a Calcium Smectite. SKB Technical Report 87-31, SKB, Stockholm, 1987

23 **Pusch,R.** A Technique for Investigation of Clay Microstructure. J. Microscopie. Vol.6, 1967 (pp.963.986)

24 **Farmer,V.C.** The Layer Silicates. In: The Infrared Spectra of Minerals. Farmer,V.C. Ed., Miner. Soc., London, 1974 (pp.331-363)

25 **VanDer Marel,H.W. & Beutelspacher,H.** Atlas of Infrared Spectroscopy of Clay Minerals and their Admixtures. Elsevier, Amsterdam, 1976, 396 p.

26 **Oinuma,K. & Hayashi,H.** Infrared Study of Mixed-layer Clay Minerals. Am. Miner. Vol.50, 1965 (pp.1213-1227)

27 **Coey,J.M.D.** Mössbauer Spectroscopy of Silicate Minerals. In: Mössbauer Spectroscopy Applied to Inorganic Chemistry. Long,G.J. Ed., Plenum Press, New York, 1984 (pp-443-509)

28 **Decarreau,A.** Spectroscopie Mössbauer. In: Materiaux Argileux. Structure, Proprietes et Applications. Soc. Fr. Miner. et Crist./ Gr.Fr.Arg., Paris, 1991 (pp.117-126)

29 **Lasaga,A.C.** Rate Laws of Chemical Reactions. In: Kinetics of Geochemical Processes. Lasaga,A.C. & Kirkpatrick,R.J. Eds., Reviews in Mineralogy, Miner. Soc. Amer., Vol.8, 1981 (pp.1-68)

30 **Eberl,D. & Hower,J.** Kinetics of Illite Formation. Geol. Soc. Amer. Bull. Vol.87, 1976 (pp.1326-1330)

31 **Vasseur,G. & Velde,B.** A Kinetic Interpretation of the Smectite to Illite Transformation. 1992 (In preparation)

32 E.R.M. Etude de la Fraction Inferieure a 0.2 μm de l'argile Fo-Ca 7 et de Ses Produits d'alteration a 200°C. Rapport E.R.M. Contrat CEA no A 218 347 FM, 1990

33 **Velde,B.** Kinetics of I/S (Illite/smectite) Transformations. MRS Strasbourg 1991 (Resume no B-II, Invited Paper), 1991

34 **Roberson,H.E. & Lahann,R.W.** Smectite to Illite Conversion Rates: Effects of Solution Chemistry. Clays & Clay Miner. Vol.29, 1981 (pp.129-135)

35 **Bouchet,A.** Mineralogie et Geochimie des Roches Alterees du Chapeau de Fer de Rouez (Sarthe). These, Univ. Poitiers, 1987, 145 p

36 **Maury,R. & Mervoyer,B.** Metamorphisme Thermique des Pelites Permiennes du Bassin de Lodeve au Contact d'Intrusions Basaltiques de Tailles Variees. Bull. Soc. Geol. Fr. Vol.15, 1973 (pp.313-320)

37 **Correia,M.J. & Maury,R.C.** Effets Thermique, Mineralogique et Chimiques de l'Intrusion d'un Dyke Basaltique dans le Toarcien de Causses. Bull. Centre Rech. Pau SNPA. Vol.9, 1975 (pp.245-259)

38 **Miwa,K., Kanno,T., Asano,H. & Wakamutso,H.** Migration Behavior of Carbon Steel Corrosion Products. Topical Meeting on Nuclear Waste Packaging (FOCUS-91), Las Vegas 1991 (In print)

39 **Nakayama,G. & Akashi,M.** The Critical Condition for the Initiation of Localized Corrosion of Mild Steels in Contact with Bentonite Used for Nuclear Waste Package. MRS XV Int. Symp. for Nucl. Waste Management, Strasbourg, 1991

40 **Pusch,R., Ranhagen,L. & Nilsson,K.** Gas Migration Through MX-80 Bentonite. NAGRA Technical Report 85-36, 1985

41 **Pusch,R., Karnland,O. & Sanden,T.** Effects of Salt Water on the Wetting Rate and Porewater Chemistry of MX-80 Clay Exposed to a Thermal Gradient. Int. Techn. Rep. SKB, Stockholm 1992

42 **Thornberg,M.R.** Weathering of Sulphide Ore Bodies. In: Geochemical Exploration in Deeply Weathered Terrains. Smith,R.E. Ed., CSIRO, Wembley, Australia, 1983 (pp.67-103)

List of SKB reports

Annual Reports

1977-78
TR 121
KBS Technical Reports 1 – 120
Summaries
Stockholm, May 1979

1979
TR 79-28
The KBS Annual Report 1979
KBS Technical Reports 79-01 – 79-27
Summaries
Stockholm, March 1980

1980
TR 80-26
The KBS Annual Report 1980
KBS Technical Reports 80-01 – 80-25
Summaries
Stockholm, March 1981

1981
TR 81-17
The KBS Annual Report 1981
KBS Technical Reports 81-01 – 81-16
Summaries
Stockholm, April 1982

1982
TR 82-28
The KBS Annual Report 1982
KBS Technical Reports 82-01 – 82-27
Summaries
Stockholm, July 1983

1983
TR 83-77
The KBS Annual Report 1983
KBS Technical Reports 83-01 – 83-76
Summaries
Stockholm, June 1984

1984
TR 85-01
Annual Research and Development Report 1984
Including Summaries of Technical Reports Issued during 1984. (Technical Reports 84-01 – 84-19)
Stockholm, June 1985

1985
TR 85-20
Annual Research and Development Report 1985
Including Summaries of Technical Reports Issued during 1985. (Technical Reports 85-01 – 85-19)
Stockholm, May 1986

1986
TR 86-31
SKB Annual Report 1986
Including Summaries of Technical Reports Issued during 1986
Stockholm, May 1987

1987
TR 87-33
SKB Annual Report 1987
Including Summaries of Technical Reports Issued during 1987
Stockholm, May 1988

1988
TR 88-32
SKB Annual Report 1988
Including Summaries of Technical Reports Issued during 1988
Stockholm, May 1989

1989
TR 89-40
SKB Annual Report 1989
Including Summaries of Technical Reports Issued during 1989
Stockholm, May 1990

1990
TR 90-46
SKB Annual Report 1990
Including Summaries of Technical Reports Issued during 1990
Stockholm, May 1991

1991
TR 91-64
SKB Annual Report 1991
Including Summaries of Technical Reports Issued during 1991
Stockholm, April 1992

1992
TR 92-46
SKB Annual Report 1992
Including Summaries of Technical Reports Issued during 1992
Stockholm, May 1993

Technical Reports
List of SKB Technical Reports 1993

TR 93-01

Stress redistribution and void growth in buttwelded canisters for spent nuclear fuel

B L Josefson[1], L Karlsson[2], H-Å Häggblad[2]
[1] Division of Solid Mechanics, Chalmers University of Technology, Göteborg, Sweden
[2] Division of Computer Aided Design, Luleå University of Technology, Luleå, Sweden

February 1993